Claudin-2 and Claudin-12 Inform our Understanding of Intestinal Mineral Absorption

by

Matthew Saurette

A thesis submitted in partial fulfillment of the requirements for the degree of

Master of Science

Department of Physiology

University of Alberta

ABSTRACT

Hyperphosphatemia, elevated serum phosphate (Pi), is an electrolyte imbalance frequently associated with chronic kidney disease (CKD) and end-stage renal disease (ESRD). There are many negative consequences of hyperphosphatemia including worsening renal function, secondary hyperparathyroidism, cardiovascular disease and mortality in this population and the general population. Therefore, reducing serum Pi is a clinical priority. Currently, the main strategies to lower serum Pi include dietary Pi restriction and phosphate-binding agents. However, restricting dietary Pi can be difficult as Western diets contain high amounts of Pi salts as additives and preservatives, which have greater bioavailability compared with organic sources. However, the mechanism responsible for altered bioavailability between the forms of Pi is unknown. Claudin-12 KO mice are a transgenic model with enhanced intestinal paracellular Pi permeability. When fed an inorganic Pi diet, they had increased Pi bioavailability compared to wild-type mice suggesting inorganic Pi moves preferentially via the paracellular pathway. Conversely, inhibiting Npt2b, the major transcellular intestinal Pi transporter with NTX-1942 reduced Pi bioavailability in wildtype mice on an organic phosphorus, but not an inorganic Pi diet. This suggests that Pi liberated from organic sources is absorbed transcellularly in the intestine, while inorganic Pi moves paracellularly leading to a higher bioavailability. Additionally, feeding claudin-12 KO mice an inorganic Pi diet results in hyperphosphatemia and is therefore a useful model for interrogating the causal link between high blood Pi, cardiovascular disease and mortality in the absence of renal dysfunction.

Claudin-2 is a cation permeable claudin, expressed in the intestine and kidney like claudin-12. Previous cell culture work has inferred a role for claudin-2 in intestinal and renal

calcium (re)absorption. To assess the role of claudin-2 in calcium homeostasis in vivo, metabolic balance studies were performed on wild-type and claudin-2 knockout mice. This revealed hypercalciuria and increased intestinal calcium absorption. Bi-ionic diffusion potential studies in Ussing chambers revealed reduced colonic calcium permeability without alterations in other segments. Analysis of wild-type and claudin-2 KO tibia's revealed unaltered bone mineralization. Similarly, plasma calcium was not different between genotypes nor was intestinal or renal calciotropic gene expression. We therefore conclude that claudin-2 knockout mice have increased renal calcium excretion compensated by enhanced net calcium absorption secondary to reduced colonic secretion.

PREFACE

The research project, of which this thesis is a part, received research ethics approval from the University of Alberta Research Ethics Board, The role of transport proteins in Epithelial Sodium, Bicarbonate Phosphate and Calcium Transport and Breeding Colonies, AUP00000213.

Some of the research conducted for this thesis forms part of an international research collaboration with Dr. Alan Yu at the University of Kansas Medical Center. Dr. R. Todd Alexander was the lead collaborator at the University of Alberta. The quantitative RT-PCR, micro-computed tomography and mouse experiments included in Chapter 4 of this thesis were conducted by myself and I performed the subsequent data analysis. A portion of Chapter 1 in this thesis references material from a literature review that was also my original work.

Chapter 4 of this thesis was published as Curry J.N, Saurette M, Askari M, Pei L., Filla M.B, Beggs M.R, Rowe P.S.N, Fields T, Sommer A.J, Tanikawa C, Kamatani Y, Evan A.P, Totonchi M, Alexander R.T, Matsuda K, Yu A.S.L, "Claudin-2 deficiency associates with hypercalciuria in mice and human kidney stone disease," *Journal of Clinical Investigation,* volume 130, issue 4, 1948-1960. Along with JNC, LP, MBF, I performed the main set of animal experiments, edited and reviewed the final manuscript. JNC and ASLY were responsible for study design and drafting the original manuscript.

ACKNOWLEDGEMENTS

I would like to thank all the past and present members of the Alexander Laboratory including: Dr. Todd Alexander, Wanling Pan, Debbie O'Neill, Megan Beggs, Justin Lee, Allein Plain, Saba Rehman, Shane Wiebe, Tate MacDonald and Rebecca Tan. I am sincerely grateful to Dr. Alexander for the many opportunities to learn and grow. Your kind and compassionate leadership style, enthusiasm for science and ability to bring out the best in your students and staff is inspirational. In addition, I would like to thank the wonderful lab technicians, Wanling Pan and Debbie O'Neill, who were always willing to lend their guidance and expertise. Your help over the years has been invaluable.

I would like to extend my thanks to the Faculty of Medicine and Dentistry and the Membrane Protein Disease Research Group for their financial support. I would also like to acknowledge Dr. Emmanuelle Cordat and laboratory members, as well as my committee members Dr. Elaine Leslie, Dr. Shereen Hamza for your guidance and feedback.

Finally, thank you to my family and friends for your continued love and support. I would not have been able to get here without you.

Table of Contents

List of Figures

List of Abbreviations

BMD–bone mineral density

BS–bone surface area

BS/BV–bone surface / bone volume

BS/TV– bone surface / tissue volume

BV–bone volume

BV/TV (%)–bone volume / tissue volume

Ca^{2+} – calcium ion

CABP9K – calbindin-D_{9k}

CaSR – calcium sensing receptor

cAMP – cyclic adenosine monophosphate

CKD – chronic kidney disease

Ct. Th– Cortical thickness

ESRD – end-stage renal disease

FGF-23 – fibroblast growth factor 23

NCX1 – sodium-calcium exchanger 1

Npt2a – sodium-phosphate cotransporter 2a

Npt2b – sodium-phosphate cotransporter 2b

Npt2c – sodium-phosphate cotransporter 2c

P – Phosphorus

PD–potential difference

Pi – inorganic phosphorus ($H_2PO_4^-$ / HPO_4^-)

PiT-1 – sodium-phosphate transporter 1

PiT-2 – sodium-phosphate transporter 2

PMCA1b – plasma membrane calcium ATPase 1b

PTH – parathyroid hormone

SMI– structure model index

TAL – thick ascending limb

Tb.N–trabecular number

Tb.Sp–trabecular spacing

Tb.Th–trabecular thickness

TS–tissue surface area

TV–tissue volume

TRPV5– transient receptor potential cation channel subfamily V member 5

TRPV6 – transient receptor potential cation channel subfamily V member 6

$1,25[OH]_2D_3$ – 1, 25-dihydroxyvitamin D_3 (active Vitamin D_3)

$25[OH]D_3$ – 25-hydroxyvitamin D_3

Chapter 1 : Introduction

Section 1.4 of the introduction was modified from published work in *Saurette M* and Alexander RT., *Exp. Biol. Med.* 2019 May, 244 (8):646-654.

1.1 Phosphate importance and homeostasis

Phosphorus (P) is an essential element for life. This is reflected in the fact that it is the second most abundant mineral, comprising 1-1.4% of free-fat mass in humans (Robert, 2012), and is involved in a wide variety of cellular processes and is a component of many biomolecules. The primary source of phosphorus is through dietary intake. Dietary phosphorus can occur as organic phosphorus, where it is bound to a carbon-containing molecule, or as inorganic phosphorus *i.e.* phosphate salts. Organic phosphorus is found in protein from meat, poultry and fish as well as phytate from plant products including cereals and legumes (Kalantar-Zadeh et al., 2010). As humans lack the enzyme phytase, a phosphatase that hydrolyzes phytic acid found in plant tissue, diets containing a greater proportion of their total P from plants have reduced intestinal absorption (*i.e.* reduced bioavailability) (S. M. Moe et al., 2011). Absorption of phosphate from protein requires its hydrolysis and cleavage by intestinal alkaline phosphatase (IAP). We propose in this thesis that this contributes to a lower bioavailability compared to diets containing inorganic phosphate as phosphate salts, typical additives and preservatives, which are readily absorbed and have a bioavailability >80% (Cupisti & Kalantar-Zadeh, 2013; Gutierrez et al., 2015).

In humans, phosphorus primarily occurs in an oxidized form as inorganic phosphorus (PO_4^{3-} or Pi) and the vast majority (~85%) of Pi is found complexed with calcium (Ca^{2+}) as the salt hydroxyapatite [$(Ca)_{10}(PO_4)_6(OH)_2$] in the extracellular matrix, conferring hardness to bone and teeth (Bhadada & Rao, 2021). In addition to forming hydroxyapatite, PO_4^{3-} also regulates the terminal differentiation of hypertrophic chondrocytes in the growth plate allowing for proper vascularization and replacement of chondrocytes with osteoblasts to form the primary spongiosa of bone (Sabbagh et al., 2005) .

The remaining PO_4^{3-} outside the skeleton is distributed intracellularly in soft tissue (~14%) and to a lesser degree in extracellular fluid (~1%) (Goretti Penido & Alon, 2012). Within cells, phosphate is critical for the maintenance of genetic information as a principle component of the backbone of ribonucleic acids (Kornberg, 1979). In addition to its structural role in DNA and RNA, phosphate contributes to the structure of cell membranes by determining the polarity of phospholipids and is often involved in the initiation of signal transduction cascades. For example, phosphoinositides, a family of membrane lipids composed of diacylglycerol (DAG) linked to a *myo*-inositol group *via* a phosphodiester bond, are involved in signal transduction pathways that control a wide variety of cellular processes from the regulation of ion transporters and pumps, to vesicle transport and actin dynamics (Balla, 2013; Chakraborty et al., 2011). Upon initiation of a signal transduction pathway, the phosphorylation and dephosphorylation of secondary messengers by protein kinases and phosphatases respectively is critical for intracellular signalling and activation of a wide variety of target proteins. However, dietary phospholipids likely contribute negligibly to overall Pi status as most are incorporated into the plasma membrane of cells. In the gastrointestinal lumen, most glycerophospholipids are hydrolysed by pancreatic phospholipase A_2 ($pPLA_2$) to free fatty acids and lysophospholipids which are then absorbed into enterocytes (Kullenberg et al., 2012). These can be reesterefied and packaged into chylomicrons or to a lesser degree very low density lipoproteins (VLDL). Another ubiquitous cellular process that PO_4^{3-} is necessary for is energy transfer and metabolism. To meet the metabolic demands of cells, a steady supply of PO_4^{3-} is necessary for glycolysis and oxidative phosphorylation to generate ATP (Lardy & Ferguson, 1969), as well as energy storage in the phosphoester bonds of other phosphonucleotides and phosphocreatine, an important high-energy molecule in myocytes (Wallimann et al., 2011).

Due to its nature as a weak polyprotic acid, phosphoric acid acts as a buffer in extracellular fluids (Goretti Penido & Alon, 2012). In plasma, around 75 % of the total phosphorus occurs as organic phosphorus, bound to carbon containing molecules and the remaining 25% is inorganic phosphorus (Peacock, 2021). Twenty percent of plasma inorganic phosphorus is bound to protein, while the majority (~80%) of the inorganic phosphorus fraction in plasma is free or complexed to counter ions such as sodium, calcium and magnesium (Nordin, 1976). This free fraction is responsible for the buffering capacity of phosphoric acid in urine and plasma. Given the ubiquitous cellular processes and biomolecules that Pi is necessary for, serum Pi is maintained in a tight range between 0.75-1.45 mM (humans) or 1.3-2.3 mM (rodent) in adults (Miyagawa et al., 2018; Perazella et al., 2018) through the coordinated regulation of intestinal absorption, bone remodelling and renal reabsorption / excretion. Serum Pi varies with age, with higher values in infancy, allowing for proper bone formation and growth, then declining to the aforementioned adult values (MacDonald et al., 2021; Saurette & Alexander, 2019). The transport processes in these tissues are under constant endocrine regulation by a variety of hormones which maintain plasma Pi at equilibrium (section 1.3). When there is a negative Pi balance (*i.e.* greater Pi is excreted than absorbed / reabsorbed) the body enhances intestinal Pi absorption and leaches Ca^{2+} and Pi from bone. If chronic, this may lead to a weakening of bone and present a risk for fracture (Office of the Surgeon, 2004). Alternatively, when there is a positive Pi balance (*i.e.* more absorbed / reabsorbed than excreted) outside of bone development, such as in chronic kidney disease (CKD), the body decreases intestinal Pi absorption and renal reabsorption. Failure to decrease serum Pi may contribute to ectopic calcifications.

Disorders of Pi homeostasis highlight the consequences of abnormally low and high blood phosphate. Diseases causing chronic hypophosphatemia including tumor-induced osteomalacia

(TIO), X-linked hypophosphatemic rickets / osteomalacia (XLH) and autosomal dominant hypophosphatemic rickets / osteomalacia (ADHR) are characterized by reduced serum Pi, normal parathyroid hormone levels, low or normal calcitriol, typically display renal Pi wasting leading to hypophosphotemic rickets, a defect in bone mineralization due to insufficient Pi (Shaikh et al., 2008). Patients with these diseases present with rickets (decreased mineralization of growth plate), lower extremity deformities, bone pain, weakness and may have dental abnormalities highlighting the necessity of proper renal Pi reabsorption to form the growing skeleton (Chanchlani et al., 2020). Conversely, when serum Pi is chronically elevated such as in chronic kidney disease / end-stage renal disease (CKD / ESRD) or tumoral calcinosis, vascular calcification is a predictable sequela contributing to cardiovascular disorders and premature death (Boyce et al., 2020; Jono et al., 2000; Yamada et al., 2014).

1.2 Calcium homeostasis

Calcium (Ca^{2+}) is involved in a wide variety of physiologic functions including blood coagulation, muscle contraction, cellular signalling, neuronal transmission and bone formation in conjunction with phosphate. Under physiologic conditions, blood Ca^{2+} and PO_4^{3-} concentrations are considered near supersaturation, therefore, a significant increase in plasma Ca^{2+} can lead to its precipitation in soft tissues (Sandin et al., 2006), potentially leading to atherosclerosis, or hypercalciuria and the formation of kidney stones. Conversely, a significant decrease in blood Ca^{2+} can lead to muscle tetany, heart arrhythmias and if chronically depressed, may lead to osteopenia / osteoporosis. Therefore, serum Ca^{2+} is tightly regulated through the coordinated interplay between intestinal absorption / secretion, renal reabsorption / excretion and bone deposition or resorption.

The majority of Ca^{2+} (>99%) is found complexed with PO_4^{3-} as hydroxyapatite in bone. The remaining 1% is distributed in teeth and soft tissue with 0.1% being extracellular. In neutral calcium balance, the transport processes maintaining plasma Ca^{2+} in the intestine, kidney and bone are constantly being regulated by endocrine and receptor-mediated mechanisms. Given the significant overlap in the distribution of Ca^{2+} and Pi, as well as the potential to form Ca-Pi precipitations, it is unsurprising the regulation of these two ions are inextricably linked (Blau & Collins, 2015; Khundmiri et al., 2016).

1.3 Regulation of calcium and phosphate homeostasis

1.3.1 1,25-dihydroxyvitamin D_3 (1,25$[OH]_2D_3$)

Production and activation of $1,25(OH)_2D_3$ or calcitriol involves multiple organs including the skin, liver and kidneys. Its biosynthesis starts in the skin with the photochemical conversion of 7-dehydrocholesterol and ergosterol to inactive vitamin-D (cholecalciferol) through exposure to ultraviolet (UV) light (Holick et al., 1977). Cholecalciferol is absorbed into the circulation from the skin and lymph and transported to the liver where it undergoes one of the two hydroxylation steps required for its activation in hepatocytes. The first hydroxylation of cholecalciferol is carried out by vitamin D 25-hydroxylase (CYP2R1) converting it to 25-hydroxyvitamin D_3 (25$[OH]D_3$; calcifidiol) (Shinkyo et al., 2004). The final hydroxylation and activation of vitamin-D largely occurs when 25-hydroxyvitamin D_3 is transported to renal proximal tubule cells, where 1-α-hydroxylase (CYP27b1) catalyzes the production of the active form of vitamin D, 1,25-dihydroxyvitamin D_3 (1,25 $[OH]_2D_3$) (Kitanaka et al., 1998). Being a steroid hormone, vitamin D_3 exerts its effects on target tissues by diffusing through the cell membrane and binding the intracellular vitamin-D receptor (VDR). Upon vitamin D_3 binding,

VDR dimerizes with another nuclear receptor, the retinoid-X-receptor (RXR) and the ligand bound VDR-RXR heterodimer translocates to the nucleus to alter expression of genes with a VDR response element (VDRE) (Kliewer et al., 1992).

Hypocalcemia, hypophosphatemia and parathyroid hormone (PTH) all induce the expression of 1-α-hydroxylase (CYP27b1) thereby increasing the synthesis of active vitamin D_3. In turn, vitamin D_3 negatively regulates PTH transcription (Silver et al., 1985) and increases transcription of the calcium-sensing receptor (CaSR) in parathyroid tissue, sensitizing it to extracellular Ca^{2+} and decreasing PTH production / secretion (Canaff & Hendy, 2002). Upon secretion, active vitamin D_3 enters the circulation and targets the intestine, and bone to increase plasma levels of Ca^{2+} and Pi (Alexander, 2020). The primary function of vitamin D_3 is to enhance intestinal absorption of Ca^{2+} and Pi. In the intestine vitamin D_3 increases the expression of transient receptor potential cation channel subfamily V member 6 (TRPV6), calbindin-D9k and the plasma membrane Ca^{2+}-ATPase (PMCA1b) which mediate transcellular Ca^{2+} absorption in the duodenum and proximal colon (Christakos, 2012; Ko et al., 2009). Vitamin D_3 may also increase intestinal Ca^{2+} absorption *via* the paracellular pathway by increasing expression of claudin-2 and claudin-12 (Fujita et al., 2008) which likely form independent Ca^{2+} permeable pores. With respect to Pi, vitamin D_3 increases protein levels of the sodium-dependent phosphate cotransporter 2b (Npt2b; *SLC34a2*) (Hattenhauer et al., 1999; Segawa et al., 2004) via a post-transcriptional mechanism and the sodium-dependent phosphate transporter 2 (PiT-2; *SLC20a2*) (Katai et al., 1999) thereby enhancing transcellular intestinal Pi transport. Unlike with Ca^{2+}, vitamin D_3 likely does not alter intestinal Pi absorption through alterations to the paracellular pathway, at least in the small intestine (Hernando et al., 2020).

The effect of vitamin D_3 on bone is more varied and depends on the body's Ca^{2+} balance. When there is hypocalcemia or hypophosphatemia, vitamin D_3, binds VDR in osteoblasts increasing expression and release of RANKL, which in turn binds its receptor RANK on osteoclasts increasing osteoclastogenesis, promoting Ca^{2+} and Pi release into circulation and preventing bone mineralization (Lieben et al., 2012). Additionally, vitamin D increases the production of fibroblast growth factor 23 (FGF-23), an important counter regulatory hormone of Pi homeostasis (discussed in detail below). In osteoblasts, the promoter for FGF-23 has a vitamin D_3 response element (VDRE), allowing for its increased production in order to enhance Pi excretion upon its release from bone (Liu et al., 2006).

1.3.2 Parathyroid hormone (PTH)

Parathyroid hormone (PTH) is a calciophosphotropic peptide hormone produced in the parathyroid gland. PTH is synthesized as a 115 residue prepro-hormone, with a 25-amino acid signal sequence, a 6-amino acid pro-sequence and an 84-amino acid sequence ([1-84] PTH) which is stored in the vesicles of chief cells following cleavage of the signal and pro-sequence (Gensure et al., 2005). Secretion of PTH (1-84) is regulated by the activity of the calcium-sensing receptor (CaSR), a G-protein coupled receptor. The binding of extracellular Ca^{2+} activates the CaSR, while high extracellular Pi inhibits CaSR activity (Almaden et al., 1996) through non-competitive antagonism at the pathophysiological concentrations of Pi seen in chronic kidney disease (P. P. Centeno et al., 2019). Activation of the CaSR leads to $G_{q/11}$ associated phospholipase C (PLC) cleavage of phosphatidylinositol 4,5-bisphosphate (PIP2) to inositol trisphosphate (IP3) and DAG (Bergwitz & Juppner, 2010; Wettschureck et al., 2007). Upon cleavage, IP3 ultimately leads to increased intracellular Ca^{2+} and the activation of calcium-

sensitive proteases which degrade the PTH stored in vesicles (Habener et al., 1975). Given hypocalcemic or hyperphosphatemic conditions, CaSR activity decreases and leads to an increase in the production and release of PTH. Once in the circulation, PTH is transported to its primary target tissues, bone and kidney, where its actions ultimately increase serum Ca^{2+} and decrease serum Pi.

In bone, PTH induces bone resorption through the indirect activation of osteoclasts. PTH binds PTHR1 on osteoblasts, stimulating production of RANKL and degradation of osteoprotegrin (OPG), ultimately leading to the differentiation and activation of osteoclasts and increase bone resorption and Ca^{2+} release into the circulation (Ma et al., 2001). Additionally, PTH increases expression of FGF-23 in osteocytes and osteoblasts.

In the kidney, PTH increases serum Ca^{2+} by enhancing reabsorption from the tubular fluid, while decreasing reabsorption of Pi. The effects of PTH on the proximal tubule involve a reduced driving force for Ca^{2+} absorption *via* an attenuation of Na^{+} reabsorption (Agus et al., 1973). PTH binds PTHR1 on the apical and basolateral membranes of the proximal tubule cells activating PKA and PKC respectively. This reduces the activity and abundance of NHE3, while PKC also inhibits the sodium-potassium ATPase leading to reduced sodium reabsorption and paracellular solvent drag of Ca^{2+} (J. J. Lee et al., 2017). PTH binding PTHR1 in the thick ascending limb (TAL) leads to increased net flux of Ca^{2+}(Di Stefano et al., 1990). Additionally, in the DCT, PTH activation of PKA increases the open probability of TRPV5 (de Groot et al., 2009) and decreases its calveolae-mediated endocytosis (Cha et al., 2008) thereby increasing transcellular Ca^{2+} absorption. Together, the tubular effects of PTH on Ca^{2+} reabsorption in the TAL and DCT outweigh the reduced Ca^{2+} reabsorption in the proximal tubule and lead to a net increased Ca^{2+} reabsorption.

In terms of renal Pi transport, PTH inhibits proximal tubule renal Pi reabsorption by reducing the membrane abundance of Npt2a, (SLC34a1) and Npt2c (SLC34a3) (J. J. Lee et al., 2017; Matsumoto et al., 2010; Segawa et al., 2005). PTH-PTHR1 binding activates PKA leading to the phosphorylation of the sodium-hydrogen exchanger regulatory factor (NHERF1) which tethers Npt2a to the cytoskeleton and allows for its endocytosis and subsequent degradation (Gisler et al., 2001; Weinman et al., 2009). The exact mechanism for reduced Npt2c abundance is unclear, however, unlike Npt2a it does not undergo lysosomal degradation (Picard et al., 2010). Ultimately, increased PTH in response to hyperphosphatemia increases bone resorption contributing to a further increase in serum Pi, however, the phosphatruic effect allows for enhanced urinary Pi excretion and the normalization of serum Pi.

1.3.3 Phosphatonins

While the role of vitamin D_3 and PTH in Ca^{2+} and Pi homeostasis has long been appreciated, more recently a group of factors principally regulating Pi have has been discovered. These factors have been coined the "phosphatonins" and include: FGF-23, FGF-7, polypeptide *N*-acetylgalactosaminyltransferase 3 (GALNT3), phosphate- regulating neutral endopeptidase (PHEX), matrix extracellular phosphoglycoprotein (MEPE), dentin matrix acidic phosphoprotein 1 (DMP1) and secreted frizzled-related protein 4 (s-FRP4).

1.3.3.1 Fibroblast growth factor-23 (FGF23)

FGF-23 is the most extensively studied phosphatonin and is a phosphaturic hormone synthesized in osteocytes and osteoblasts. FGF-23 is translated as a 32 kDa protein and upon cleavage of the signal sequence and after *O*-glycosylation by GALNT3 is secreted into the

circulation as active full-length FGF-23 (Martin et al., 2012). Its effects on Pi homeostasis were discovered in an attempt to identify the cause of autosomal dominant hypophosphatemic rickets (ADHR) (Consortium, 2000). It was found that ADHR was caused by various missense mutations surrounding a furin-like cleavage site ($R_{176}XXR_{179}$) (Consortium, 2000), and that *O*-glycosylation of FGF-23 by GALNT3 extends the half-life of FGF-23 by reducing its proteolysis by subtilisin-like proprotein convertases (Kato et al., 2006). FGF-23 production and secretion from osteoblasts and osteocytes is regulated by classical hormonal (PTH, Vitamin D_3) and local factors in bone, including PHEX and DMP1. Once thought to be the protease responsible for inactivation of FGF-23, PHEX likely indirectly decreases the expression of FGF-23 *via* cleavage of the proprotein convertase PC2, which along with its coactivator 7B2, mediates FGF-23 cleavage (Yuan et al., 2013). Along with PHEX, DMP1 is also expressed in osteocytes and osteoblasts and regulates matrix mineralization (Lu et al., 2011).It has been shown to reduce FGF-23 production as inactivating mutations in the gene recapitulate autosomal recessive hypophosphatemic rickets and DMP1 null mice have increased serum FGF-23 (Feng et al., 2006). The molecular mechanism by which DMP1 modulates FGF-23 production is not clear, although it involves a common pathway with PHEX (Martin et al., 2011).

The production of FGF-23 is stimulated by high serum Pi, vitamin D_3 and PTH (Haussler et al., 2012; Lopez et al., 2011). Interestingly, the type III Pi transporter, PiT-2, was shown to be involved in Pi sensing in bone and responsible for regulating FGF-23 secretion in response to a Pi challenge (Bon et al., 2018). When released, FGF-23 acts on target tissues through the binding of FGF receptors (FGFR) and the membrane co-receptor alpha-klotho (Kurosu et al., 2006). In the kidney, FGF-23 binds FGFR1, 3, and 4 (Han et al., 2016). FGF-23 binding FGFR1/klotho leads to the endocytosis of Npt2a and Npt2c *via* increased ERK1/2 phosphorylation and

activation of SGK1 which phosphorylates the same PDZ domain of NHERF1 that PTH targets (Andrukhova et al., 2012; Weinman et al., 2011). In hyperphosphatemic conditions or during bone resorption when both Ca^{2+} and Pi are released, this leads to phosphaturia in order to normalize serum Pi. The exact site of action of FGF-23 in the kidney causing a reduction in membrane expression of Npt2a/c in the proximal tubule is unclear as alpha-klotho is predominantly expressed in the distal tubule; this may suggest distal to proximal paracrine signalling, but is still incompletely understood (Olauson et al., 2012). Additionally, FGF-23–FGFR1 binding in the distal tubule may increase transcellular Ca^{2+} reabsorption *via* increased transcription of TRPV5, CaBP28k, NCX and PMCA1b (Han et al., 2016). FGF-23 and vitamin D_3 are in a negative feedback loop, with vitamin D_3 increasing the production of FGF-23 which in turn negatively regulates the production of vitamin D_3 *via* decreased transcription of CYP27b1, which encodes 1-α-hydroxylase, and increased transcription of CYP24a1 encoding the 24-hydroxylase which inactivates vitamin D_3 (T. Shimada et al., 2004). This effect is mediated *via* FGF-23 binding to FGFR 3 and 4 (Perwad et al., 2007). Due to decreased production / increased inactivation of vitamin D_3, FGF-23 also indirectly decreases intestinal absorption of Ca^{2+} and Pi from the intestine (Miyamoto et al., 2005).

1.3.3.2 Matrix extracellular phosphoglycoprotein (MEPE)

MEPE is a member of the SIBLING (Small Integrin Binding Ligand N-Glycoprotein) family and is expressed exclusively in osteoblasts, osteocytes and odontoblasts (Rowe et al., 2004). MEPE promotes phosphaturia when ASARM (Acidic Serine Aspartate Rich Motifs) peptides are released upon its proteolysis by cathepsin B. PHEX inhibits this proteolysis *via* binding of the ASARM motif in MEPE and global PHEX KO mice (Hyp mouse model for X-

linked hypophosphatemic rickets) have elevated MEPE, FGF-23 and have hypophosphatemia (Yuan et al., 2008). In the general population, serum MEPE is associated with serum Pi levels and bone mineralization suggesting a role in normal physiology (Jain et al., 2004). MEPE exerts its physiologic effects locally in bone, but modulates Pi absorption in the intestine and reabsorption in the kidney. Increasing serum MEPE levels in mice decreases Npt2a expression in the proximal tubule and leads to hyperphosphatruia and hypophosphatemia in a dose-dependent manner (Dobbie et al., 2008). Additionally, using an *in-situ* intestinal loop model, MEPE was shown to decrease intestinal Pi absorption from the jejunum in rats independently of changes in other phosphaturic hormones like PTH, vitamin D_3 and FGF-23 (Marks et al., 2008). When MEPE is overexpressed in bone and kidney osteoclastogenesis was impaired which inhibited bone resorption and reduced the $CaxPO_4$ product thereby reducing renal calcifications (David et al., 2009).

1.3.3.3 Secreted frizzled related protein-4 (sFRP4)

Similar to MEPE, sFRP4 was found to be highly expressed in some tumors of patients with osteomalacia who have hypophosphatemia, hypocalcemia and impaired bone mineralization (De Beur et al., 2002). Further, resection of these tumors improved renal Pi reabsorption, normalizing serum Pi. Conversely, extracts of these tumors inhibited Pi uptake in opossum kidney (OK) cells suggesting a factor secreted from these tumors may be responsible (Wilkins et al., 1995). This factor was identified as secreted frizzled related protein-4, which acts as a decoy receptor for Wnt ligand thus antagonizing Wnt/ß-catenin signalling in the kidney (Berndt et al., 2003). Infusion of recombinant sFRP4 increases the fractional excretion of Pi in rats with a PTH-independent mechanism (levels of cAMP were unaltered). sFRP4 was proposed to play a role in

adaptation to high Pi challenge as its expression is elevated in the kidneys of rats fed a chronic high Pi diet, but not a low Pi diet (Sommer et al., 2007). However, a significant role of sFRP4 in long-term regulation of serum Pi has been disputed given results from sFRP4 overexpressing and genetic KO mice. Mice overexpressing sFRP4 had increased expression of Npt2a and 1-α-hydroxylase, but did not have altered urinary Pi excretion and maintained normophosphatemia (H. Y. Cho et al., 2010). Additionally, genetic ablation of *Srp4* does not alter urine or serum Pi (Christov et al., 2011). Further, sFRP4 was unable to compensate for the loss of the major phosphatonin FGF-23 or its essential co-receptor α-klotho. While the single FGF-23 and α-klotho KO mice have elevated plasma Pi and Ca^{2+} they do not have altered urine or serum biochemical parameters compared to sFRP4/FGF-23 and sFRP4/ α-klotho dKO mice (Christov et al., 2011). While loss of sFRP4 does not appear to play a significant role in long-term Pi regulation, its loss does affect bone mineralization, suggesting a more important role locally in bone.

1.3.4 Dietary Pi

Intestinal Pi absorption is increased by active vitamin D_3, however, there is also clear regulation by dietary Pi itself. Pi is able to regulate expression of the key intestinal transcellular Pi transporter, Npt2b, independently of vitamin D_3 (Segawa et al., 2004). While Npt2b protein expression is significantly reduced in VDR KO mice compared to WT mice, following administration of a low-Pi diet (0.5% Pi) protein expression increased and immunofluorescence indicated proper localization of the transporter in the brush boarder membrane of enterocytes. Functionally, this also corresponded to an increase in sodium-dependent Pi uptake in BBMVs isolated from the intestines of these mice to levels similar to mice fed a normal Pi diet.

Additionally, dietary Pi appears to regulate renal Pi reabsorption independently of PTH as thyroparathyroidecomized rats fed a low Pi diet were able to maintain plasma Pi (Stoll et al., 1979). This is thought to be mediated by increased transcription of Npt2a in mice fed a low Pi diet. The molecular mechanism by which Pi content regulates Npt2a transcription was delineated by Kido *et al* (1999). Using DNA footprint analysis which permits interrogation of DNA-protein interactions, they identified a phosphate responsive element (PRE) in the promoter of *SLC34a1* which was able to bind the transcription factor (TFE3). When dietary Pi was restricted there was greater renal mRNA expression of TFE3 and enhanced Npt2a expression suggesting a mechanism by which dietary Pi influences renal Pi reabsorption independently of hormones. Dietary Pi may also affect the post-translational stability of Npt2a mRNA. Cytosolic proteins are able to interact with the 5'-UTR of Npt2a mRNA, which serves as a cis-acting stability element, thereby enhancing its translation (Moz et al., 1999). When cytosolic proteins isolated from rats fed a low-Pi diet were used in an *in-vitro* degradation assay, there was enhanced binding to this cis-regulatory region leading to increased stability and enhanced translation of Npt2a (Moz et al., 2003). Therefore, through both translational and post-translational mechanisms, dietary Pi affects both renal Pi reabsorption and intestinal Pi absorption independently of hormonal alterations.

1.4 Phosphate (Pi) transport

1.4.1 Renal phosphate reabsorption

As urinary Pi excretion / reabsorption is the main mechanism maintaining serum Pi within its physiologic range (Blaine et al., 2015), the kidneys are a key organ in maintaining Pi homeostasis. The glomerulus freely filters Pi and in adults ~90% of the Pi is reabsorbed back into the bloodstream; the vast majority of filtered Pi (>90%) is reabsorbed from the proximal

tubule (J. J. Lee et al., 2017) with the distal tubule potentially playing a minor role (Jaeger et al., 1980). The two pathways that Pi could be reabsorbed by are the transcellular, mediated by transporters, or the paracellular, mediated by a group of tight-junction proteins called claudins. In the kidney, Pi reabsorption is exclusively transcellular (Kaufman & Hamburger, 1987) and driven by the secondary active transport of sodium. The transporters mediating apical entry into proximal tubule cells include the sodium-dependent cotransporters Npt2a (SLC34a1), Npt2c (SLC34a3) and PiT-2 (SLC20a2) (Biber et al., 2013) (Figure 1). Npt2a and Npt2c preferentially transport divalent Pi (HPO_4^{2-}) while Npt2a has a stoichiometry of 3 Na^+: 1 HPO_4^{2-} contrasting to the electroneutral transport of Npt2c which transports 2 Na^+: 1 HPO_4^{2-}(Forster et al., 1999). PiT-2 has higher affinity for monovalent Pi ($H_2PO_4^-$) and is electrogenic (Bottger et al., 2006). In renal brush boarder membrane vesicles (BBMV), PiT-2 mediated uptake varied from 3 to 40 % of the total Pi uptake between pH 7.5 and 6 respectively (Villa-Bellosta & Sorribas, 2010). As the pH of proximal tubular fluid is greater than 6.6 even in conditions of metabolic acidosis, the contribution of PiT-2 is likely negligible (DuBose et al., 1979).

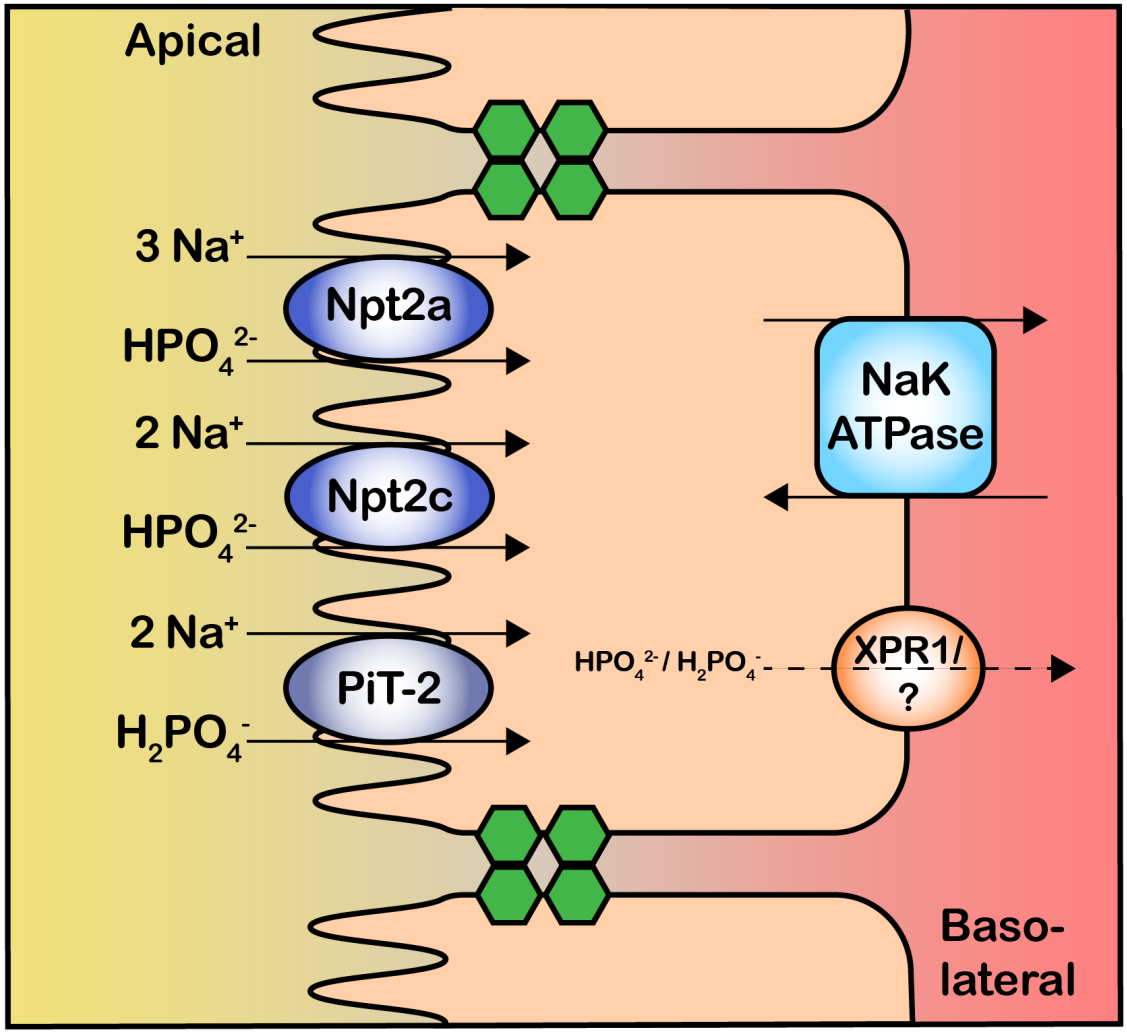

Figure 1.1. Proximal tubule phosphate (Pi) reabsorption. Reabsorption of Pi in the proximal tubule is transcellular and secondarily active utilizing the sodium gradient maintained by basolateral Na-K ATPase. The preference of Pi species and stoichiometric ratio of transport is depicted. Basolateral extrusion of Pi may be mediated by the xenotropic and polytropic retroviral receptor (XPR1).

There are key species differences in regards to the relative importance of the various transporters in renal Pi reabsorption. In mice, Npt2a likely plays a more dominant role in renal Pi reabsorption post-weaning relative to Npt2c (Segawa et al., 2009; Tenenhouse et al., 2003). In humans, Npt2a and Npt2c likely both play important roles as mutations in either of these transporters cause renal Pi wasting and hypophosphatemia (Bergwitz et al., 2006; Schlingmann et al., 2016). Unlike in mice, Npt2a may play a more important role during development in humans (MacDonald et al., 2021). Individuals with mutations in SLC34a3 have hereditary hypophosphatemic rickets with hypercalciuria (HHRH) which develops in childhood and appears to be lifelong (Lorenz-Depiereux et al., 2006). In contrast, patients with mutations in SLC34a1 have a range of Pi wasting phenotypes (Rajagopal et al., 2014; Schlingmann et al., 2016) and the improvement in their clinical presentation throughout the lifespan implies a relatively larger role for Npt2a during development.

The exact mechanism of basolateral Pi efflux is still uncertain. However, it may involve the xenotropic and polytropic retroviral receptor 1 (XPR1). XPR1 shares sequence homology to phosphate transporter 1 (PHO1) in *Arabadopsis thaliana* and mutations in the gene in humans causes primary familial brain calcification, suggesting a potential role in Pi export in mammals (Legati et al., 2015). Recently it was shown that XPR1 localizes to the proximal tubule and that tubule specific XPR1 KO mice develop hyperphosphaturia, hypophosphatemia and rickets (Ansermet et al., 2017).

1.4.2 Intestinal phosphate transport

Dietary Pi occurs as a mixture of "organic P" and inorganic Pi, in the form of sodium / potassium phosphate preservatives. Prior to intestinal absorption, Pi from organic sources must

be liberated *via* enzymatic cleavage by the enzymes trypsin and intestinal alkaline phosphatase (IAP), located on the brush boarder of enterocytes (Moog & Glazier, 1972). Once liberated from organic sources, the Pi is free and unbound and therefore identical to that supplied as inorganic Pi salts. As Pi is liberated from organic sources along the length of the gastrointestinal tract, this may lead to lower concentrations at the brush boarder membrane than the concentration of Pi that would be present due to the ingestion of a large bolus of Pi from inorganic sources. Given Pi from inorganic sources does not need to be digested to be absorbed, this can be expected to increase the concentrative driving force in earlier segments of the small intestine relative to a diet with Pi derived from an organic source with the same overall dietary P content. This difference might help explain why diets containing Pi from organic sources have a lower bioavailability (~40-60% bioavailable) compared to diets with high amounts of inorganic Pi (>90% bioavailable) (Cupisti & Kalantar-Zadeh, 2013). In rodents and humans, intestinal Pi transport occurs throughout the small intestine and in the colon (Knöpfel, 2017; Marks et al., 2015; Saurette & Alexander, 2019). Classically, intestinal Pi transport has been separated into a saturable sodium-dependent pathway and a sodium-independent pathway that does not appear to saturate (McHardy & Parsons, 1956; Sabbagh et al., 2011). The relative importance of the various pathways depends on dietary Pi content, intestinal segment (presence of transporters), sojourn time, species and form of dietary Pi, a subject of this thesis. Importantly, there are differences in both the contribution of each intestinal segment to net Pi absorption as well as species differences in the expression profiles of the various Pi transporters in rodents and humans (discussed below). In mice, the ileum is the site of maximal Pi absorption while in both rats and humans the jejunum and duodenum have highest absorption, reflecting the expression pattern of the major transcellular Pi transporter Npt2b (Marks et al., 2015; Radanovic et al., 2005).

1.4.2.1 Transcellular Pi transport

Transcellular intestinal Pi transport is mediated by the sodium-dependent transporters Npt2b (SLC34a2), PiT-1 (SLC20a1) and PiT-2 (SLC20a2) (Figure 2). The rate limiting step of transcellular transport is the apical entry into enterocytes. Like the other members of the type II sodium-phosphate cotransporter (SLC34) family, Npt2b preferentially transports divalent Pi (HPO_4^{2-}) in a stoichiometric ratio of 3 Na^+: 1 HPO_4^{2-}. Transport by Npt2b was originally characterized in *Xenopus laevis* oocytes as sodium-dependent with a K_m^{Pi} of 10-50 μM, i.e. it is a high- affinity Pi transporter (Hilfiker et al., 1998; Virkki et al., 2006). Conversely, the type III transporter (SLC20) family preferentially transports monovalent Pi ($H_2PO_4^-$) in a stoichiometric ratio of 2 Na^+: 1 $H_2PO_4^-$ making both PiT-1 and PiT-2 electrogenic. When PiT-1 and -2 were expressed in *X. laevis* oocytes, they both have a K_m^{Pi} between 25- 89 μM (L. Bai et al., 2000; Tatsumi et al., 1998).

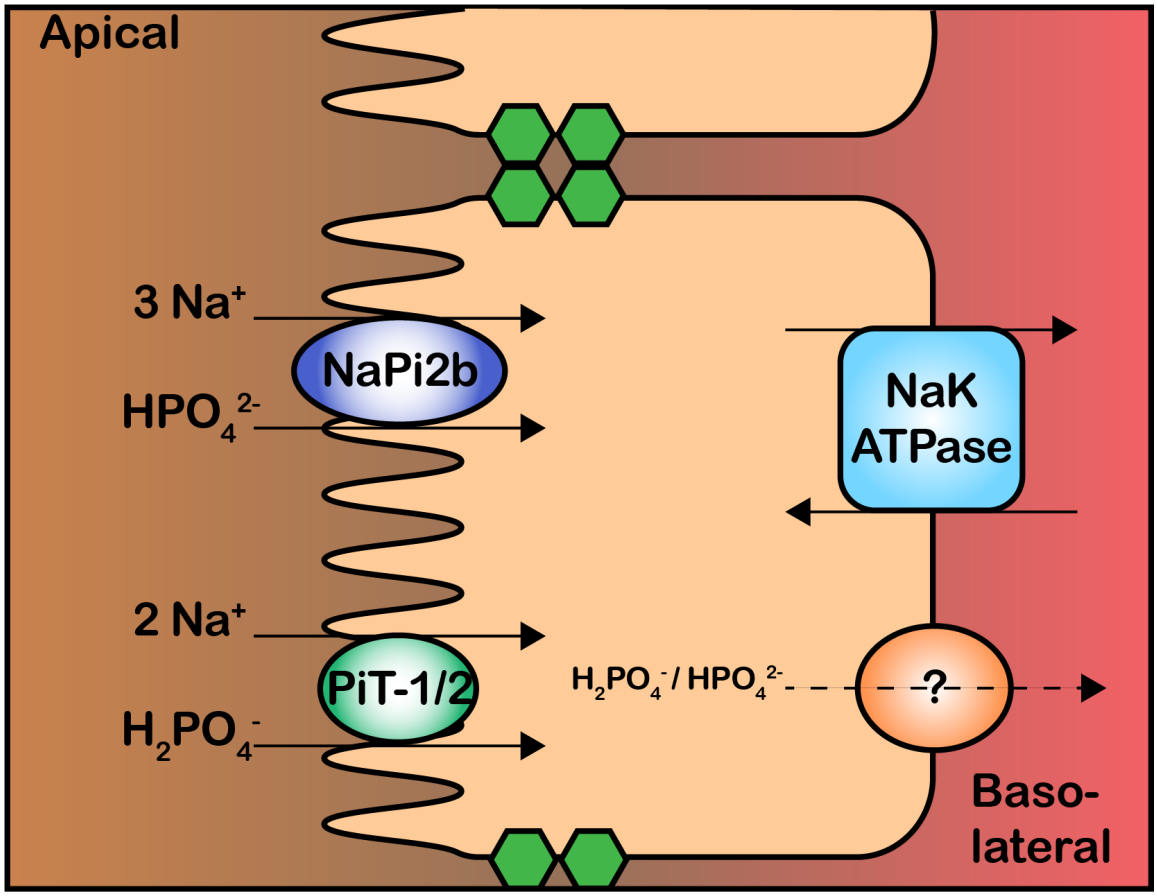

Figure 1.2 Transcellular intestinal phosphate (Pi) absorption. (Adapted from Saurette and Alexander, 2019). Transcellular, sodium-dependent, Pi absorption is secondarily active utilizing the sodium-concentration gradient maintained by the Na+-K+ ATPase. The apical transporter mediating the bulk of this is Npt2b, however, PiT-1 and -2 may play a minor role. The localization of each transporter is both species and intestinal segment specific. Currently, it is unknown which transporter mediates basolateral Pi efflux.

The expression of the transcellular Pi transporters is both species and segment specific. In mice, Npt2b mRNA and protein expression is greatest in the ileum, with less expression in the jejunum and none present in the duodenum (Marks et al., 2006). Conversely, in rats Npt2b expression is greatest in the duodenum and jejunum with no mRNA or protein detectable in the ileum (Marks et al., 2006). While mRNA transcript levels and *in-vivo* Pi absorption normalized to area is greater in the duodenum for rats, due to the relatively short sojourn for this segment, the maximum overall Pi absorption occurs in the jejunum (Bronner, 2003). Early studies investigating the regional differences in Pi absorption in humans indicate the proximal small intestine has a higher absorptive capacity, and thus in terms of segmental Pi absorption, humans have greater similarity to the rat model system (Borowitz & Ghishan, 1989; Walton & Gray, 1979). PiT-1 and -2 are widely expressed and originally thought to play a housekeeping role in cellular Pi homeostasis (Collins et al., 2004). However, apical expression of the two transporters has been demonstrated in enterocytes indicating their potential contribution to sodium-dependent Pi absorption and systemic Pi homeostasis. In mice, the jejunum and ileum express PiT-1 and -2 (Candeal et al., 2017; Marks et al., 2010) (Table 1.1). Conversely, PiT-1 and -2 are expressed in the duodenum and jejunum of rats, with PiT-2 being expressed in the ileum (Candeal et al., 2017; Giral et al., 2009; Marks et al., 2010) (Table 1.1).

Table 1.1 *Presence of sodium-dependent Pi transporters in small intestinal segments*

Species	Duodenum	Jejunum	Ileum
Mouse	PiT-1 PiT-2	Npt2b PiT-1 PiT-2	Npt2b PiT-1 PiT-2
Rat	Npt2b PiT-1 PiT-2	Npt2b PiT-1 PiT-2	PiT-2
Human	?	?	?

Despite the potential to transport Pi in the intestine, the overall contribution of the type II transporters PiT-1 and -2 to intestinal Pi absorption is likely negligible. Studies utilizing intestinal-specific Npt2b KO and tamoxifen- inducible global Npt2b KO mice demonstrate the loss of Npt2b increases fecal Pi content, consistent with decreased intestinal absorption, and that compensatory increased renal reabsorption allows for the maintenance of normophosphatemia. Sodium-dependent Pi uptake into intestinal BBMVs from these mice is abolished consistent with a negligible contribution of PiT-1 / -2 (Hernando et al., 2015; Sabbagh et al., 2009). This is further supported by evidence that the majority of sodium-dependent Pi uptake was sensitive to the Nptb inhibitor, phosphonoformate (PFA), which does not inhibit type III transporters (PiTs) (Candeal et al., 2017). While these studies demonstrate the importance of Npt2b *ex-vivo*, further evidence from mice using an intestinal loop model demonstrate that it mediates ~90% of the transcellular transport *in-vivo* (King et al., 2018). In brief, Pi transport into blood from the ileum (where transport is almost exclusively transcellular) of Npt2b KO mice was virtually abolished, demonstrating the predominant role of Np2b in transcellular Pi uptake.

Transcellular Pi transport, mediated by Npt2b, likely predominates in conditions of low luminal Pi such as in a low-Pi diet challenge or periods of fasting consistent with the low K_m^{Pi} (high affinity) of Npt2b. Intestinal- specific Npt2b KO mice maintain normophosphatemia on a normal and high Pi diet through compensatory decreases in urinary Pi excretion (Knopfel et al., 2017). However, when challenged with a low Pi diet, the mice are unable to compensate through enhanced intestinal absorption and instead resorb bone, as evidenced by an increase in the number of osteoclasts in the primary spongiosa and decreased cortical and trabecular bone mineral density (BMD).

Alternatively, given normal dietary Pi conditions and especially in humans consuming a typical "Western" diet (*i.e.* with larger amounts of inorganic Pi preservatives), the transcellular pathway likely plays a smaller role in overall intestinal Pi absorption (*Saurette* & Alexander, 2019). While global Npt2b KO mice are embryonically lethal (Shibasaki et al., 2009), global tamoxifen-inducible Npt2b KO mice and intestinal-specific Npt2b KO mice maintain normophosphatemia on regular chow diets suggesting that loss of the prominent transcellular absorptive route can be compensated for by alternative mechanisms in rodent models (Hernando et al., 2015; Ikuta et al., 2018; Sabbagh et al., 2009). In humans, homozygous inactivating mutations in SLC34a2 are associated with pulmonary alveolar microlithiasis (PAM) (Huqun et al., 2007). Np2b is expressed in type II pneumocytes, which produce surfactant. The lipid component of surfactant includes phosphatidylcholine, phosphoglycerol and cholesterol and during the metabolism of phospholipids, liberated Pi is recycled *via* Npt2b. Therefore, loss of the transporter leads to the formation of Ca^{2+}-Pi precipitates (microliths) in the alveolar space (Traebert et al., 1999). Despite the formation of microliths, the deletion of Npt2b in humans does not lead to altered serum Pi, indicating Pi homeostasis is maintained (Tachibana et al., 2009).

Finally, the success of specific Npt2b inhibitors at reducing hyperphosphatemia in rodent models of CKD (Sabbagh et al., 2009; Schiavi et al., 2012; Taniguchi et al., 2015) suggested it may be a good therapeutic target to reduce plasma Pi in persons with CKD and ESRD. Unfortunately, this failed to translate to humans. When the specific Npt2b inhibitor, ASP3325, was administered to healthy human volunteers (phase 1 trial) or patients with hyperphosphatemia and ESRD who were receiving hemodialysis (phase 2 trial), it failed to alter urine or fecal Pi excretion (Larsson et al., 2018). In the hemodialysis patients, ASP3325 also failed to reduce

serum Pi, PTH and FGF-23 providing further evidence that Npt2b mediated transcellular Pi absorption is less physiologically relevant in humans.

1.4.2.2 Paracellular Pi transport

Compared with transcellular Pi absorption, relatively little is known about paracellular Pi transport and its molecular mediators, though classic studies in humans demonstrate linear, increasing Pi absorption that is non-saturating with increasing intraluminal Pi concentration (Davis et al., 1983; Walton & Gray, 1979), characteristic of paracellular transport. Diffusion of ions and small molecules through the paracellular pathway depends on the concentration gradient across the epithelium, the electrical gradient (potential difference) and the permselectivity of the tight junctions. The luminal concentration of Pi depends on the dietary Pi load and form. In rodents, the luminal Pi concentration has been measured between 4-30 mM depending on the intestinal segment and diet composition (Knopfel et al., 2019; Marks et al., 2015) (Figure 1.3).

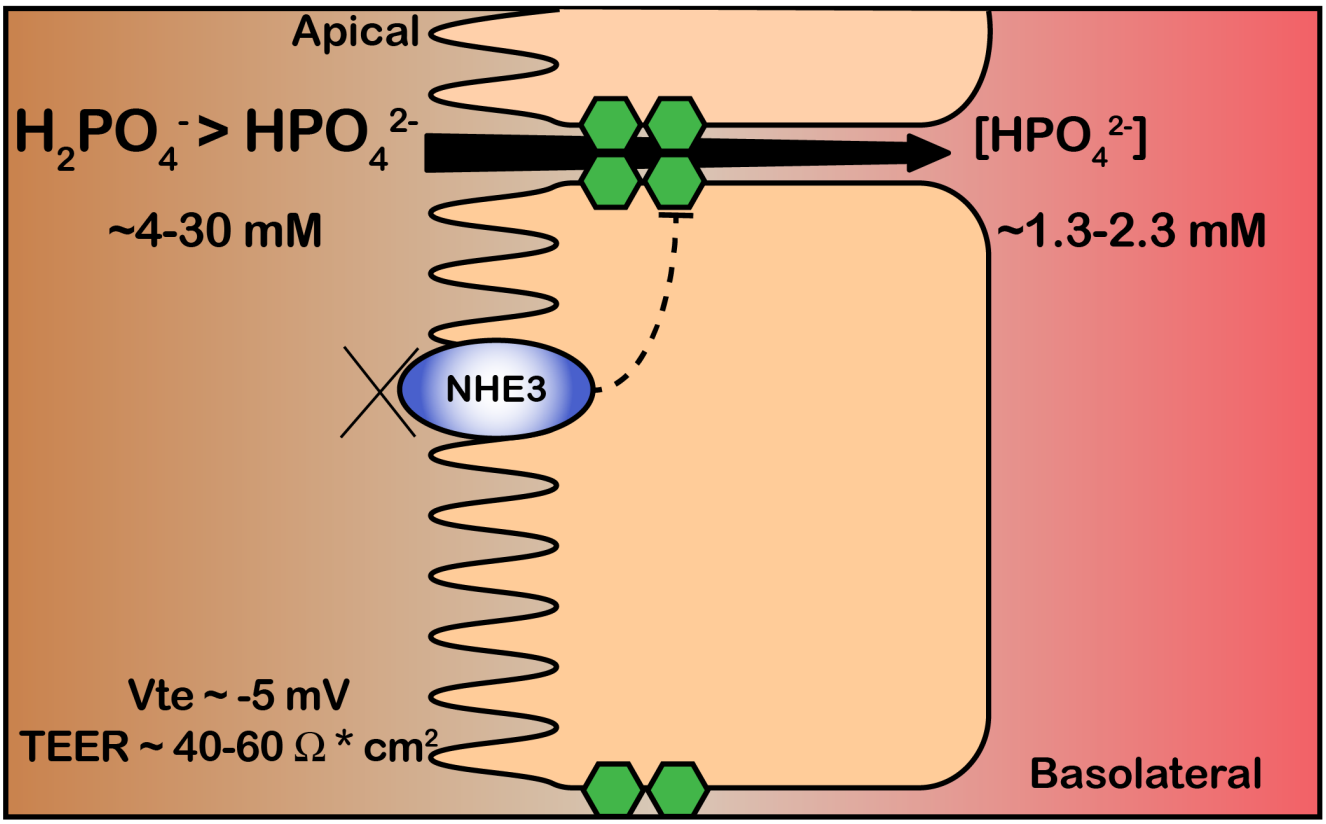

Figure 1.3. Paracellular intestinal phosphate (Pi) absorption in rodents. (Adapted from Saurette and Alexander 2019). Paracellular Pi absorption is favored by the chemical and electrical gradients. The tight junction is more permeable to monovalent Pi, however, the identity of the tight junction protein(s) mediating this process is unknown. Inhibition of the sodium-hydrogen exchanger (NHE3) leads to an increased transepithelial electrical resistance (TEER) and a reduction in the absolute permeability to phosphate (King et al., 2018).

In humans, the luminal Pi concentration has been measured in aspirated jejunal fluid between 0.5-17.5 mM (Davis et al., 1983). Conversely, the serum Pi in adult rodents ranges between 1.3-2.3 mM (Miyagawa et al., 2018) and 0.75-1.45 mM in adult humans (Perazella et al., 2018) and given the fenestrations in the capillaries, Pi is likely able to freely diffuse into blood from the interstitial space . Clearly, the concentration gradient between lumen and blood favors Pi absorption. As Pi from organic sources must be cleaved from a protein first to be absorbed while Pi from inorganic sources is free, the source of Pi may alter the concentrative driving force along the length of the intestine. Free Pi liberated from organic sources is expected to be at a lower concentration in the small intestinal than when supplied as a salt (same total P content), which contributes a larger initial Pi "bolus" and thus concentration gradient. Additionally, the potential difference across the intestinal epithelium contributes to the driving force for paracellular transport. In rodents and humans, the transmural electrical potential difference is around 5 mV (lumen negative) (Geall & Summerskill, 1969), however, there have been reports of a transmural potential difference as large as 12 mV in the jejunum and ileum in humans (Gustke et al., 1981). Given Pi is an anion, the electrical gradient favors Pi absorption. Within the intestinal lumen, Pi exists as $H_2PO_4^-$ or HPO_4^{2-} depending on the pH of the intestinal segment (N.B the pH ranges from ~6 in the duodenum to 7.4 in the terminal ileum in humans (Fallingborg, 1999)). Along with the potential difference, the valence of Pi affects its electrical driving force. Therefore, HPO_4^{2-} experiences a greater electrical driving force than $H_2PO_4^-$. The tight junctions in rodents discriminate between Pi species with the intestinal epithelium, however, there is conflicting evidence with respect to its permeability characteristics. Diffusion potential experiments completed in the Alexander lab found the intestinal epithelium has a greater permeability for $H_2PO_4^{2-} > HPO_4^-$ (King et al., 2018). However, Knopfel *et al* found a

greater permeability for $H_2PO_4^-$ > HPO_4^{2-} (2019). If this alternative prevails, it may highlight a synergism between the transcellular and paracellular pathway, as $H_2PO_4^-$ would be preferentially transported by the paracellular pathway (especially in the proximal small intestine with more acidic pH) while HPO_4^{2-}, the preferred Pi species for Npt2b, is preferentially transported *via* the transcellular pathway.

Additionally, all segments of the small intestine and colon are permeable to Pi indicating the capacity for paracellular transport throughout. Claudins, a family of tight-junction proteins, are transmembrane adhesion proteins which form homo- and heterotypic interactions with claudins on adjacent cells and are able to regulate the permselectivity of epithelia (Anderson & Van Itallie, 2009). There are at least 24 claudins in mammals and the first extracellular loop determines the charge selectivity and resistance of the pores that they form (Colegio et al., 2003). Some tight junctions contribute to epithelia with high TEERs ("tight" epithelia), while other epithelia are considered "leaky", including the gastrointestinal track. The ion selectivity of claudins is particularly relevant in "leaky" epithelia where larger quantities of ions are able to flow. Depending on the charge of amino acid residues in the first extracellular loop, claudins can be categorized as structural (no particular charge selectivity), anion selective or cation selective. For example, claudins-2 and -12 are cation selective and can act as paracellular Ca^{2+} channels in the small intestine (Fujita et al., 2008). The expression of the various claudins differs between species and epithelia, therefore, the unique combinations of claudins in the tight junction influences the resistance and permeability characteristics of an epithelium (Gunzel & Yu, 2013). To date, no claudin has been associated with governing paracellular Pi transport and unfortunately, the molecular identity of the Pi pore is unknown.

The sodium-hydrogen exchanger isoform 3 (NHE3) is an ion-counter transporter located in the kidneys, small intestine and colon (Biemesderfer et al., 1997; Bookstein et al., 1994; Hoogerwerf et al., 1996) which plays a role in regulating paracellular Pi transport (Figure 3.1). It mediates the electroneutral exchange of an extracellular sodium for an intracellular proton. Although NHE 1-3 and 7 are expressed in the intestine, NHE3 is the predominant isoform contributing to intestinal Na^+ absorption (Gawenis et al., 2002; Zachos et al., 2005). *Ex-vivo* experiments using human ileal NHE3 KO monolayers demonstrate a reduced Pi flux, which suggests NHE3 may play a role in Pi absorption (King et al., 2018). Given the role of NHE3 in sodium absorption, minimally absorbable NHE3-specific inhibitors were developed as antihypertensives. In addition to their effects on sodium and water balance, these inhibitors including SAR218034 and tenapanor hydrochloride, also increase fecal Pi and decrease urinary Pi in humans, healthy rats ((King et al., 2018; Linz et al., 2012; Spencer et al., 2014) and $5/6^{th}$ nephrectomy (NPX) rats (Labonte et al., 2015), a model for CKD. Transcellular transport is not affected by tenapanor in cell culture and it fails to reduce Pi flux in both human ileal NHE3 KO monolayers and mouse ileum (N.B. mouse ileal Pi transport is mediated almost exclusively by Npt2b) suggesting direct inhibition of NHE3 is responsible for reduced Pi flux and not non-specific inhibition of transcellular Pi transporters (King et al., 2018; Labonte et al., 2015). Conversely, King *et al* demonstrated the mechanism whereby tenapanor reduced intestinal Pi absorption is *via* decreased paracellular Pi absorption (2018). However, the molecular mechanism linking NHE3 inhibition and reduced paracellular Pi permeability is still incompletely understood. When human ileum monolayers are mounted in Ussing chambers and either treated with tenapanor or the apical media is acidified, there is a rapid increase in TEER due to a reduced cytosolic pH (pHi). The rapid time scale that this occurred on led to the

hypothesis that the reduced pHi leads to a conformational change in a tight junction protein. Several studies lend support to the rational for this hypothesis. The first utilized a trans-tight junction patch clamp technique allowing the measurement of conductance across a single claudin channel (Weber et al., 2015). Using this model, Weber *et al* discovered that the claudin-2 channel is dynamically gated alternating between an open and closed conformation. Finally, an *in-silico* study by the same group found that local gating kinetics of singular claudin-2 channels describe the global barrier function of an epithelium (Weber & Turner, 2017). This lends support to the idea that altering intracellular pH may modulate the barrier function of the gastrointestinal tract and inhibit paracellular Pi absorption.

1.5 Calcium (Ca^{2+}) transport

1.5.1 Renal Ca^{2+} transport

The kidney reabsorbs the vast majority (98-99%) of filtered Ca^{2+} ions, a process that is tightly coupled to sodium reabsorption. The bulk of Ca^{2+} (~70%) is reabsorbed *via* a passive paracellular process in the proximal tubule (PT) of the nephron, with about 25% of Ca^{2+} reabsorption occurring paracellularly in the thick ascending limb (TAL) and the remaining 5% occurring by active transcellular processes in the distal convoluted tubule (DCT) and collecting duct (CNT).

1.5.1.1 Paracellular Ca^{2+} transport

As with renal Pi reabsorption, the majority of Ca^{2+}(~70%) is reabsorbed in the proximal tubule (Seldin, 1999; Suki, 1979). While Pi transport in this segment is transcellular, Ca^{2+} reabsorption is predominantly paracellular in this segment. Active transcellular Ca^{2+} reabsorption

may occur in the PT, but is less than 10% of reabsorption from this segment (Ullrich et al., 1976). Conversely, microperfusion of the proximal convoluted tubule (PCT) in mammals in the absence of a transepithelial potential difference demonstrates that Ca^{2+} transport occurs in a paracellular fashion (Ng et al., 1984). Micropuncture experiments demonstrate parallel absorption of Na^{+} and Ca^{2+} and pharmacological treatment with PTH, acetazolamide, furosemide and hydrochlorothiazide is unable to decouple absorption of the two ions (Agus et al., 1973; Beck & Goldberg, 1973; Edwards et al., 1973; Suki, 1979). Na^{+} reabsorption in the proximal tubule occurs both paracellularly and transcellularly. In the PCT, the potential difference is initially lumen negative due to the action of SGLT2 (Barratt et al., 1974). Despite this, Na^{+} moves against its electrochemical gradient paracellularly through the cation and water permeable tight junction proteins claudin-2, driven by a process called solvent drag (Muto et al., 2010). Solvent drag in the PCT depends on the active transport of Na^{+}, largely *via* NHE3, and this is the principle route of Na^{+} absorption in the proximal tubule (Curthoys & Moe, 2014; Pan et al., 2012; Schultheis et al., 1998). The active reabsorption of Na^{+} generates an osmotic gradient for water reabsorption which diffuses transcellularly through aquaporin-1 (AQP-1) and paracellularly through the cation and water permeable claudin-2 (Amasheh et al., 2002; Schnermann et al., 2013). Solvent drag occurs when water diffusing through tight junctions "drags" other ions with it (Figure 4, top tight junction).

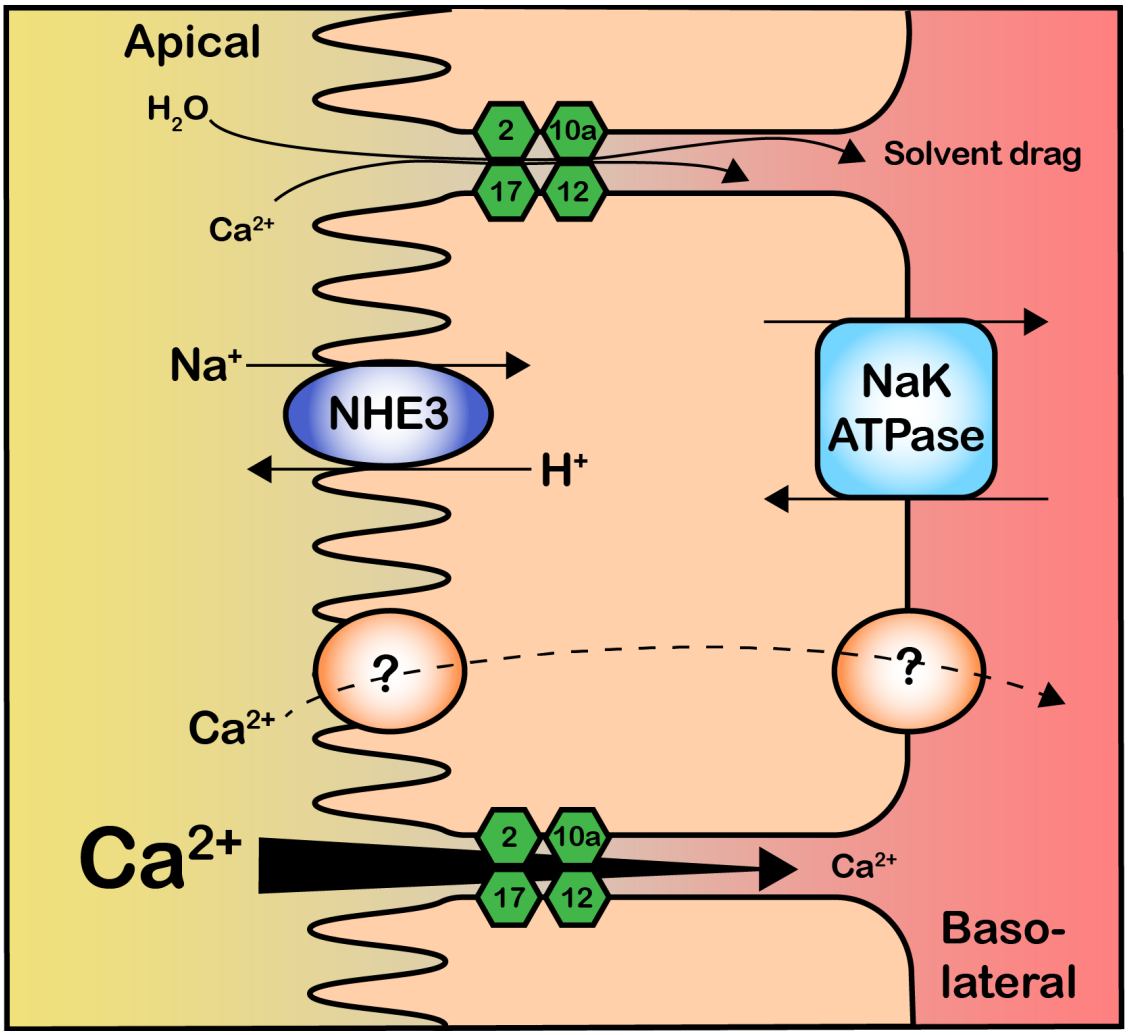

Figure 1.4. Proximal tubule (PT) Ca^{2+} reabsorption. (Adapted from Lee et al. 2017). Ca^{2+} reabosorption in the proximal tubule is mainly via the paracellular pathway (90%). This process is mediated by claudins-2 and -12 and is dependent on the active reabsorption of Na^{+} by the sodium-hydrogen exchanger isoform 3 (NHE3) and the basolateral Na^{+}-K^{+} ATPase. Osmotic reabsorption of water through the tight junction brings along Ca^{2+} and Na^{+} in a process called solvent drag (top junction). Reabsorption of Na^{+} and water in the early PT concentrates tubular Ca^{2+} driving paracellular flux in the late PT. The transcellular Ca^{2+} absorption pathway in the proximal stright tubule is a dashed line and represents <10% of absorption in this segment.

In the PCT, NHE3 mediated solvent drag is also responsible for paracellular Ca^{2+} reabsorption (Pan et al., 2012). Reabsorption of chloride and bicarbonate in the early proximal tubule generates a lumen positive potential difference by S2 / S3 favoring reabsorption of cations (Barratt et al., 1974). The reabsorption of Na^+ and water in the early proximal tubule generates a tubular fluid to ultrafiltrate calcium ratio (TF/UF_{Ca}) greater than 1 by the late proximal tubule suggesting a concentration gradient for paracellular Ca^{2+} reabsorption (Figure 1.4, bottom junction) (Suki, 1979; Sutton & Dirks, 1975). Therefore, by the late proximal tubule both the electrical and chemical gradients favor passive paracellular Ca^{2+} reabsorption. As with the gastrointestinal epithelium, the proximal tubule is also considered "leaky" (Yu, 2015) and has the lowest TEER in the body, of 5-7 $\Omega \bullet cm^2$. This allows a greater flux of ions to move paracellularly and the expression of various claudins determines its permselectivity. Claudin-10a and -17 are expressed in the PT, however, these are anion selective likely contributing to paracellular Cl^- reabsorption (Gunzel et al., 2009; Krug et al., 2012). Conversly, claudin-2 and -12 are expressed in the proximal tubule, forming independent cation permeable pores (Alexander Laboratory, unpublished data) and contribute to paracellular Ca^{2+} flux (Amasheh et al., 2002; Enck et al., 2001; Plain et al., 2020). Claudin-2 KO mice have have a proximal tubule Ca^{2+} reabsorption defect (renal leak) and consequently develop hypercalciuria and nephrocalcinosis (Curry et al., 2020). In contrast to claudin-2 KO mice, claudin-12 KO mice do not display hypercalciuria despite evidence that claudin-12 confers calcium permeability in the proximal tubule (Plain et al., 2020). Normocalciuria was maintained in these mice through compensatory increased Ca^{2+} reabsorption in the TAL.

In the TAL, around 20-25% of filtered Ca^{2+} is reabsorbed (Suki, 1979). Ca^{2+} absorption occurs paracellularly and relies on a large positive transepithelial potential difference generated

through the concerted action of the sodium-potassium-chloride cotransporter (NKCC2) and the renal outer medullary potassium channel (ROMK). In brief, Na^+, K^+ and two Cl^- are reabsorbed across the apical membrane *via* NKCC2. Upon entry into TAL cells, Na^+ and Cl^- are reabsorbed back into the peritubular capillary by the Na^+-K^+ ATPase and CLC-Kb channels respectively. The continuation of transport by NKCC2 relies on ROMK as K^+ is limiting and, therefore, the K^+ ion transported apically by NKCC2 is recycled back into the tubular lumen. A net absorption of anions generates a positive 5-10 mV potential difference in the lumen of the medullary TAL (Greger & Schlatter, 1983) which further increases to +30 mV in the cortex (Mandon et al., 1993) given considerable paracellular Na^+ backflux when the chemical gradient reverses . This suggests a greater electrical driving force for paracellular Ca^{2+} transport in the cortical TAL (Suki et al., 1980).

Although there are other claudins expressed in the TAL, only the effects of claudins-16, -19, -10 and -14 on the permselectivity of the TAL have been characterized. The properties of claudins-16 and -19 were determined mainly *in-vitro* leading to a variability in results depending on the endogenous expression of other claudins in each cell line (Hou et al., 2008) However, claudin-16 knock-down mice recapitulate features of patients suffering from familial hypomagnesemia with hypercalciuria and nephrocalcinosis (FHHNC), who have enhanced fractional excretion of Mg^{2+} and Ca^{2+} and develop nephrocalcinosis (Hou et al., 2007). Additionally, FHHNC disease causing mutations in claudin-16 and -19 cause a reduction in cation selectivity or reduce the ability to block anion flux respectively. When co-expressed, claudin-16 and -19 form a cation permeable pore, allowing for permeation of Ca^{2+} and Mg^{2+} (Hou et al., 2008). Deletion of claudin-10 from the TAL leads to hypermagnesmia, no change in Ca^{2+} balance and isolated perfused TAL lacking claudin-10 have reduced permeability to sodium

and increased relative permeability of Ca^{2+} over Na^{+} (Breiderhoff et al., 2012). Together, this suggests the TAL is permeable to Ca^{2+}. Conversly, claudin-14 is a negative regulator of claudin-16 (Gong et al., 2012) and during states of hypercalcemia, extracellular Ca^{2+} activation of CaSR in the TAL leads to increased expression of claudin-14 in the tight junction which acts as a non-selective cation barrier (Dimke et al., 2013; Frische et al., 2021; Gong et al., 2012). In addition to blocking absorption of Ca^{2+}, claudin-14 expression would also reduce Na^{+} backflux and the magnitude of the transepithelial potential difference driving Ca^{2+} absorption. Recently, it was shown that potassium channel tetramerization domain containing 1(KCTD1) regulates paracellular Ca^{2+} reabsorption in the TAL (Marneros, 2021). Previously this protein was shown to be important in the differentiation of TALs and DCTs, however, its deficiency also reduces paracellular Ca^{2+} reabsorption. This is thought to be due to reduced NKCC2, claudin-16, claudin-19 and increased claudin-14.

1.5.1.2 Transcellular Ca^{2+} transport

While the majority of Ca^{2+} transport in the proximal tubule is paracellular, there is evidence of a small portion of this occurring transcellularly in the PST (S2 and S3 regions) (Almeida et al., 1981). It is unclear which transporter mediates this. There is evidence of a nifedipine sensitive channel (L-type) in rabbits (J. J. Lee et al., 2017; Zhang & O'Neil, 1996) and the cation-permeable transient receptor potential channel 1 (TRPC1) may play a role in transcellular Ca^{2+} reabsorption in the proximal tubule of rats (Goel et al., 2006). The molecular details of transcellular Ca^{2+} reabsorption in the proximal tubule are thus unclear.

The DCT and CNT are sites of regulated active Ca^{2+} reabsorption which fine tunes the amount of Ca^{2+} in the urine. The DCT is subdivided into the DCT1 and DCT2, with the later

expressing the epithelial Na^+ channel (ENaC) (Campean et al., 2001). While the DCT1 does not express any Ca^{2+} channel machinery, the DCT2, CNT and initial parts of the collecting duct express Ca^{2+} transport proteins (Loffing & Kaissling, 2003; Loffing et al., 2001). Apical entry of Ca^{2+} is mediated by the transient receptor potential vanilloid 5 channel (TRPV5) and its expression is under the control of vitamin D_3 (Hofmeister et al., 2009). When Ca^{2+} enters the cell, it is buffered and shuttled to the basolateral membrane by calbindin-D28k (Koster et al., 1995). Basolateral extrusion of Ca^{2+} into the interstitium is carried out by the plasma membrane Ca^{2+}-ATPase 1 and 4 (PMCA1 and 4) (Alexander et al., 2015) and the Na^+ / Ca^{2+} exchanger type 1 (NCX1) (Reilly et al., 1993). Although classic micropuncture experiments estimate that between 3-7% of filtered Ca^{2+} is reabsorbed distally, TRPV5 KO mice have massive renal Ca^{2+} loss causing osteopenia and compensatory increases in Ca^{2+} transport machinery in the intestine (Hoenderop et al., 2003).

1.5.2 Intestinal Ca^{2+} transport

Ca^{2+} transport occurs throughout the small intestine (Beggs & Alexander, 2017; Bronner et al., 1986) and has been reported to be increased in the proximal small intestine and colon under conditions of low dietary Ca^{2+} intake. The contribution of each small intestinal segment to Ca^{2+} absorption varies in terms of rate of absorption: the duodenum has the greatest rate of absorption (Birge et al., 1969) while this varies in the jejunum and ileum depending on dietary Ca^{2+} intake (Bronner & Pansu, 1999). A number of other factors influence segmental differences in net Ca^{2+} absorption including solubility, intraluminal Ca^{2+} concentration, transepithelial potential difference, sojourn time and the permeability of each segment to Ca^{2+}(Bronner & Pansu, 1999). Cumulatively, it appears that due to a longer sojourn time in the ileum, this segment contributes

the most to net Ca^{2+} absorption (Duflos et al., 1995). Ca^{2+} absorption in the intestine occurs both *via* the paracellular pathway, through tight junctions mediated by claudins, and transcellularly, *via* transporter-mediated processes.

1.5.2.1 Transcellular Ca^{2+} transport

The duodenum, cecum and proximal colon are the major sites of transcellular Ca^{2+} absorption as evidenced by voltage-independent Ca^{2+} transport from the intestinal lumen to blood (Hoenderop et al., 2005; Karbach, 1989; Rievaj et al., 2013a). The current model for Ca^{2+} reabsorption in these segments is analogous to active Ca^{2+} transport in the DCT/CNT of the kidney, involving apical entry into enterocytes, intracellular buffering and ferrying of Ca^{2+} to basolateral extrusion into serosal blood (Figure 5). Apical transport of Ca^{2+} into enterocytes is mediated in part by the transient receptor potential vanilloid 6 (TRPV6) channel (Figure 1.5).

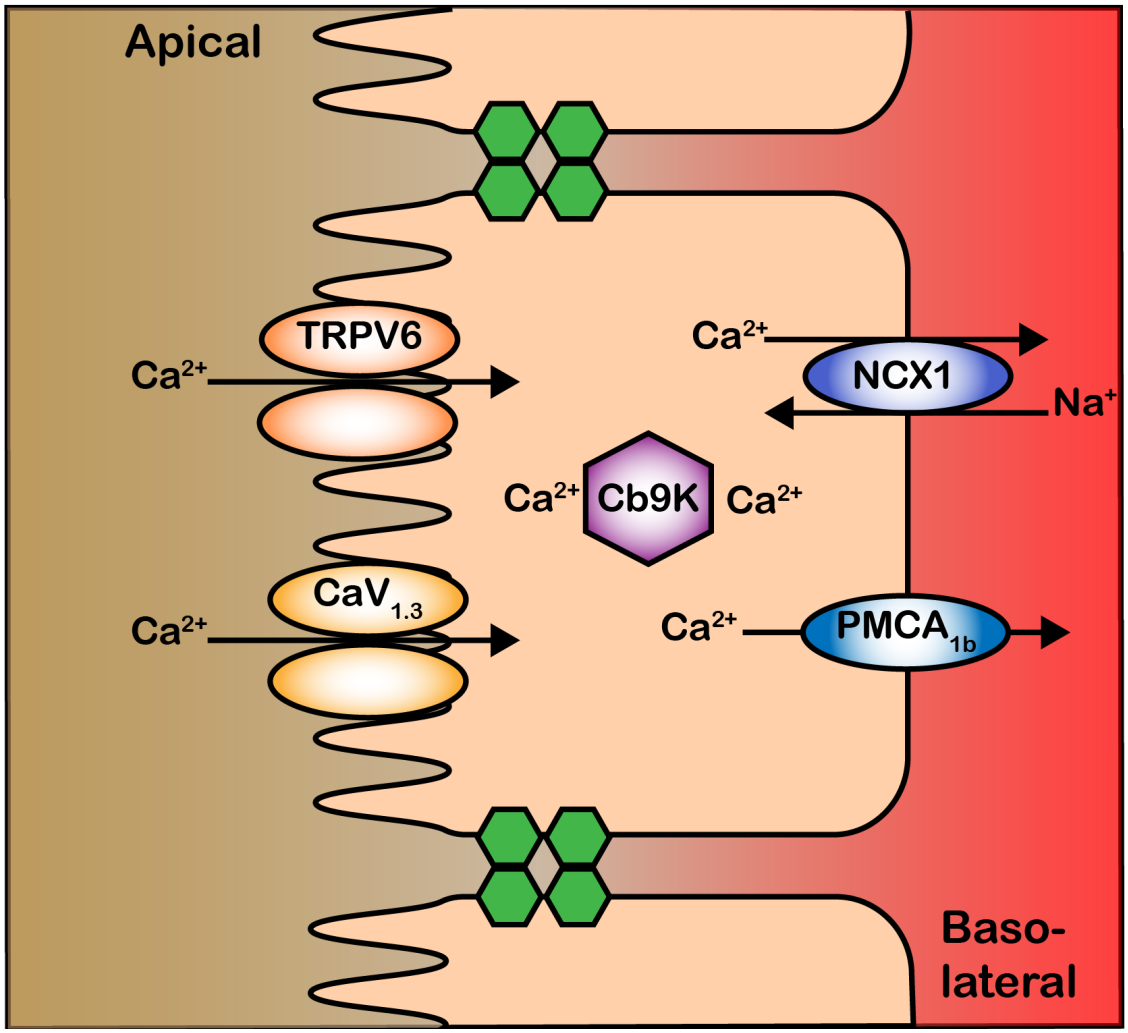

Figure 1.5. Intestinal transcellular Ca^{2+} transport. Active transcellular Ca^{2+} transport in the intestine occurs in the duodenum, cecum and colon in mice. Apical Ca^{2+} entry into the cell is mediated by the transient receptor potential vanilloid 6 (TRPV6) Ca^{2+} channel in the duodenum, jejunum and colon; the L-type Ca^{2+} channel $CaV_{1.3}$ mediates apical Ca^{2+} entry in the jejunum and ileum in mice. Upon entry, Ca^{2+} is buffered and shuttled to the basolateral membrane by calbindin-D9k (Cb9K). Ca^{2+} extrusion into serosal blood is mediated by the Na^{+}-Ca^{2+} exchanger 1 (NCX1) and the plasma membrane Ca^{2+}-ATPase (PMCA1b).

The expression of Trpv6 is species dependent. In humans, it is solely expressed in the duodenum while in mice expression of *Trpv6* is detected in the duodenum, jejunum and colon (Lameris et al., 2015). Supporting a role for TRPV6 in Ca^{2+} homeostasis, TRV6 KO mice have reduced Ca^{2+} transport in the duodenum when measured with the everted sac technique (Benn et al., 2008), develop hypocalcemia and have reduced femoral bone mineral density to compensate for reduced intestinal Ca^{2+} absorption (Bianco et al., 2007). While some evidence suggests TRPV6 appears to play a substantial role in transcellular Ca^{2+} absorption, the fact that there is residual Ca^{2+} transport in duodenal everted sacs of TRPV6 KO mice fed a low Ca^{2+} diet suggests there is an alternative pathway for active Ca^{2+} transport. Additionally, while an alternative TRPV6 genetic mutant (D541A, pore inactivating mutation) has reduced intestinal Ca^{2+} absorption, they do not have altered bone mineralization demonstrating alternative intestinal absorptive pathways may compensate (Woudenberg-Vrenken et al., 2012). An alternative apical transporter that may play a compensatory role is the apical L-type calcium channel (Cav 1.3) (Kellett, 2011). This channel is expressed in the jejunum and ileum of rats and an *in-vivo* jejunal loop model demonstrates that nifedapine (L-type Ca^{2+} channel blocker) reduces Ca^{2+} absorption, which does not block TRPV6 (Morgan et al., 2003).

Upon entry into the cell, Ca^{2+} must be buffered as increased cytosolic Ca^{2+} is an apoptotic signal (Rizzuto et al., 2003). A vitamin D_3 sensitive protein thought to mediate this process was first identified in the intestinal epithelium of chicks, now known as calbindin-D9k (CaBP9k) (Wasserman et al., 1969; Wasserman & Taylor, 1966). The protein expression pattern of CaBP9k along the small intestine closely matches that of TRPV6 with significant expression in the duodenum, cecum and colon and none/minimal expression in the jejunum and ileum (Lameris et al., 2015). Furthermore, CaBP9k co-localizes with TRPV6 supporting a role in

shuttling Ca^{2+} (Nijenhuis et al., 2003). Despite the essential role of intracellular Ca^{2+} buffering, CaBP9k KO mice survive and do not have altered Ca^{2+} absorption *in-vivo* (G. S. Lee et al., 2007) suggesting it is not essential.

Basolateral Ca^{2+} extrusion is mediated by the sodium-calcium exchanger 1 (NCX1) and the plasma-membrane Ca^{2+}-ATPase (PMCA1b) (Hoenderop et al., 2005). PMCA1b is ubiquitously expressed in all intestinal segments in mice (Lameris et al., 2015) and expression of PMCA1b and NCX1 were increased in chick enterocytes fed a low-Ca^{2+} diet suggesting a role in Ca^{2+} absorption (V. A. Centeno et al., 2004). Additionally, transgenic mice lacking NCX1 are embryonically lethal (C. H. Cho et al., 2003) and mice lacking PMCA1 have dysfunction in cellular Ca^{2+} homeostasis (Prasad et al., 2004; Wang et al., 2017). Given the importance of keeping intracellular Ca^{2+} concentrations low, this supports a major role of these proteins in Ca^{2+} efflux.

1.5.2.2 Paracellular Ca^{2+} transport

Paracellular Ca^{2+} transport is a major mechanism of absorption throughout the small intestine, which shows voltage-dependent Ca^{2+} transport throughout (Karbach, 1992). As with paracellular Ca^{2+} transport in the kidney, paracellular Ca^{2+} flux in the intestine is through both solvent drag, again mediated by NHE3 and distally by a concentrative driving force. Consistent with NHE3 playing a role in paracellular Ca^{2+} absorption, NHE3 KO mice have impaired intestinal Na^{+}, Pi as well as Ca^{2+} reabsorption, highlighting the important coupling of Na^{+} absorption with other ions (Pan et al., 2012; Rievaj et al., 2013a). Given the gastrointestinal tract has a TEER of ~5 mV (lumen negative), a luminal free Ca^{2+} concentration of at least 1.74 mM is needed to overcome the unfavorable electric gradient (Alexander et al., 2014). As sodium and

water are reabsorbed in the proximal small intestine, this concentrates luminal Ca^{2+} providing a chemical driving force for paracellular Ca^{2+} transport. Post-weaning, there is evidence of net paracellular Ca^{2+} absorption from the duodenum, secretion in the jejunum and absorption from the ileum of mice (Beggs & Alexander, 2017). Additionally, while it was previously thought the colon played a negligible role, there is evidence of paracellular Ca^{2+} reabsorption from the colon as well as the cecum (Hylander et al., 1980, 1990; Rievaj et al., 2013a).

In addition to an electrochemical driving force, permeability to Ca^{2+} is necessary for paracellular absorption. Given the presence of paracellular Ca^{2+} absorption, the molecular mediators providing permselectivity to the epithelium were investigated. Claudin-2, -12 and -15 were discovered to localize to the intestinal epithelium and are implicated in forming cation permeable pores, allowing for Ca^{2+} and Na^{+} absorption (Amasheh et al., 2002; Fujita et al., 2008; Yu et al., 2009) (Figure 1.5).

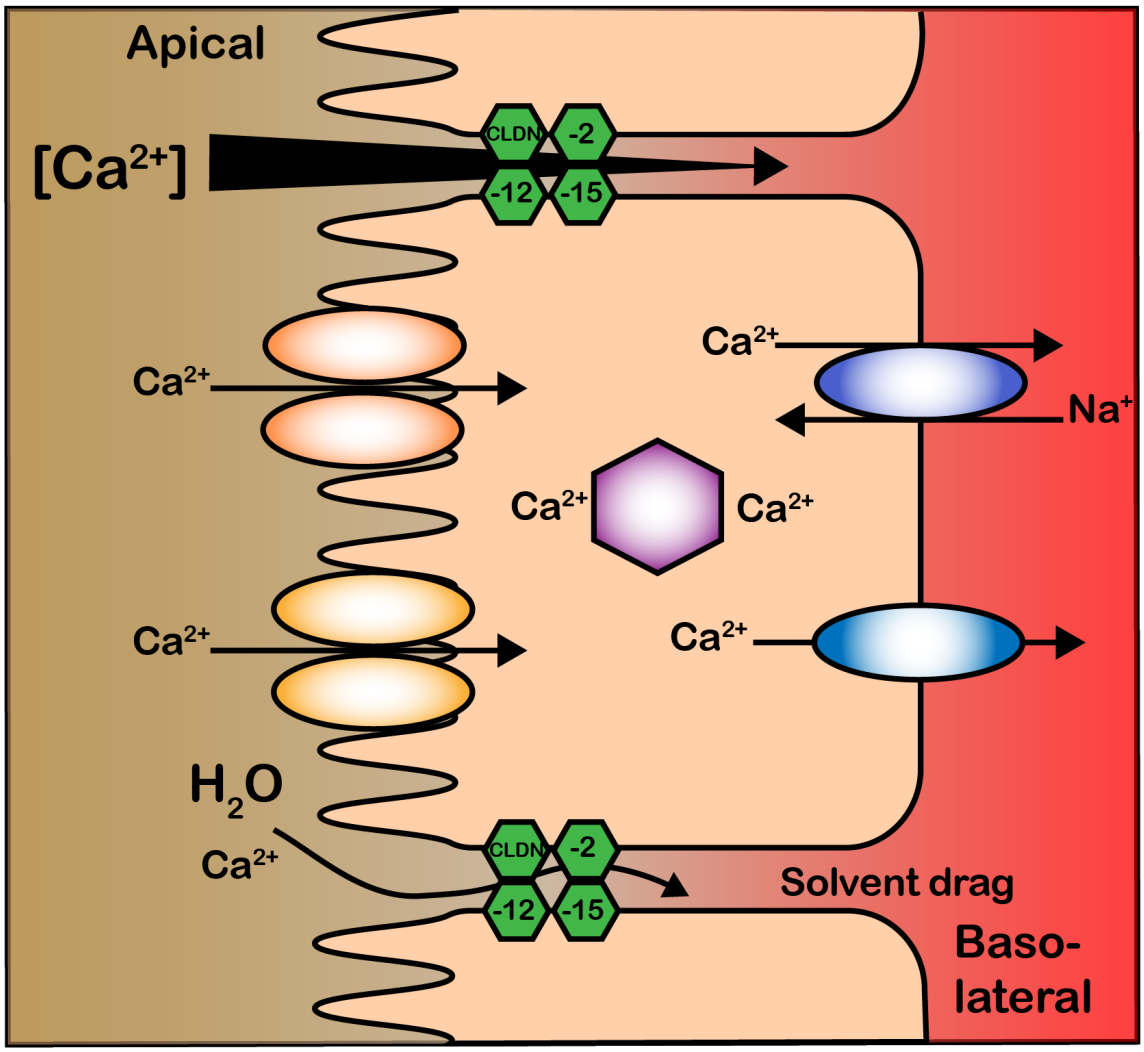

Figure 1.6. Intestinal paracellular Ca^{2+} transport. Passive paracellular Ca^{2+} transport occurs throughout the small intestine, cecum and colon. Permselectivity of the tight junction is determined by the expression of claudins and claudins -2, -12 and -15 are proposed to mediate Ca^{2+} transport. Solvent drag driven by sodium reabsorption occurs in the proximal small intestine (bottom junction) while sodium and water reabsorption increases the luminal Ca^{2+} concentration providing a chemical driving force favoring Ca^{2+} reabsorption in more distal segments (top junction). Depending on the electrochemical gradient there can also paracellular Ca^{2+} secretion.

The expression of claudin-2 and -12 were shown to be regulated by vitamin D_3 levels (Fujita et al., 2008). To investigate the roles of claudin-2 and -12 in mediating paracellular Ca^{2+} transport, transgenic KO mouse models were employed. Claudin-2 KO mice have reduced permeability to Ca^{2+} (PCa^{2+}) in the proximal colon, which contributed reduced paracellular Ca^{2+} secretion as compensation for a renal Ca^{2+} leak (Curry et al., 2020). Additionally, Ussing chamber experiments demonstrate that loss of claudin-12 reduces colonic PCa^{2+}, however, these mice do not have altered fecal Ca^{2+} or Ca^{2+} balance suggesting potential compensation by claudin-2 (Plain et al., 2020). Recently, the Alexander lab generated a claudin-2 / -12 double KO mouse model which exhibits an additive reduction in colonic PCa^{2+} consistent with claudin-2 and claudin-12 forming independent Ca^{2+} permeable pores (Beggs et al., Alexander Laboratory, unpublished data). Claudin-15 mediates paracellular Na^+ and water absorption, however, unlike claudin-2 is unable to meditate solvent drag (Tamura et al., 2011). Loss of claudin-15 thus causes reduced permeation of Na^+ and retention of water in the lumen leading to megaintestine (Tamura et al., 2008). Although it is unclear if claudin-15 confers Ca^{2+} permeability, by preventing the permeation of water, it could indirectly decrease solvent drag of Ca^{2+} as well as the concentrative driving for paracellular Ca^{2+} absorption. Ultimately studies on claudin-15 KO mice will need to be performed to assess the role of claudin-15 in intestinal calcium absorption.

1.6 Overall Rationale

Hyperphosphatemia, elevated serum phosphate (Pi), is an electrolyte imbalance frequently occurring in chronic kidney disease and end-stage renal disease (ESRD) (Da et al., 2015; Gonzalez-Parra et al., 2012; Palmer et al., 2011). In these patients, as well as the general population (W. Bai et al., 2016), high blood Pi is associated with a number of negative sequelae

including further worsening of kidney function, secondary hyperparathyroidism and vascular calcification. Lowering plasma Pi is therefore a clinical priority (Kidney Disease: Improving Global Outcomes, 2017). The main strategies used to achieve this aim are dietary Pi restriction and drugs that bind Pi in the intestinal lumen, enhancing excretion.

However, there are problems with both of these approaches to reducing serum Pi. As Pi is prevalent in protein, dietary Pi restriction involves restricting this and potentially causing protein malnutrition. In addition, the typical Western diet contains an abundance of sodium and potassium phosphate additives and preservatives (Carrigan et al., 2014; Leon et al., 2013). While it is well appreciated that the source of dietary Pi influences its bioavailability, with inorganic Pi sources being highly bioavailable, the molecular details underpinning this difference is not understood. Therefore, we set out to understand why "organic P" has lower bioavaiability than "inorganic Pi". As per our introduction, we posited that organic Pi was predominantly transported *via* the transcellular pathway, while inorganic Pi was absorbed largely by the paracellular pathway. To test this hypothesis, we created two different diets with equal total amounts of dietary P (0.7%), but in one diet the P was predominately from organic sources (protein), while in the other it was predominately from inorganic sources (Pi salts). We fed this diet to wild-type and claudin-12 KO mice (N.B. biophysical studies inferred claudin-12 contributed a paracellular blocking function) and used various pharmacological inhibitors of the predominant intestinal Pi transporter, Npt2b, in order to interrogate which pathway, paracellular or transcellular, that Pi was absorbed by. Understanding the molecular details underpinning the varying bioavailability from different sources will allow for the development of improved therapies to reduce intestinal Pi absorption i.e. diets low in inorganic Pi and paracellular Pi blockers.

The second approach to lowering plasma Pi, phosphate-binding drugs, is problematic as these binders are often required in high-doses leading to a large tablet burden, non-adherence to treatment and are associated with gastrointestinal intolerance (Cannata-Andia & Martin, 2016; Chiu et al., 2009; Fissell et al., 2016). A better alternative would be to target intestinal Pi transport directly. The NHE3 inhibitor Tenapanor was recently shown to reduce intestinal Pi absorption by reducing paracellular Pi transport (King et al., 2018), which is likely the predominant route for intestinal Pi transport in humans eating a Western diet (Saurette & Alexander, 2019). However, the molecular mediators of paracellular Pi transport (*i.e.* claudins) are unknown. While the exact mechanism of action for how Tenapanor reduces paracellular Pi permeability is unknown, preliminary studies from the Alexander Lab suggest that claudin-12 is necessary for the Tenapanor mediated reduction in intestinal Pi absorption. Therefore, we also sought to understand the role of claudin-12 in regulating paracellular Pi transport.

Along with claudin-12, claudin-2 has also been implicated as a paracellular cation pore in renal and intestinal epithelia (Curry et al., 2020; Muto et al., 2010; Plain et al., 2020). Importantly, these mice have hypercalciuria and develop nephrocalcinosis while maintaining plasma Ca^{2+}. The Alexander Laboratory therefore generated claudin-2 KO mice to better understand the role of this protein in regulating paracellular Ca^{2+} absorption. It was an additional aim to better understand how claudin-2 regulates paracellular Ca^{2+} absorption in the intestines and PT. To this end, we characterized the Ca^{2+} phenotype of claudin-2 KO mice in balance studies and investigated potential compensatory mechanisms in the bone (using micro-computed tomography) and intestine which allow the KO mice to maintain normocalcemia.

1.7 Specific Hypotheses

I hypothesize that “inorganic Pi”, being free and unbound, is able to move down its electrochemical gradient *via* the paracellular pathway while “organic P” must first be digested to be absorbed leading to lower luminal Pi concentrations that requires a secondary active process for transcellular absorption.

Given the reported role of claudin-12 as a paracellular cation pore, I hypothesize that claudin-12 forms a paracellular Pi barrier.

I hypothesis that claudin-2 forms a paracellular cation pore across the proximal tubule and intestine.

Chapter 2 : Material and Methods

2.1 Ethics approval and animal studies

All animal experiments were approved by the Animal Care and Use Committee for Health Science of the University of Alberta (under ethics protocol - AUP00000213) following the Guide for the Care and Use of Laboratory Animals (Canadian Council on Animal Care). Mice with global, constitutive knockout of the claudin-2 gene ($Cldn2^{tm1Lex/Mmcd}$) were purchased from the Mutant Mouse Regional Resource Centers. In brief, $Cldn2^{tm1Lex/Mmcd}$ mice were generated by replacing the single coding exon on the X chromosome with a *βGeo/Puro* cassette by homologous recombination and originally maintained on a B6;129F2 background (B6;129S5-$Cldn2^{tm1Lex/Mmcd}$). At the University of Alberta, the mice were backcrossed for 9 generations onto an FVB/N (from Taconics Inc.) background, as kidney disease tends to be more severe in this strain of mice. The global, constitutive claudin-12 knockout strain was generated through the UC Davies Knock Out Mouse Project (KOMP) as previously described (Plain et al., 2020). In brief, a targeting vector (Velocigene cassette ZEN-Ub1, KOMP Repository category number 13208L1) was used to replace exon 4 of the claudin-12 gene (chromosome 5) with a neomycin resistance gene and lacZ reporter gene by homologous recombination in VGB6 embryonic stem (ES) cells derived from the mouse strain C57BL/6NTac. Heterozygous mice were generated using these recombinant ES cells and were then crossed with each other to generate claudin-12 knockout mice. Wildtype FVB/N (Jackson laboratories), claudin-2 knockout and claudin-12 knockout mice were housed in virus-free conditions and maintained on a 12-h light-dark schedule. Standard pelleted chow (PicoLab Rodent Diet 5053: 21% wt/wt protein, 5.0% wt/wt fat, 0.81% wt/wt Ca^{2+}, and 2.2 IU/g vitamin D_3) and drinking water were available *ad libitum* between metabolic balance studies.

2.1.1 Collection of biological samples

At the end of each metabolic balance study, the animals were euthanized with an intraperitoneal injection of sodium-pentobarbital (50 mg/kg) and tissues collected. Blood was collected *via* cardiac puncture, centrifuged and the serum aliquoted and snap frozen in liquid nitrogen. After euthanasia, intestine and kidney were removed by sharp dissection, immediately snap frozen in liquid nitrogen and stored at -80ºC until further use. Intestinal segments were defined and isolated as previously described (Rievaj et al., 2013b). In short, the first 4.6 cm of the small intestine distal to the pyloric sphincter represented the duodenum. The jejunum was represented by segments 10 to 14.8 cm distal to the pylorus. For ileum, intestine between 3.2 and 6.8 cm proximal to the ileocecal junction was used.

2.2 Metabolic balance studies

2.2.1 Inorganic phosphate and organic phosphorus balance studies

Balance studies were performed on wildtype FVB/N (n=18, 10 female and 8 male) and cldn12 KO (n=21, 9 female and 12 male) mice between 10-15 weeks of age. Animals were placed individually into metabolic cages (Techniplast), permitting the collection of urine (under mineral oil) and feces for each 24-hour interval. For 72 hours, the animals were kept in metabolic cages and fed an *"organic P"* diet containing phosphorus from protein and phytate (0.7% wt/wt P / 1% Ca^{2+} wt/wt, Teklad rodent diet 2918, Table 2.1). After 72 hours, the animals were moved to static cages and fed a pelleted *"inorganic Pi"* diet consisting of 0.4% wt/wt P / ≤ 0.1% wt/wt Ca^{2+} (TD. 95027 Table 1) supplemented to 0.7% wt/wt P and 1% wt/wt Ca^{2+} with $CaCl_2 \cdot 2\ H_2O$ (5.18 g / kg chow), NaH_2PO_4 (12.5 g / kg chow) and $CaCO_3$ (22.5 g / kg chow). After 4 days in static cages, the animals were placed into metabolic cages and fed the *"inorganic Pi"* diet for 72

hours. Urine (under mineral oil) and feces were again collected every 24 hours. After 72 hours in the metabolic cages, the animals were euthanized and tissues were collected for further analysis. The experiment was then repeated with diets delivered in the reverse order. In short, the animals were placed into metabolic cages for 72 hours, fed the "*inorganic Pi"* diet (TD. 95027, supplemented to 0.7% wt/wt P and 1% wt/wt Ca^{2+}) and urine (under mineral oil) and feces collected. They were then placed in static cages for 4 days and fed an *"organic P"* diet (0.7% wt/wt P / 1% Ca^{2+} wt/wt, Teklad rodent diet 2918). On the final day, they were placed back into metabolic cages on the *"organic P"* diet for an additional 72- hours to permit the collection of their urine and feces. After the final 72 hours in metabolic cages, the animals were sacrificed and their tissues collected.

Table 2.1. *Mineral composition of organic P and inorganic Pi diets*

Mineral	"Organic" P diet	"Inorganic Pi" diet
Calcium (Ca^{2+})	1.0%	1.0%
Total P	0.7%	0.7%
Organic P	0.7%	0.4%
Inorganic Pi (PO_4^{3-})	0.0%	0.3%
Sodium (Na^{+})	0.2%	0.3%
Chloride (Cl^{-})	0.4%	0.4%
Magnesium (Mg^{2+})	0.2%	0.1%
Potassium (K^{+})	0.6%	0.7%

Table 2.2. *Macronutrient composition of organic P and inorganic Pi diets*

Macronutrient (%by weight)	"Organic" P diet	"Inorganic Pi" diet
Crude Protein	18.6%	17.7%
Fat	6.2%	6.2%
Carbohydrate (available)	44.2%	63.4%

2.2.2 Phosphonoformate (PFA) balance studies

Balance studies were performed using wildtype FVB/N (n=17) and claudin-12 KO (n=17) mice between 10-15 weeks of age. Animals were housed individually in metabolic cages (Techniplast) for 72 hours, permitting the collection of urine (under mineral oil) and feces. They were fed an *"organic P"* diet (Teklad rodent diet 2918). Half of the wildtype FVB/N and claudin-12 KO mice received the diet supplemented with PFA (3.75 mg / g chow). An animal consuming an average of 4 g of chow per day ingests 15 mg PFA per day. Assuming a 30 g animal, the daily dose of PFA was 500 mg PFA/ kg • day. After 72 hours, the animals were placed back into static cages for a drug washout period of 4 days and fed an *"organic P"* diet (Teklad rodent diet 2918). After the drug washout period, animals were placed back into metabolic cages for an additional 72 hours and fed an *"organic P"* diet (Teklad rodent diet 2918) with each animal receiving the opposite drug treatment *i.e.* animals who did not receive PFA for the first 72 hours in metabolic cages received it the second time they were in metabolic cages and vice-versa. At the end of the second 72 hours in metabolic cages the animals were sacrificed and their tissues collected as described above. This experimental design was repeated as described a second time using the *"inorganic Pi"* diet (TD. 95027, supplemented to 0.7% wt/wt P and 1% wt/wt Ca^{2+}).

2.2.3 NTX1942 balance studies

Balance studies were performed using wildtype FVB/N (n=16) mice between 10-15 weeks of age Animals were placed individually into metabolic cages (Techniplast), permitting the collection of urine (under mineral oil) and feces every 24 hours for 72 hours (set 1). Half of the animals received the *"organic P"* diet (0.7% wt/wt P and 1% wt/wt Ca^{2+}, Teklad rodent diet

2918) while half the animals received the *"inorganic Pi"* diet (TD. 95027, supplemented to 0.7% wt/wt P and 1% wt/wt Ca^{2+}) and each animal received the same diet throughout the course of the experiment. After 72 hours in metabolic cages, the animals were transferred back to their static cages for 48 hours. They were subsequently placed into metabolic cages for an additional 72 hours (set 2) with each animal receiving the same diet treatment as set 1 supplemented with NTX1942 (6 mg / g chow). The dose received was calculated assuming a mass of 30 g for an animal and an average daily chow consumption of 4 g. This yields an average daily dose of 200 mg / kg • day. After a final 72 hours in metabolic cages, the mice were sacrificed and tissues collected for further analysis.

2.3 Real-time quantitative PCR

Total RNA from intestinal segments and kidney was isolated by a phenol-chloroform separation using TRIzol reagent (Invitrogen, Carlsbad, CA) as per the manufacturer's instructions. After addition of DNaseI (AmpGrade, Invitrogen, Carlsbad, CA), RNA was reversed transcribed to cDNA from 1 µg of RNA using the SensiFAST cDNA Synthesis Kit (Bioline, Cincinnati, OH) according to the manufacturer's instructions. mRNA quantification of genes in claudin-2 knockout mice was performed by TaqMan assay using the ABI Prism 7900 HT Sequence Detection System (Applied Biosystems) and primers / probes listed in Table 3. Primers and probes (Integrated DNA Technologies, San Diego, CA) designed for Npt2a (*SLC34A1*), Npt2b (*SLC34A2*), Npt2c (*SLC34A3*), PiT1 (*SLC20A1*), PiT2 (*SLC20A2*), claudin-2 (*CLDN2*), claudin-3 (*CLDN3*), claudin-4 (*CLDN4*), claudin-12 (*CLDN12*), claudin-15 (*CLDN15*), claudin-23 (*CLDN23*) and iALP (*IAP*) (Table 3) were used to quantify mRNA expression of genes from wildtype FVB/N and claudin-12 knockout mice tissue using an

Applied Biosystems QuantStudio pro 6 (Thermo Fisher, Waltham, MA). Expression levels were normalized to either ezrin (*EZR*) or 18s.

Table 2.3. *Primers and probes for qRT-PCR*

Gene	5'-Forward sequence-3'	5'-Reverse sequence-3'	5'-Probe-3'
TRPV6	TCACACACCTTCCCACAATC	CTGTCTCCTCCCAGGTCTAATA	CACAGAACTCTTCCCAGGGTGCTC
CalbD9k	TGGATAAGAATGGCGATGGAG	GCTAGAGCTTCAGGATTGGAG	ACAGCACCTACTGATTGAACGCACG
ATP2B1 (PMCA1b)	CGCCATCTTCTGCACCATT	CAGCCATTGCTCTATTGAAAGTTC	CAGCTGAAAGGCTTCCCGCCAAA
SLC34A1 (Npt2a)	ID: Mm00441450_m1		
SLC34A2 (Npt2b)	GGAGCACACGAACAAGTAGAG	AGGACACTGGGATCAAATGG	ACCAAAGGGAAGACGCTCTGCAT
SLC34A3 (Npt2c)	ID: Mm00551746_m1		
SLC20A1 (PiT-1)	AATTGGTAAAGCTCGTAAGCCATT	TTCCTTGTTCGTGCGTTCATC	CCGTAAGGCAGATCC
SLC20A2 (PiT-2)	CTCAGGAAGGACGCGATCAA	GACCGTGGAAACGCTAATGG	CATGGTTGGTTCAGCTG
CLDN2	AGGTGAGGGAAATAGAAAAGCTAG	TGAGGGTAGAATGACTTTGGC	ATGGAGTGAAGGCAGAGATGAGAAGAGG
CLDN3	CACCAAGATCCTCTATTCTGCG	GGTTCATCGACTGCTGGTAG	CCCCTCTATTCTGCG
CLDN4	ID: Mm00515514_s1		
CLDN12	CCTGCTGTTCGTTTGGTATTG	TGATGAATAGGGCTGTGAGTAAG	TTGTCCTCTCCTTTCTGGCAACCG
CLDN15	AGACAGTGGGACAAGAAATGG	CTTCCCTACAAGCCTTCTACG	AGCTGATGTCACTCTCATCCGAGGT
CLDN23	CCTAGTATTTGGAGAGGAGTTTGG	TGAACTTCTGCCAGTACATCTG	TAGAACCCTGGTCGCCTTCCTCTAA
CLDND1	ACATAGCAACTCACGGAGC	TTTACCCTTCGTCAGCTTGG	CCAATCAACGCCCCAAAGCACAT
IAP (iALP)	TCTGCATCTGAGTACCAATTACG	TGATGTACCGTGCCAAGAAAG	TCACCACTCCCACAGACTTCCCT
ß-actin	ID: Mm01205647_g1		
Ezrin	TGTGATGTCCTGGATGAGTTC	TTCCTACCTGGCTGAAACTTG	ACCCTGTCCAGTTTAAATTCCGGGC

2.4 Serum and Urine Creatinine Measurement

Creatinine in serum was measured using the Diazyme Creatinine Liquid Reagents Assay (Catalogue number DZ072B, Diazyme, Poway, CA) according to the manufacturer's instructions. In brief, fresh serum samples were diluted in 0.85% saline and reacted through a series of enzymatic reactions converting creatinine to creatine via creatininase, which was further converted to sarcosine by creatine amidinohydrolase. The sarcosine is oxidized through the addition of sarcosine oxidase producing hydrogen peroxide. In the presence of peroxidase, the hydrogen peroxide forms a colored dye and the quantity produced measured at 550 nm using a BioTek Synergy Mx florescence plate reader (Agilent, Santa Clara, CA).

Creatinine in urine was measured by high-performance liquid chromatography (HPLC). All measurements were performed using a Dionex UltiMate 3000 HPLC System (Thermo Scientific, ISO-3100SD PUMP category number 5040.0011; TCC-3000SD Column Thermostat, category number 5730.0010, and VWD-3100 DETECTOR, category number 5074.0005, Thermo Fisher Scientific Inc., Mississauga, ON, Canada). The HPLC eluent was prepared as per manufacturer's instructions. The eluent contained acetonitrile (category number A-0626-17, Thermo Scientific)/Trifluoroacetic acid (category number T-3258-PB05), Thermo Scientific, Mississauga, ON, Canada) in ddH_2O. Reagents were filtered using 0.2 μM syringe filters (Thermo Scientific, category number 03-391-1B, Mississauga, ON, Canada). Calibration standard curves were made using creatinine from Acros Organics, NJ, USA (category number AC228940250). Data handling was completed with Thermo Scientific Chromeleon 7 Chromatography Data System (CDS) software.

2.5 Urine and Fecal Ion Measurement

Feces collected during metabolic balance studies were dried for 3 days at 60ºC (Lab-Line Imperial III incubator, Mumbai, India), then homogenized with a mortar and pestle. A sample between 50-100 mg of the homogenized feces was digested using 300 µL of 70% nitric acid (15.7 M). The feces were then heated for 30 minutes at 65ºC. An additional 700 µL of nitric acid was added and samples were heated at 85ºC for an additional 60 minutes to release ions from the organic matter. The fecal samples were removed from heat and 1 mL of hydrogen peroxide added to each.

Urine electrolytes were measured by ion chromatography (Dionex Aquion Ion Chromatography System, Thermo Fisher Scientific Inc., Mississauga, ON, Canada) with an autosampler. Samples were diluted 1:100 in ddH_2O and carried in 4.5 mM Na_2CO_3/1.5 mM $NaHCO_3$ in ddH_2O for anion eluent, 20 mM Methanesulfonic acid in ddH_2O for cation eluent. Calibration curves were created with serial dilutions of Dionex five anion and six cation-I standards (Dionex, Thermo Fisher Scientific Inc., Mississauga, ON, Canada). Results were analyzed using Chromeleon 7 Chromatography Data System software (Thermo Scientific). Urine and fecal phosphate were measured using a colorimetric assay (BioVision, Milpitas, CA) in which free phosphate forms a chromogenic complex with malachite green and ammonium molybdate whose absorbance was read at 650 nm using a BioTek Synergy Mx florescence plate reader (Agilent, Santa Clara, CA). Urinary ion excretion was normalized both to urine creatinine and the mass of each ion ingested. The fecal ion concentrations were used to determine the oral bioavailability which was calculated as:

$$\text{Oral bioavailability (\%)} = \left(1 - \frac{\text{Mass excreted (mg)}}{\text{Mass ingested (mg)}}\right) \times 100 \ .$$

2.6 Hormone Measurements by Enzyme-Linked Immunosorbent Assays (ELISA)

Plasma intact parathyroid hormone (PTH 1-84) was measured *via* a mouse PTH 1-84 ELISA kit (Immunotopics, San Diego, CA) as per the manufacturer's instructions as previously described (Pan et al., 2012). Likewise, fibroblast growth factor 23 (FGF-23) was measured by ELISA according to the manufacturer's instructions (FGF-23 ELISA Kit, Kainos, category number CY-4000, Tokyo, Japan).

2.7 Bi-ionic Dilution Potential Experiments

Bi-ionic diffusion potential experiments were performed on Caco2bbe cells essentially as previously described (King et al., 2018). Six-well Snapwell polyester filter inserts (Corning, Corning, NY) were seeded with $2.0 \bullet 10^6$ caco2bbe cells and grown to confluency for 20 days before the dilution potential experiments. Initial baseline conditions were corrected by filling each hemichamber with 4 mL of normal Krebs Ringer Buffer (KRB) (140 mM NaCl, 0.4 mM KH_2PO_4, 2.4 mM K_2HPO_4, 1.2 mM $MgCl_2 \bullet 6H_2O$, 0.5 mM Ca^{2+}-gluconate • H_2O, 10 mM glucose, pH 8.0) and bubbling continuously with 5% vol/vol CO_2, 95% vol/vol O_2 at 37ºC. To eliminate electrical bias, the voltage and fluid resistance across the empty sliders was set to 0 mV and 0 $\Omega \cdot cm^2$ respectively using an EVC 4000 (WPI, Sarasota, FL). Voltage measurements were made using Ag/AgCl electrodes connected to each hemichamber by 3 M KCl agarose bridges and the data recorded using a PowerLab 8SP series (ADInstruments, Bella Vista, NSW, Australia). For the analysis, the dilution potentials were corrected for liquid junction potentials (Barry & Lynch, 1991) and TEER measurements for the resistance of an empty filter.

Snapwell inserts were mounted in the Ussing chamber (P2300 sliders, Physiologic Instruments, San Diego, CA) and incubated with 4 mL KRB in the apical and basolateral

hemichambers and bubbled continuously with 5% vol/vol CO_2, 95% vol/vol O_2 at 37ºC. After 20 minutes, the transepithelial resistance (TEER) was determined by pulsing 90 μA for 3 seconds, measuring the subsequent change in voltage and then calculated using Ohm's law. TEER measurements were made after each buffer change to monitor the stability of the cells throughout the experiment and channels whose resistances changed by >30% over the course of the experiment were eliminated from the analysis. A dilution potential was induced by replacing the apical KRB with low NaCl buffer (55 mM NaCl, 0.4 mM KH_2PO_4, 2.4 mM K_2HPO_4, 1.2 mM $MgCl_2 \cdot 6H_2O$, 0.5 mM Ca^{2+}-gluconate$\cdot H_2O$, 135 mM mannitol, 10 mM glucose, pH 8.0). Once the peak current was reached, the low NaCl buffer was replaced by normal KRB for 5 minutes, until baseline current was reached. Another dilution potential was induced by replacing normal KRB in the apical hemichamber with a high PO_4 buffer (70 mM Na_2HPO_4, 5.3 mM KH_2PO_4, 1.2 mM $MgCl_2 \cdot 6H_2O$, 1.3 mM Ca^{2+}-gluconate$\cdot H_2O$, 95 mM mannitol, 10 mM glucose, pH 8.0). Again, once the peak current was reached, the high PO_4 buffer was switched back to normal KRB for 5 minutes. Following these two dilution potential recordings, the measurements were repeated in the presence of 5 mM phosphonoformate (PFA) or vehicle (water) throughout the experiment. To ensure the viability of the cells at the end of the experiment, 10 μM forskolin was applied bilaterally to all chambers and the resulting change in voltage recorded. Samples that did not display an increase of >40% in the potential difference (PD) were excluded.

The sodium-to-chloride permeability (P_{Na}/P_{Cl}) ratio was calculated using the Goldman-Hodgkin-Katz equation and the NaCl dilution potentials measured. The absolute permeability of sodium (P_{Na}) and chloride (P_{Cl}) was calculated using the simplified Kimizuka-Koketsu equation (Kimizuka & Koketsu, 1964) (equations i and ii). The absolute permeability of phosphate (equation iii) was calculated from the HPO_4^{2-}—Cl^- bionic diffusion potential using the Goldman-

Hodgkin-Katz equation for HPO_4^{2-} , Na^+ and Cl^- (equation iv) at equilibrium, where the sum of the individual ion fluxes is zero, and knowing the P_{Na}/P_{Cl}, P_{Na}, and P_{Cl}. The solutions were designed so that differences in the activities of other ions in solution were negligible and no other dilution potentials were induced.

$$\text{(i)}\ \ P_{Na} = G\frac{RT}{F^2}\frac{1}{aNa^+_{ctrl}\left(1+\frac{P_{Cl}}{P_{Na}}\right)}$$

$$\text{(ii)}\ P_{Cl} = G\frac{RT}{F^2}\frac{1}{aCl^+_{ctrl}\left(1+\frac{P_{Na}}{P_{Cl}}\right)}$$

$$\text{(iii)}P_{HPO_4^{2-}} = (e^u + 1)\frac{P_{Na}\left(aNa^+_{bl} - e^u aNa^+_{ap}\right) + P_{Cl}\left(aCl^-_{ap} - e^u aCl^-_{bl}\right)}{4\left(e^{2u}aHPO_4^{2-}{}_{bl} - aHPO_4^{2-}{}_{ap}\right)}$$

$$\text{(iv)}J_x = P_x z_x{}^2 E_m \frac{F^2}{RT}\frac{aX_{ap} - aX_{bl}e^{-z_x u}}{1-e^{-z_x u}},\ u = \frac{FE_m}{RT},\ E_m = E_{ap} - E_{bl}$$

In the equations above J_x is the flux, P_x is the permeability, z_x is the valence, and aX is the activity of the ion. Further, R is the gas constant, T is the temperature in kelvins, F is Faraday's constant, while 'ap' stands for apical and 'bl' stands for basolateral.

2.8 Micro-computed tomography

Micro-computed tomography (μ-CT) experiments were performed on wildtype FVB/N and Cldn2 KO animals essentially as previously described (Pan et al., 2012). After euthanasia, the right tibias were isolated by sharp dissection, fixed in 4% paraformaldehyde and stored at -4ºC. At the time of the experiment, dissected tibias were wrapped in tissue (KimTech, Kimberly-Clark) sprayed with 70% ethanol prior to scanning to prevent desiccation and placed in Eppendorf tubes within a polystyrene foam tube during scanning to prevent movement artifacts. The right tibial metaphasis was scanned using a Skyscan 1076 micro-computed tomography (CT) imager (Skyscan NV, Kontich, Belgium). Image projections were taken at 9-μm resolution

using an X-ray voltage and current of 25 kVp and 222 μA respectively, with beam filtration through a 0.5 mm aluminum filter, at a 0.5º rotation step. A modified Feldkamp back projection algorithm was used for image reconstruction and the raw image data was Gaussian filtered and globally thresholded at a fixed range of 0.0 - 0.07752 to separate the mineral phase from background. The bridging of the metaphaseal growth plate was used as an anatomical landmark for the origin of trabecular bone. A region of interest 100 slices in the direction of the metaphasis, starting 20 slices below this landmark was used for analysis. Within the region of interest, trabecular bone was segmented from cortical bone in the transaxial slices using the vendor-supplied software (CT-analyser, Skyscan NV) with semi-automated contouring. After calibrating using known hydroxyapatite "phantoms", morphometric analysis of trabecular and cortical bone was completed to determine the bone volume ratio [bone volume/tissue volume (BV/TV)], trabecular thickness (Tb.Th), trabecular separation (Tb.Sp), trabecular number (Tb.N) and volumetric bone mineral density (g/cm^3).

2.9 Statistical Analysis

Data are presented as means ± standard deviation (SD). Outliers in data sets were first identified and removed using the ROUT method with a false discovery rate of 1%. Assumptions of normality were tested using by creating a histogram, QQ plot and testing normality with the D'Agostino-Pearson test. If the data were not Gaussian and transformation did not result in normality, a Mann-Whitney non-parametric test was used. One-way ANOVA or students' t-tests (GraphPad, La Jolla, CA) were carried out to determine statistical significance as appropriate, and values < 0.05 were considered statistically significant. The Tukey's Honest Significant Difference

(HSD) post-hoc test was used when determining significance when multiple comparisons were made between groups.

Chapter 3 : Organic and Inorganic Pi Results

The author performed all experiments and data analysis included in this chapter, with the exception of Figure 3.3 which was carried out by the laboratory technician Debbie O'Neill.

3.1 Diets of inorganic Pi have enhanced bioavailability

3.1.1 Altered form of dietary Pi affects urinary excretion of inorganic phosphorus (Pi)

We first sought to determine if altering the form of dietary phosphorus (*i.e.* organic P or inorganic Pi) affects its intestinal absorption. To this end, we placed FVB/N (Wild Type; WT) mice into metabolic cages on an "organic P" diet (0.7% wt/wt P, 1% Ca^{2+} wt/wt, Teklad rodent diet 2918), where the dietary Pi came from protein, for 72 hours (n=18, 10 female, 8 male). Following the 72 hours, the diet was subsequently switched to the "inorganic Pi" (0.7% wt/wt P, 1% Ca^{2+} wt/wt, TD. 95027) diet for an additional 72 hours, where 0.4% P came from protein and 0.3% P was supplemented with inorganic Pi salts (N.B diet order was reversed for roughly half the animals). No alterations in body weight, chow, water consumption, urine volume or fecal mass were observed (Table 3.1) in the animals between the different diets.

As urinary Pi excretion directly correlates with intestinal Pi absorption (King et al., 2018), it is used as an indirect marker of intestinal Pi uptake. Consistent with the known difference in intestinal absorption between organic and inorganic P sources (Cupisti & Kalantar-Zadeh, 2013; Gutierrez et al., 2015), urinary Pi excretion was significantly greater ($P < 0.0001$) in WT mice consuming an inorganic Pi diet compared to an organic P diet when normalized to amount eaten (Table 3.2) or urine creatinine (Table 3.3) (**Figure 3.1**). Male and female WT mice consuming either an inorganic Pi or organic Pi diet did not have significantly different urinary Pi excretion and both sexes had increased excretion of Pi on the inorganic Pi diet. Therefore, the data from both sexes were combined in the respective groups. Urinary excretion of Cl^- and Mg^{2+} on the inorganic Pi diet were significantly lower ($P< 0.05$, Tukey HSD test) than on an organic P diet (Table 3.1-2). This is consistent with reduced Mg^{2+} on the inorganic Pi diet, however, there was no difference in Cl^- between diets. Conversely, the urinary excretion of Na^+ was

significantly greater on the inorganic Pi diet (Table 3.1-2), while diet condition did not affect urinary Ca^{2+} or K^{+} excretion (N.B. diet ion amounts are in Table 2.1 and there was 50% more Na^{+} in the inorganic Pi diet).

Table 3.1. *Metabolic cage data for organic / inorganic phosphate diet study*

	Organic P Diet			**Inorganic Pi Diet**		
	WT	**Cldn-12 KO**	***P*-value**	**WT**	**Cldn-12 KO**	***P*-value**
Sample size (n)	18	21		18	21	
Body Weight (g)	26.08 ± 4.26	27.74 ± 4.53	0.25	27.48 ± 2.97	27.89 ± 3.7	0.71
Chow eaten (g/g body weight)	0.17 ± 0.04	0.18 ± 0.04	0.83	0.15 ± 0.03	0.16 ± 0.03	0.20
Water intake (mL/24 hour/g body weight)	0.16 ± 0.04	0.14 ± 0.04	0.19	0.14 ± 0.04	0.12 ± 0.03	0.06
Urine volume (mL/24 hour/g body weight)	0.032 ± 0.017	0.030 ± 0.011	0.66	0.036 ± 0.024	0.041 ± 0.012	0.41
Fecal excretion, wet (g/24 hour/g body weight)	0.065 ± 0.021	0.069 ± 0.020	0.59	0.013 ± 0.003	0.015 ± 0.003	0.014

Data presented as mean ± SD compared by unpaired t-test.

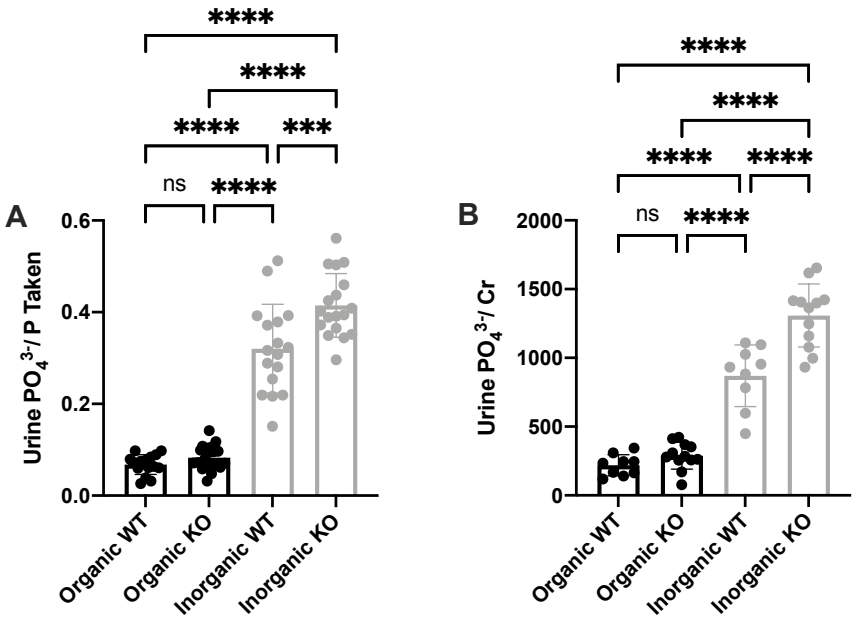

Figure 3.1. 24 hour urinary PO_4^{3-} excretion of wildtype and claudin-12 KO mice on an organic P and inorganic Pi diet. Mice were housed in metabolic cages for 3 days on each diet (0.7% total P) allowing collection of urine and determination of dietary consumption by weighing the food. 24 hour urinary PO_4^{3-} excretion was measured from hour 48 to 72 and normalized to phosphorus ingested **(A)** (n= 18 WT, 21 KO) or urinary creatinine **(B)** (n=10 WT, 12 KO). Data presented as mean ± SD and comparisons were made by one-way ANOVA and Tukey's HSD test for multiple comparisons. *P < 0.05, **P < 0.01, ***P < 0.001, ****P< 0.0001.

Table 3.2: *Urine biochemistry for organic / inorganic phosphate diet study*

	N	WT	N	Cldn-12 KO	*P*-value
"Organic P" diet					
Urine (/Amount eaten)					
Ca^{2+} (mg / mg eaten)	18	0.004 (0.003-0.005)	21	0.004 (0.003-0.005)	0.89
Cl^- (mg / mg eaten)	18	0.65 ± 0.18	21	0.62 ± 0.23	0.64
PO_4^{3-} (mg / mg eaten)	18	0.07 ± 0.02	21	0.08 ± 0.03	0.07
Mg^{2+} (mg / mg eaten)	18	0.10 (0.08-0.13)	21	0.09 (0.07-0.11)	0.28
K^+ (mg / mg eaten)	18	0.67 ± 0.13	21	0.69 ± 0.17	0.68
Na^+ (mg / mg eaten)	18	0.44 ± 0.13	21	0.45 ± 0.10	0.91
"Inorganic P" diet					
Urine (/Amount eaten)					
Ca^{2+} (mg / mg eaten)	18	0.004 (0.003-0.006)	21	0.004 (0.003-0.005)	0.80
Cl^- (mg / mg eaten)	18	0.45 ± 0.14 *#	21	0.52 ± 0.10	0.08
PO_4^{3-} (mg / mg eaten)	18	0.32 ± 0.10 *#	21	0.41 ± 0.07 *#	0.002
Mg^{2+} (mg / mg eaten)	18	0.06 (0.04-0.09) *#	21	0.08 (0.07-0.08)	0.29
K^+ (mg / mg eaten)	18	0.59 ± 0.14	21	0.65 ± 0.10	0.14
Na^+ (mg / mg eaten)	18	0.71 ± 0.17 *#	21	0.78 ± 0.15 *#	0.20

Data are presented as mean ± SD compared by unpaired t-test, or as median (IQR) compared by Mann-Whitney test. Comparisons between WT and claudin-12 KO were made by students unpaired t-test or Mann-Whitney are indicated by the P-value and considered significant for $P < 0.05$. * indicates significance ($P < 0.05$) versus WT organic P diet and # indicates significance ($P < 0.05$) versus Cldn-12 KO organic Pi diet by Tukey multiple comparison's test.

Table 3.3: *Urine biochemistry for organic / inorganic phosphate diet study normalized to Creatinine*

	N	WT	N	Cldn-12 KO	*P*-value
"Organic P" diet					
Urine (/ Creatinine)					
Ca^{2+}	10	14.2 (10.9-20.5)-	12	14.5 (10.3-18.9)	0.91
Cl^-	10	1153 ± 316	12	1277 ± 313	0.66
PO_4^{3-}	10	218.7 ± 76.8	12	288.1 ± 97.8	0.79
Mg^{2+}	10	120.7 ± 54.9	12	119.5 ± 49.9	0.99
K^+	10	1700 ± 296	12	1873 ± 373	0.60
Na^+	10	624.6 ± 159.9	12	627.6 ± 207.9	>0.99
"Inorganic Pi" diet					
Urine (/ Creatinine)					
Ca^{2+}	10	11.6 (8.8-17.1)	12	11.9 (9.8-16.5)	0.99
Cl^-	10	679 ± 176 *#	12	810 ± 143 *#	0.64
PO_4^{3-}	10	869.8 ± 224.5 *#	12	1308 ± 229.2 *#	<0.0001
Mg^{2+}	10	32.1 ± 2.8 *#	12	42.6 ± 9.5 *#	0.93
K^+	10	1372 ± 317 #	12	1696 ± 260	0.10
Na^+	10	1088 ± 249.9 *#	12	1327 ± 229.1 *#	0.07

Data presented as mean ± SD or as median (IQR) compared by one-way ANOVA and Tukey's HSD test. Comparisons between WT and claudin-12 KO were made by Tukey's HSD test are indicated by the P-value and considered significant for $P < 0.05$. * indicates significance ($P < 0.05$) versus WT organic P diet and # indicates significance ($P < 0.05$) versus Cldn-12 KO organic Pi diet.

3.1.2 Type of dietary Pi affects fecal excretion of inorganic phosphorus (Pi)

Next, we measured fecal Pi excretion to calculate intestinal Pi absorption as a percentage of P consumed *i.e.* bioavailability, for each day on both diets. These data were combined for all 3 days on either the organic or inorganic Pi diet (three-day average) and were consistent with the previously reported increased bioavailability of inorganic Pi. Male and female WT mice consuming either an inorganic Pi or organic Pi diet did not have significantly different bioavailability, and both sexes had increased bioavaialibility of Pi on the inorganic Pi diet (**Figure 3.2 A-B)**. Therefore, the data from both sexes were combined. The bioavailability increased from 37.93 ± 13.45 % on an organic P diet to 51.53 ± 8.50 % on the inorganic Pi diet **(Figure 3.2 C)**.

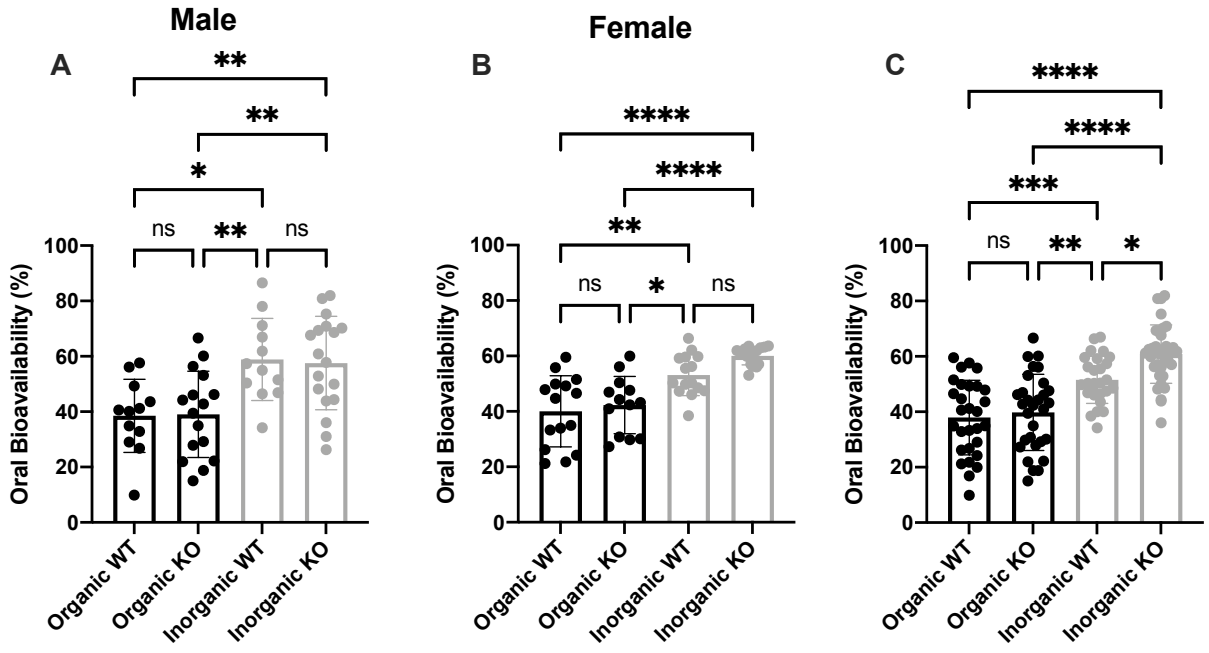

Figure 3.2. Oral P bioavailability of wildtype and claudin-12 KO mice on an organic P and inorganic Pi diet. Mice were housed in metabolic cages for 3 days on each diet (0.7% total P) permitting collection of feces and determination of dietary consumption by weighing the food. Oral Pi bioavailability as a % of total phosphorus consumed was measured for each day and the values for all three days plotted. **(A)** Male WT (n = 4) and claudin-12 KO (n = 6) mice; **(B)** Female WT (n = 6) and claudin-12 KO (n = 6) mice; **(C)** Combined male and female WT (n = 10) and claudin-12 KO (n = 12) mice. Data presented as mean ± SD and comparisons were made by one-way ANOVA and Tukey's HSD test for multiple comparisons. *P < 0.05, **P < 0.01, ***P < 0.001, ****P< 0.0001.

3.2 Claudin-12 is a paracellular Pi blocker

3.2.1 Deletion of claudin-12 enhances urinary Pi excretion

Previous studies from the Alexander laboratory revealed when claudin-12 KO mice were fed inorganic Pi diets to altered calcium content, but not regular organic chow, resulted in greater urine Pi in the claudin-12 KO mice (Plain et al., 2020). Claudin-12 is a tight junction protein, regulated by vitamin D_3 (Fujita et al., 2008). This suggested that claudin-12 might act as a paracellular Pi blocker in the gut. Therefore, after confirming enhanced Pi bioavailability and urinary Pi excretion in WT mice consuming an inorganic Pi diet, we next sought to interrogate if claudin-12 acts as a paracellular Pi pore or blocker. To do this, a technician in the laboratory performed Pi-Cl^- bionic diffusion potential studies in Ussing chambers on jejunal segments *ex-vivo*. The jejunum was employed as there is negligible transcellular Pi absorption from this segment. There were no alterations in the TEER, relative permeability of Na^+ to Cl^- (pNa^+/ pCl^-) or the absolute permeability to Na^+ and Cl^- **(Figure 3.3 A-D)**. Although the relative permeability of HPO_4^{2-} to Cl^- was unchanged **(Figure 3.3 E)**, the absolute permeability to HPO_4^{2-} was increased in the claudin-12 KO mice in the jejunum **(Figure 3.3 F)**.

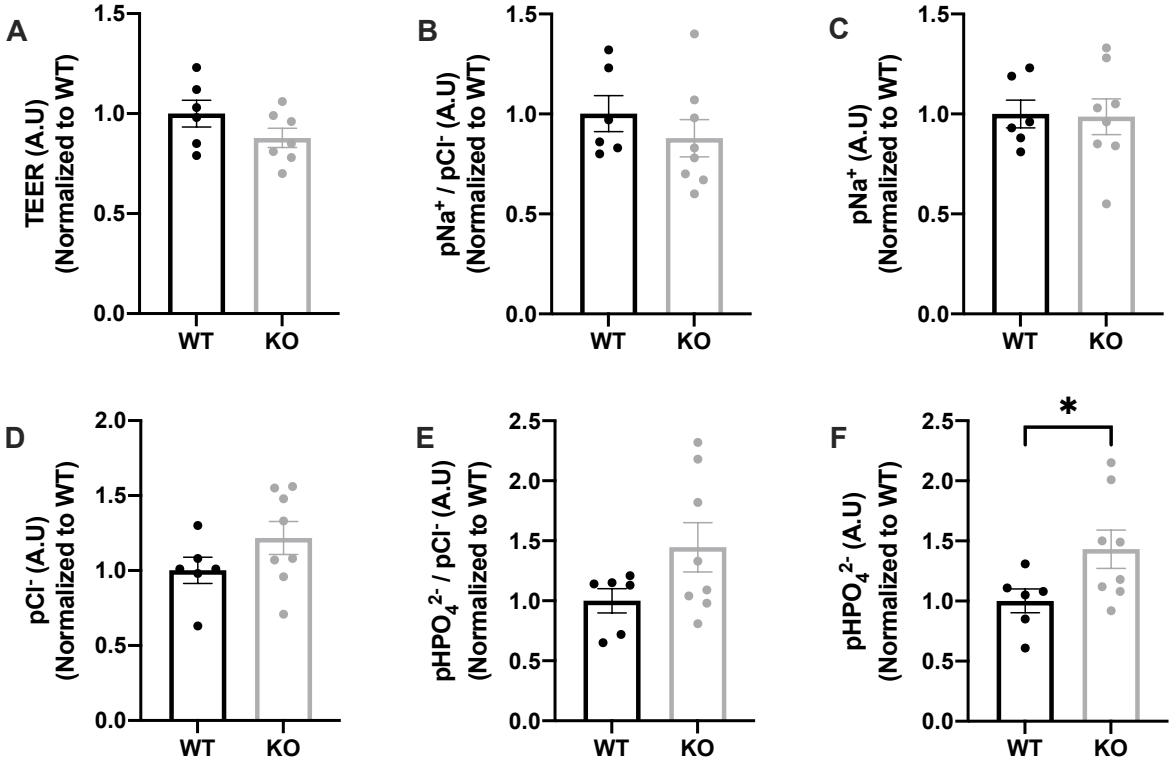

Figure 3.3. Claudin-12 KO mice have increased $pHPO_4^{2-}$ in the jejunum. Bionic diffusion potentials were induced across segments of jejunum from WT or claudin-12 KO mice mounted in Ussing chambers at pH 8.0 (n = 6 WT, 8 KO). The values were normalized to WT. There were no alterations in **A)** Transepithelial electrical resistance (TEER) (P = 0.16), **B)** relative permeability of sodium to chloride (pNa^+ / pCl^-) (P = 0.37), **C)** absolute permeability to sodium (pNa^+) (P = 0.91), **D)** absolute permeability to chloride (pCl^-) (P = 0.17), **E)** relative permeability of Pi to chloride ($pHPO_4^{2-}$ / pCl^-) (P = 0.10). However, the absolute permeability to Pi **F)** was increased in claudin-12 KO mice (P = 0.04). Data presented as mean ± SD; * P < 0.05.

Having established that claudin-12 is a paracellular Pi blocker we employed these animals to interrogate whether inorganic Pi was predominantly reabsorbed *via* the paracellular pathway vs organic Pi which is instead absorbed *via* the transcellular pathway. We hypothesized that we would therefore observe increased Pi bioavailability when claudin-12 KO mice were fed an inorganic Pi, but not an organic P diet. To this end we performed organic to inorganic Pi diet metabolic cage studies with claudin-12 KO mice. In brief, we placed claudin-12 KO mice on the organic P (0.7% wt/wt P, 1% Ca^{2+} wt/wt, TD. 2918) diet for three days permitting the collection of urine and feces. The diet was then switched to the inorganic Pi diet (0.7% wt/wt P, 1% Ca^{2+} wt/wt, TD. 95027); the treatment order was reversed in half the animals. As with WT mice, no alterations in body weight, chow or water consumption, urine volume or fecal mass were observed (Table 3.1) between the diets and genotypes. Similarly, there was significantly greater ($P < 0.05$) urinary Pi excretion in claudin-12 KO mice on an inorganic Pi diet when normalized to amount ingested **(Figure 3.1 A)** and urine creatinine **(Figure 3.1 B)**. Consistent with our hypothesis, claudin-12 KO mice had a greater increase in urinary Pi excretion compared with WT mice when they were fed the inorganic Pi diet **(Figure 3.1 A-B)** suggesting enhanced intestinal Pi absorption in the null animals. Unlike with Pi, there were no significant differences detected in the urinary excretion of Ca^{2+}, Cl^-, Mg^{2+}, and K^+ (Tables 3.2) between diets when normalized to amount ingested, consistent with claudin-12 specifically affecting intestinal Pi absoprtion. However, when normalized to urine creatinine, there was a significant decrease in urinary Cl^- and Mg^{2+} (Table 3.3). Urinary Na^+ excretion was significantly greater in claudin-12 KO mice when normalized either to amount ingested (Table 3.2) or urine creatinine (Table 3.3). Importantly, there were no significant differences in urinary excretion of other electrolytes

besides Pi between WT and claudin-12 KO mice on both the organic and inorganic Pi diets. This is consistent with claudin-12 being a paracellular Pi specific blocker.

3.2.2 Deletion of claudin-12 enhances Pi bioavailability

To directly assess if deletion of claudin-12 affects Pi bioavailability, we again measured fecal Pi excretion to determine its bioavailability. The data were combined for all days on both diets (three-day average) and consistent with previously reported increased bioavailability of Pi. Again, no difference in bioavailability was detected between sexes and male and female claudin-12 mice consuming an inorganic Pi diet both had a significantly greater bioavailability than on an organic P diet (**Figure 3.2 A-B)**. Thus, again male and female data was combined. Consistent with the observed increase in urinary Pi excretion in claudin-12 KO mice **(Figure 3.1 A-B)**, there was a significant increase in Pi bioavailability compared to WT littermates **(Figure 3.2 C)**.

3.2.3 Claudin-12 KO mice develop hyperphosphatemia and have a decreased serum Ca^{2+} on an inorganic Pi diet

Given enhanced Pi bioavailability in claudin-12 KO mice, we next assessed if this led to an altered serum Pi or if renal Pi excretion maintained normophosphatemia. WT mice did not have alterations in serum Pi between the organic P (2.59 ± 0.22 mM) and inorganic Pi (3.12 ± 0.59 mM) diets (Table 3.4). In contrast, the claudin-12 KO mice had a serum Pi of 3.71 ± 0.96 mM, which was significantly greater ($P < 0.05$) than on the organic P diet (2.55 ± 0.31 mM). However, there was no significant difference in serum Pi between genotypes on either the organic or inorganic Pi diets. These results imply that claudin-12 behaves as a paracellular Pi blocker, such that its deletion enhances intestinal Pi absorption and contributes to

hyperphosphatemia when null mice are fed an inorganic Pi diet. Interestingly, on the organic P diet the claudin-12 KO mice have a significantly decreased serum K^+ (Table 3.4) despite no alterations in urinary K^+ excretion.

Table 3.4: *Serum biochemistry for organic / inorganic phosphate diet study.*

	N	WT	N	Cldn-12 KO	*P*-value
"Organic P" Diet					
Calcium (mM)	8	2.68 ± 0.12	9	2.70 ± 0.17	0.78
Phosphate (mM)	8	2.59 ± 0.22	9	2.55 ± 0.31	0.33
Sodium (mM)	8	173.5 (170.5-174.5)	9	174.7 (171.5-183.2)	0.41
Potassium (mM)	8	8.24 ± 0.79	9	6.83 ± 0.92	0.005
Chloride (mM)	8	119.80 ± 3.13	9	119.80 ± 4.25	0.99
"Inorganic Pi" Diet					
Calcium (mM)	10	2.33 (2.23-2.55) *#	12	2.39 (2.27-2.66) #	0.45
Phosphate (mM)	10	3.12 ± 0.59	12	3.71 ± 0.96 *#	0.10
Sodium (mM)	10	176.00 ± 10.77	12	181.30 ± 15.31	0.37
Potassium (mM)	10	7.62 (7.38-8.49) #	12	7.72 (7.13-8.29)	0.54
Chloride (mM)	10	128.4 (123.6-143.8)	12	127.8 (123.6-135.5) *#	0.67

Data presented as mean ± SD compared by unpaired t-test, or as median (IQR) compared by Mann-Whitney test. Comparisons between WT and claudin-12 KO were made by students unpaired t-test or Mann-Whitney. The P-values are indicated and were considered significant for $P < 0.05$. * indicates significance ($P < 0.05$) versus WT organic P diet and # indicates significance ($P < 0.05$) versus Cldn-12 KO organic Pi diet by Tukey multiple comparison's test.

3.2.4 Form of dietary Pi alters Pi status leading to alterations in FGF-23

Because we observed increases in serum Pi and enhanced urinary Pi excretion in WT and claudin-12 KO animals fed the inorganic Pi diet, we investigated which hormonal mediators were responsible for the enhanced excretion. To this end we measured the major calciophosphotropic hormones parathyroid hormone (PTH) and fibroblast growth factor 23 (FGF-23) in mice after consuming either the organic or inorganic Pi diet. While PTH production and release are predicted to increase given the decrease in serum Ca^{2+} and increase in serum Pi on the inorganic Pi diet, we did not observe an alteration in PTH between diets or genotypes **(Figure 3.4 A)**. Consistent with the increased serum Pi in claudin-12 KO mice on an inorganic Pi diet, there was significantly increased serum FGF-23 relative to animals fed the organic P diet **(Figure 3.4 B)**. While serum Pi was not significantly increased in WT mice consuming the inorganic Pi diet, there was also a significant increase in FGF-23 **(Figure 3.4 B)**. The increased FGF-23 may be responsible for the lack of increase in serum PTH on the inorganic Pi diet as FGF-23 inhibits the gene expression and release of PTH in the parathyroid gland (Silver & Naveh-Many, 2010).

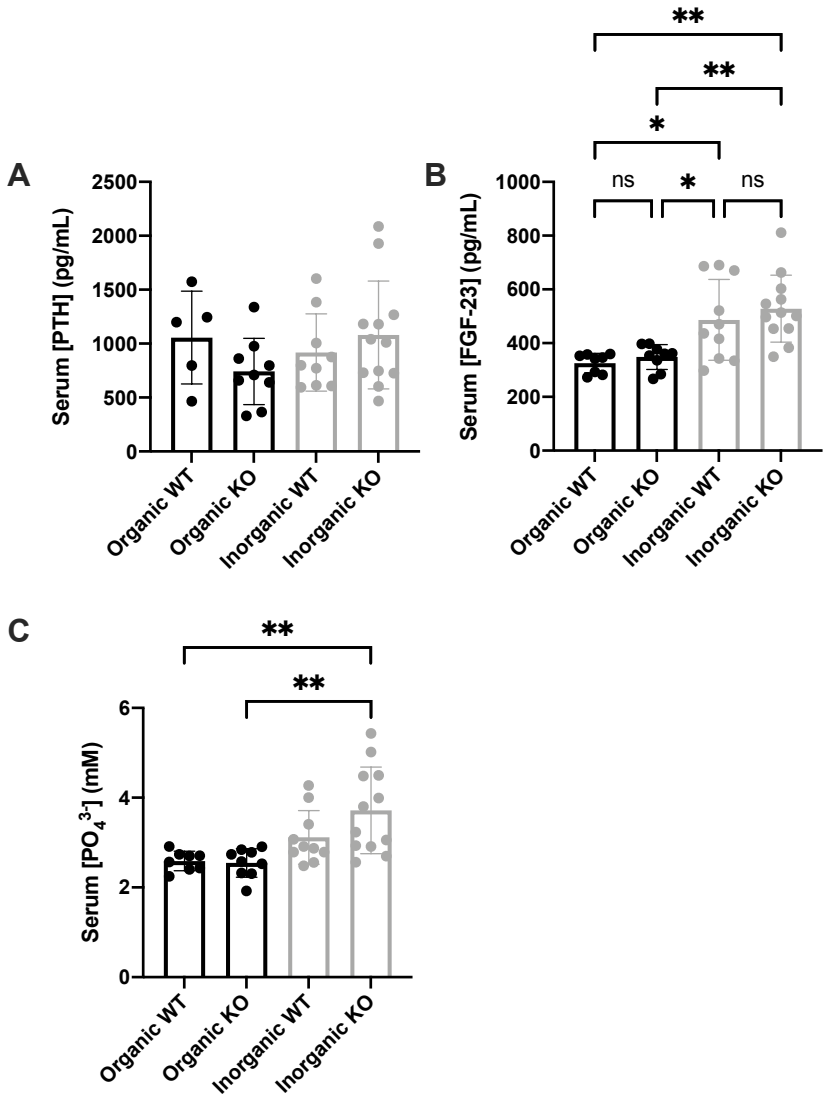

Figure 3.4.**Calciophosphotropic hormone levels in wildtype and claudin-12 KO mice consuming organic P or inorganic Pi diets.** Mice were sacrificed after 3 days on each respective diet, serum collected and levels of the phosphotropic hormones, FGF23 and PTH, were measured. **(A)** Serum intact PTH levels in wildtype (n = 5 organic P, 9 inorganic Pi) and claudin-12 KO (n = 9 organic P and 12 inorganic Pi). **(B)** Serum FGF-23 levels in wildtype (n = 8 organic P and 10 inorganic Pi) and claudin-12 KO (n = 9 organic P, 12 inorganic Pi) mice. **(C)** Serum PO_4^{3-} levels in wildtype (n =8 organic P, 10 inorganic Pi) and claudin-12 KO (n = 9 organic P, 12 inorganic Pi) mice. Data presented as mean ± SD and comparisons were made by one-way ANOVA and Tukey's HSD test for multiple comparisons. *P < 0.05, **P < 0.01.

3.3 Altering dietary Pi form affects gene expression of Pi transport mediators in the small intestine

To assess whether there were compensatory alterations in intestinal Pi transport in response to the change in the form of dietary Pi, we completed quantitative real-time polymerase chain reaction (qRT-PCR) to look at changes in gene expression of the major transcellular Pi transporters and tight junction proteins that may mediate paracellular Pi movement.

3.3.1 Dietary Pi form alters expression of tight junction proteins in the duodenum

As Npt2b is not expressed in the duodenum of mice (King et al., 2018; Marks et al., 2006; Radanovic et al., 2005), the expression of the type III Pi transporters *SLC20a1* (PiT-1) and *SLC20a2* (PiT-2) were measured to assess the sodium-dependent transcellular pathway. There were no significant differences in the expression of either SLC20a1 **(Figure 3.5 A)** or SLC20a2 **(Figure 3.5 B)**, consistent with the transporters playing a minimal role in Pi reabsorption. Interestingly, *CLDN2* expression was significantly reduced on an inorganic Pi diet **(Figure 3.5 C)**. Claudin-2 and claudin-12 are regulated by vitamin D_3 (Fujita et al., 2008) and therefore, the decreased expression of claudin-2 may be a result of FGF-23 inhibition **(Figure 3.4 B)** of vitamin D_3 production. Ultimately, in the claudin-12 KO mice, this reduction in claudin-2 expression in the duodenum may contribute to the reduced plasma Ca^{2+} (Table 3.4) observed. Similar to the pattern of *CLDN2* expression, *CLDN3* and *CLDN4* expression were decreased on the inorganic Pi diet **(Figure 3.5 D-E)**. Claudin-4 is anion selective and allows Cl^- permeation in the collecting duct of renal tubules (Hou et al., 2010). This may suggest a reduction in the anion selectivity in the duodenum, although direct measurement of permeability in Ussing chambers would be necessary to determine this. Claudin-3 plays a structural role, forming a general barrier

(Milatz et al., 2010) in the paracellular pathway. Recently lithocholic acid, normally upregulated in CKD, was shown to enhance paracellular Pi flux via a reduction in claudin-3 expression in a VDR dependent manner (Hashimoto et al., 2020). The reduction in *CLDN3* expression on the inorganic Pi diet may indicate altered geometry of the tight junction strands formed (Nakamura et al., 2019) and alteration in permeability characteristics. Claudin-15 forms a paracellular Na^+ and water permeable pore in the small intestine (Tamura et al., 2011; Tamura et al., 2008). Consistent with increased Na^+ in the inorganic Pi diet (0.3%) and enhanced urinary Na^+ excretion (Tables 3.2 and 3.3), there is increased *CLDN15* expression in WT mice on the inorganic Pi diet **(Figure 3.4 F)** which may contribute to enhanced intestinal Na^+ secretion and excretion in the feces.

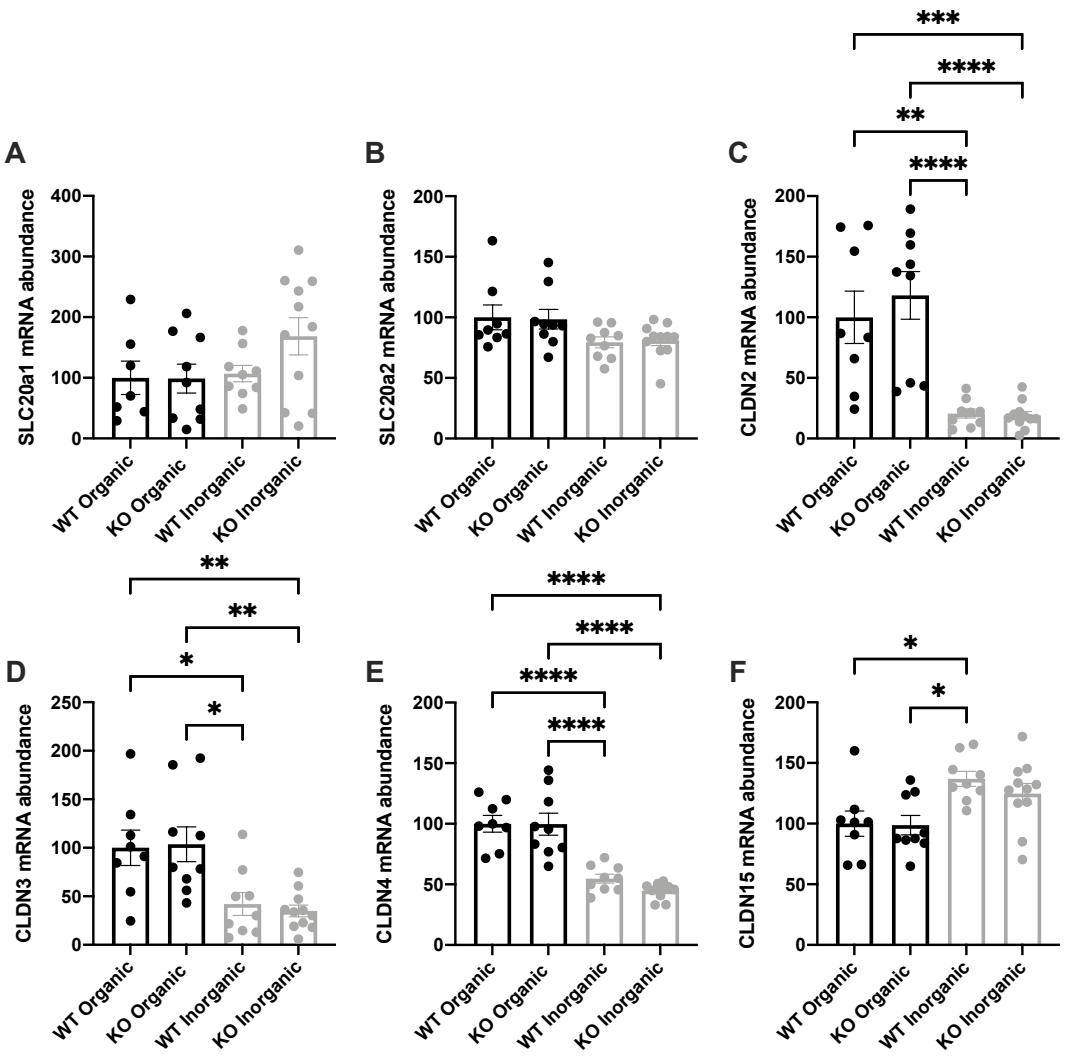

Figure 3.5. Duodenum gene expression in wildtype and claudin-12 KO mice consuming an organic P or inorganic Pi diet. mRNA abundance of duodenum genes expressing **(A)** *SLC20a1* encoding PiT-1 ($P = 0.14$), **(B)** *SLC20a2* encoding PiT-2 ($P = 0.07$), **(C)** Claudin-2 ($P < 0.0001$), **(D)** Claudin-3 ($P = 0.0006$), **(E)** Claudin-4 ($P < 0.0001$) and **(F)** Claudin-15 ($P = 0.006$). Results are normalized to *Ezrin* and expressed relative to WT on the organic P diet. Data presented as mean ± SD and comparisons were made by one-way ANOVA and Tukey's HSD test for multiple comparisons. N = 8 WT Organic, 9 WT Inorganic; N = 9 KO Organic, 11 KO Inorganic.

3.3.2 Dietary Pi form alters expression PiT-2 in the jejunum

Consistent with the presence of sodium-dependent Pi transport in the jejunum (Marks et al., 2006) of mice, *SLC34a2* (Npt2b), *SLC20a1* (PiT-1) and *SLC20a2* (PiT-2) were all expressed in the jejunum. Altering dietary Pi did not lead to any alterations in the expression of the major transcellular Pi transporter *SLC34a2* (Npt2b) in WT or claudin-12 KO mice **(Figure 3.6 A)**. Additionally, expression of *SLC20a1*(PiT-1) was not altered between dietary Pi form consumed or genotype of the mice **(Figure 3.6 B)**. However, the expression of *SLC20a2* (PiT-2) was significantly decreased in WT and claudin-12 KO mice consuming an inorganic Pi diet **(Figure 3.6 C)**. The alteration in *SLC20a2* (PiT-2) expression, but not *SLC20a1* (PiT-1) after 3 days on an inorganic Pi diet is consistent with the known difference in adaptation time of mRNA and protein expression in response to altered dietary Pi content (Candeal et al., 2017). Interestingly, we observed this alteration in expression of *SLC20a2* (PiT-2) given an increased proportion of inorganic Pi, with no alteration to total dietary P content. Unlike in the duodenum, we did not observe any alterations in expression of *CLDN2* **(Figure 3.6 D)** or *CLDN4* **(Figure 3.6 E)** between diets or genotypes, except for reduced *CLDN4* expression in claudin-12 KO on an inorganic Pi diet.

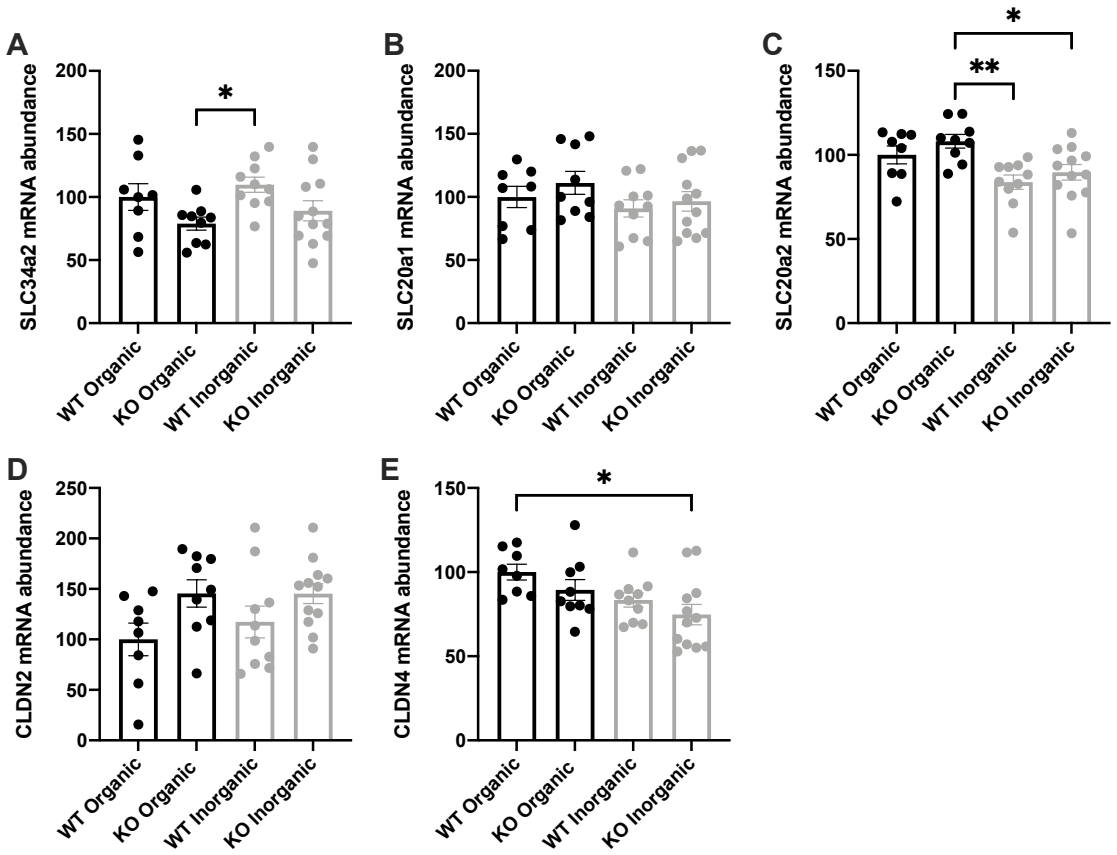

Figure 3.6. Jejunum gene expression in wildtype and claudin-12 KO mice consuming an organic P or inorganic Pi diet. mRNA abundance of jejunum genes expressing **(A)** *SLC34a2* encoding Npt2b (P = 0.04), **(B)** *SLC20a1* encoding PiT-1 (P = 0.37), **(C)** *SLC20a2* encoding PiT-2 (P = 0.003), **(D)** Claudin-2 (P = 0.07) and **(E)** Claudin-4 (P = 0.02). Results are normalized to *Ezrin* and expressed relative to WT on the organic P diet. Data presented as mean ± SD and comparisons were made by one-way ANOVA and Tukey's HSD test for multiple comparisons. N = 8 WT Organic, 10 WT Inorganic; N = 9 KO Organic, 11 KO Inorganic.

3.3.3 Alteration of dietary Pi form and genotype affects transcellular Pi transporter and tight junction protein expression in the ileum

Consistent with the ileum having the greatest Pi absorption and highest expression of transcellular Pi transporters in mice (Marks et al., 2006; Radanovic et al., 2005), all transcellular Pi transporters were detected in this segment **(Figure 3.7 A-C)**. While there was no effect of dietary Pi form on the expression of *SLC34a2* (Npt2b) in WT mice **(Figure 3.7 A)**, the claudin-12 KO mice had significantly reduced expression on the inorganic Pi diet. In addition to the diet effect, loss of claudin-12 further reduced the expression of *SLC34a2* (Npt2b) relative to WT mice on the inorganic P diet. This is consistent with a compensatory reduction in transcellular Pi transport as paracellular Pi absorption is increased on the inorganic Pi diet in claudin-12 KO mice. Similarly, the expression of the type III transporter *SLC20a1* (PiT-1) was decreased in both WT and claudin-12 KO mice on an inorganic Pi diet **(Figure 3.7 B)**. The expression of SLC20a2 (PiT-2) was significantly decreased in claudin-12 KO mice fed the inorganic Pi diet, while no effect of diet was observed in WT mice **(Figure 3.7 C)**. Together this is consistent with dietary Pi form affecting expression of transcellular Pi transporters. No alterations were observed in the expression of the tight junction proteins *CLDN2* **(Figure 3.7 D)** and *CLDND1* **(Figure 3.7 I)**. Similarly, expression of *IAP,* encoding the enzyme intestinal alkaline phosphatase which liberates Pi from protein, was not altered between diets or genotypes **(Figure 3.7 H)**. This is consistent with the similar protein contents of the organic P diet (18.6%) and inorganic Pi diet (17.7%) (Table 2.2). As in the duodenum, *CLDN3* **(Figure 3.7 E)** expression was significantly reduced on an inorganic Pi diet in WT mice, but the diet effect was not observed in the claudin-12 KO mice in this segment. Conversely, *CLDN4* expression was reduced in claudin-12 KO mice fed an inorganic Pi diet **(Figure 3.7 F)**, but not in their WT littermates. Similar to the

expression of *CLDN3*, the inorganic Pi diet reduced expression of *CLDN23* in WT mice **(Figure 3.7 G)**, but there was no diet effect in the claudin-12 KO mice.

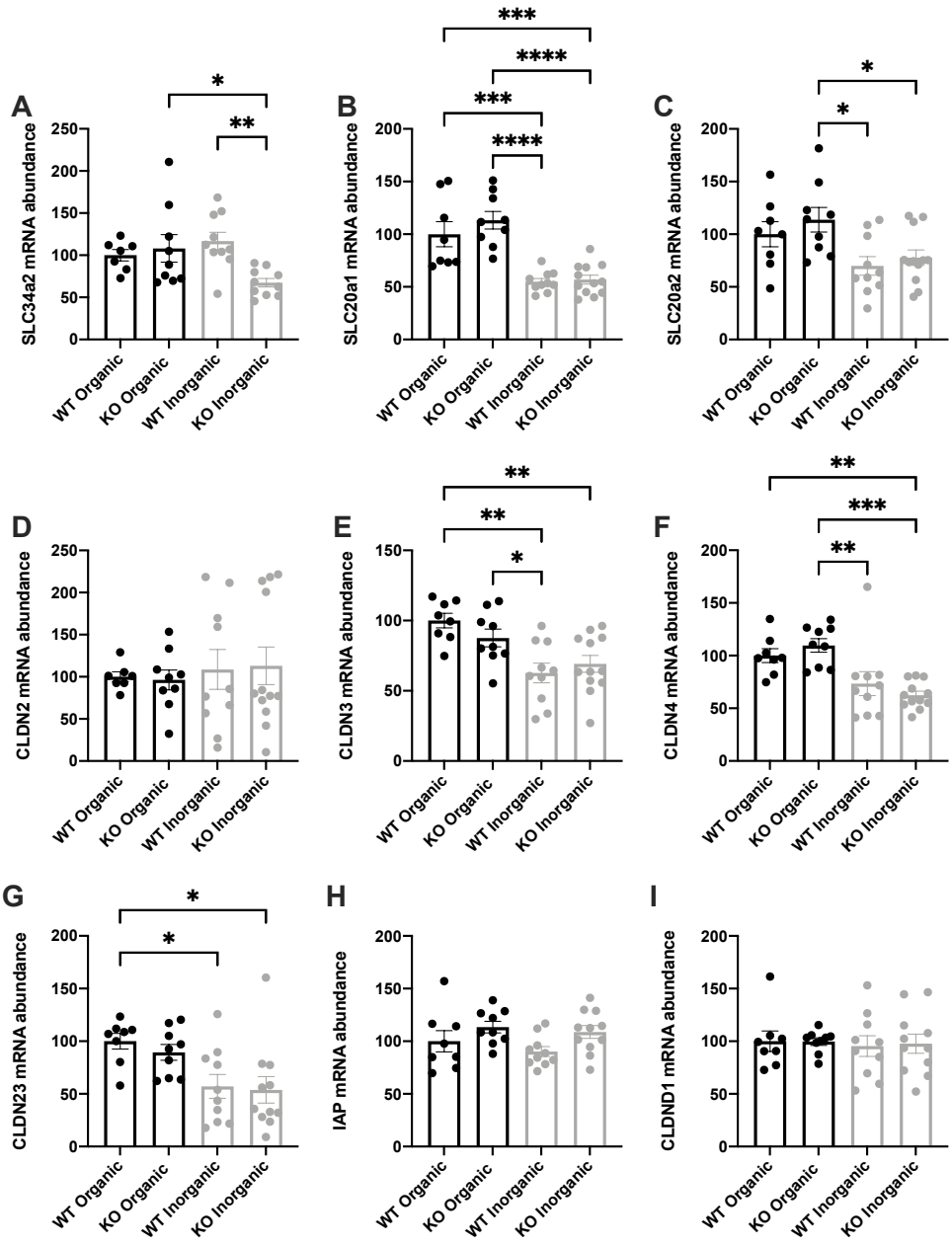

Figure 3.7. Ileum gene expression in wildtype and claudin-12 KO mice consuming an organic P or inorganic Pi diet. mRNA abundance of ileum genes **(A)** *SLC34a2* encoding Npt2b (P = 0.01), **(B)** *SLC20a1* encoding PiT-1 (P < 0.0001), **(C)** *SLC20a2* encoding PiT-2 (P = 0.01), **(D)** Claudin-2 (P = 0.92), **(E)** Claudin-3 (P = 0.0009), **(F)** Claudin-4 (P = 0.0001), **(G)** Claudin-23 (0.007), **(H)** IAP, encoding intestinal alkaline phosphatase (P = 0.07) and **(I)** CLDND1 encoding claudin-domain containing protein 1 (P = 0.06). Results are normalized to *Ezrin* and expressed relative to WT on the organic P diet. Data presented as mean ± SD and comparisons were made by one-way ANOVA and Tukey's HSD test for multiple comparisons. N = 8 WT Organic, 10 WT Inorganic; N = 9 KO Organic, 11 KO Inorganic.

3.4 Inhibition of Npt2b reduces organic P but not inorganic Pi bioavailability

3.4.1 Phosphonoformate (PFA), a Npt2b inhibitor, unfortunately appears to be absorbed systemically

Pi bioavailability on the inorganic Pi diet (0.7% P) was 60.85 ± 1.81% in WT mice, significantly greater than 37.93 ± 2.49% on the organic P diet (P = 0.0002, Tukey HSD). Claudin-12 KO mice, a model with increased paracellular Pi permeability demonstrates increased Pi bioavailability when the animals were fed an inorganic Pi but not organic P diet, consistent with inorganic Pi being absorbed by the paracellular pathway. We next wanted to directly test if organic P is absorbed by the transcellular pathway. To do this, we repeated the inorganic Pi and organic P balance studies with the addition of PFA, a Npt2b inhibitor. In brief, we put WT and claudin-12 KO mice into metabolic cages on the organic P diet (0.7% wt/wt P, 1% Ca^{2+} wt/wt) with half the mice receiving the diet supplemented with PFA (3.75 mg / g chow) for 72 hrs. After a drug washout period, mice were placed back into metabolic cages and it was repeated with the treatments reversed. This design was then implemented with the inorganic Pi diet (0.7% wt/wt P, 1% Ca^{2+} wt/wt). There were no differences in body weights, water / chow intake, urine volume or fecal excretion (Table 3.5) between treatment groups on either diet. As PFA was administered orally with the diet, this suggests the dose received was not significantly different. Consistent with the increased urinary Pi excretion on the inorganic Pi diet **(Figure 3.1)** observed in the previous organic phosphorus and inorganic Pi balance studies, urinary Pi excretion was increased in WT and claudin-12 KO mice consuming the inorganic Pi diet **(Figure 3.8 B, D, F, H)**. We assessed 24 hr urinary Pi excretion during the first and last day in metabolic cages. During the first 24 hours, we observed a significant increase in Pi excretion in WT and claudin-12 KO mice receiving PFA on the organic P diet **(Figure 3.8 C)**, but not the inorganic Pi

diet **(Figure 3.8 D)**. While we predicted inhibition of Npt2b would reduce intestinal Pi absorption in mice fed the organic P diet to a greater extent than the inorganic Pi diet, the opposite was observed at 24 hours. As PFA also inhibits Npt2a/c, this result is consistent with PFA being absorbed systemically and enhancing renal Pi excretion by inhibiting renal Pi reabsorption (Loghman-Adham, 1996) thus confounding our ability to interpret the intestinal specific effects. Further, the lack of increase in urinary Pi excretion with the addition of PFA to the inorganic Pi diet may be due to reduced PFA bioavailability. Given Pi and PFA are both absorbed by Nptb, presumably a greater free luminal Pi concentration on an inorganic Pi diet would compete for binding and intestinal absorption of PFA (Swaan & Tukker, 1995).

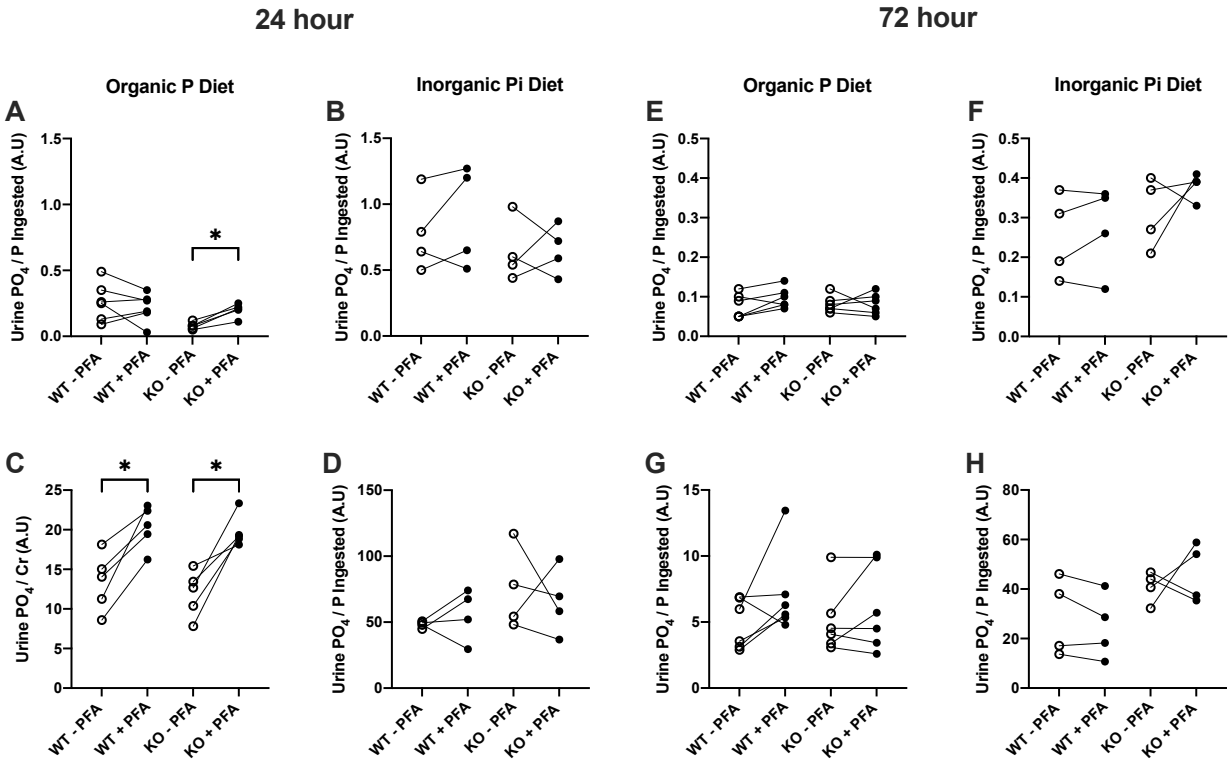

Figure 3.8. Effect of phosphonoformate (PFA) on urinary PO_4^{3-} excretion in wildtype and claudin-12 KO mice. Mice were placed into metabolic cages for 3 days on an organic P (0.7% P; n = 5 WT, 5 KO) or inorganic Pi (0.7% P; n = 4 WT, 4 KO) diet and subsequently received the same diet supplemented with PFA (3.75 mg / g chow) for an additional 3 days. 24-hour urine PO_4^{3-} excretion was measured for the first **(A-D)** and last **(E-H)** day the mice were in metabolic cages for each treatment. Urine PO_4^{3-} excretion was normalized to amount ingested **(A, B, E, F)** or urine creatinine **(C, D, G, H)** and the raw values are presented; asterisks indicate a statistical difference between conditions (student's paired t-test; *$P < 0.05$).

Table 3.5: *Metabolic cage data for PFA metabolic cage study.*

	Organic P Diet			Inorganic Pi Diet		
	No drug	**PFA**	***P*-value**	**No drug**	**PFA**	***P*-value**
Wild-type						
Sample size (n)	6	6		4	4	
Body Weight (g)	30.46 ± 2.61	31.28 ± 2.36	0.57	33.81 ± 3.07	33.63 ± 3.17	0.83
Chow eaten (g/g body weight)	0.15 ± 0.04	0.15 ± 0.04	0.94	0.14 ± 0.03	0.13 ± 0.02	0.69
Water intake (mL/24 hour/g body weight)	0.14 ± 0.04	0.12 ± 0.02	0.08	0.07 ± 0.02	0.10 ± 0.03	0.19
Urine volume (mL/24 hour/g body weight)	0.03 ± 0.01	0.03 ± 0.01	0.53	0.02 ± 0.01	0.03 ± 0.02	0.45
Fecal excretion, wet (g/24 hour/g body weight)	0.05 ± 0.02	0.05 ± 0.01	0.47	0.01 ± 0.002	0.01 ± 0.002	0.81
Cldn-12 KO						
Sample size (n)	6	6		4	4	
Body Weight (g)	30.70 ± 3.77	30.95 ± 3.03	0.70	27.68 ± 2.52	27.95 ± 3.19	0.79
Chow eaten (g/g body weight)	0.15 ± 0.04	0.17 ± 0.03	0.36	0.19 ± 0.02	0.19 ± 0.04	0.74
Water intake (mL/24 hour/g body weight)	0.13 ± 0.02	0.13 ± 0.03	0.91	0.12 ± 0.03	0.14 ± 0.04	0.13
Urine volume (mL/24 hour/g body weight)	0.03 ± 0.01	0.02 ± 0.02	0.27	0.04 ± 0.01	0.05 ± 0.02	0.34
Fecal excretion, wet (g/24 hour/g body weight)	0.05 ± 0.02	0.06 ± 0.02	0.33	0.02 ± 0.002	0.02 ± 0.004	0.63

Data presented as mean ± SD compared by paired t-test, or as median (IQR) compared by Mann-Whitney test.

As we hypothesized that PFA was absorbed systemically leading to enhanced renal Pi excretion on the organic Pi diet, likely through inhibition of Npt2a and Npt2c, we assessed Pi bioavailability. This measurement utilizes fecal Pi excretion and therefore avoids the potential confounding effects of PFA on renal Pi excretion. Consistent with the known differences in bioavailability between organic and inorganic Pi (Cupisti & Kalantar-Zadeh, 2013; Gutierrez et al., 2015) and our previous balance studies, we observed a greater bioavailability in WT and claudin-12 KO mice consuming the inorganic Pi diet **(Figure 3.9 B)**. However, coadministration of PFA with either diet did not alter Pi bioavailability **(Figure 3.9 A-B)**. There are a few potential explanations for the unaltered bioavailability. As fecal Pi excretion was ~40% on the organic P diet, large changes in intestinal absorption are required to be detected as intestinal loss. Alternatively, PFA may be enhancing intestinal paracellular Pi transport. To investigate if PFA was altering the permeability of tight junctions to Pi thereby enhancing paracellular Pi transport, bionic dilution potential experiments were conducted.

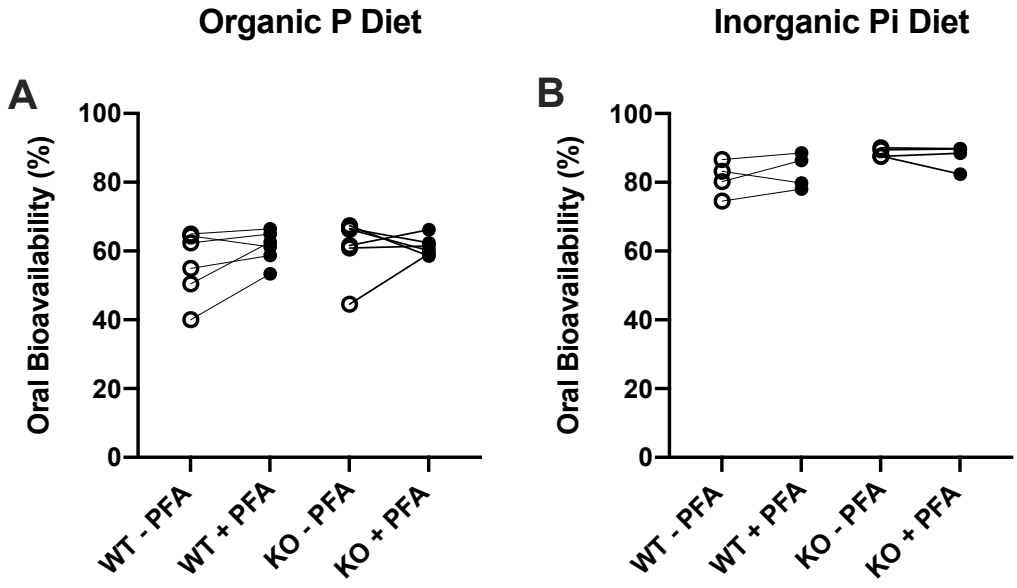

Figure 3.9. Phosphonoformate (PFA) does not alter oral P bioavailability in wildtype and claudin-12 KO mice. Mice were placed into metabolic cages for 3 days on an organic P (0.7% P; n = 5 WT, 5 KO) or inorganic Pi (0.7% P; n = 4 WT, 4 KO) diet and subsequently received the same diet supplemented with PFA (3.75 mg / g chow) for an additional 3 days; the treatment order was reversed for half the mice. Feces were collected for the first 24 hours for each treatment condition and PO_4^{3-} bioavailability determined as a % of P consumed. Raw values are presented for each animal and a student's paired t-test used to compare treatment conditions within each genotype.

3.4.2 PFA does not alter paracellular Pi permeability in caco2-bbe cells

To assess the effect of PFA on tight junction Pi permeability, we conducted bi-ionic diffusion potential measurements in Ussing chambers across caco2 brush boarder epithelial (bbe) monolayers. At baseline, we did not observe any differences in the transepithelial electrical resistance (TEER) between monolayers prior to treatment with vehicle or PFA **(Figure 3.10 A)**. Paired experiments were then conducted, first measuring the permeability characteristics of the monolayers without any treatment then repeating with the addition of PFA (5 mM) or vehicle (H_2O). Throughout the course of the experiment, the TEER decreased in both the vehicle and PFA treated groups so for all parameters measured we assessed differences by calculating the % change from baseline. First, a Na^+ to Cl^- dilution potential was imposed by adding a low-Na^+ solution (pH 8.0) to the apical side and we measured the diffusion potential across the monolayer. The relative permeability of Na^+ to Cl^- (pNa^+/ pCl^-) was calculated using the Goldman-Hodgkin-Katz (GHK) equation along with the resitance and we did not observe any alterations to the % change from baseline between PFA and vehicle treated monolayers **(Figure 3.10 B)**. We then imposed a HPO_4^{2-} to Cl^- diffusion potential across the monolayer using a high Pi solution (pH 8.0) and calculated the relative permeability of Pi to Cl^- ($pHPO_4^{2-}$/pCl^-). We did not observe any alterations in $pHPO_4^{2-}$ / pCl^- between treatment conditions **(Figure 3.10 E)**. Using pNa^+ / pCl^- , $pHPO_4^{2-}$ / pCl^- and the resistance we calculated the absolute permeability of the monolayers to Na^+, Cl^- and HPO_4^{2-} and assessed the % change from baseline upon addition of PFA or vehicle. Consistent with the relative permeability ratios, we did not observe any alterations in the % change from baseline between treatment conditions for pNa^+, pCl^- or $pHPO_4^{2-}$ **(Figure 3.10 C, D, F)**. Together, this suggests that PFA does not alter the permeability characteristics of caco2bbe monolayers. Further, this does not provide support for PFA

enhancing paracellular Pi transport and increasing Pi bioavailability. The colon is also permeable to Pi and contributes to Pi absorption (Knöpfel, 2017; Saurette & Alexander, 2019), therefore altered Pi transport in this segment may contribute to the maintained bioavailability in PFA treated animals, however, this was not assessed.

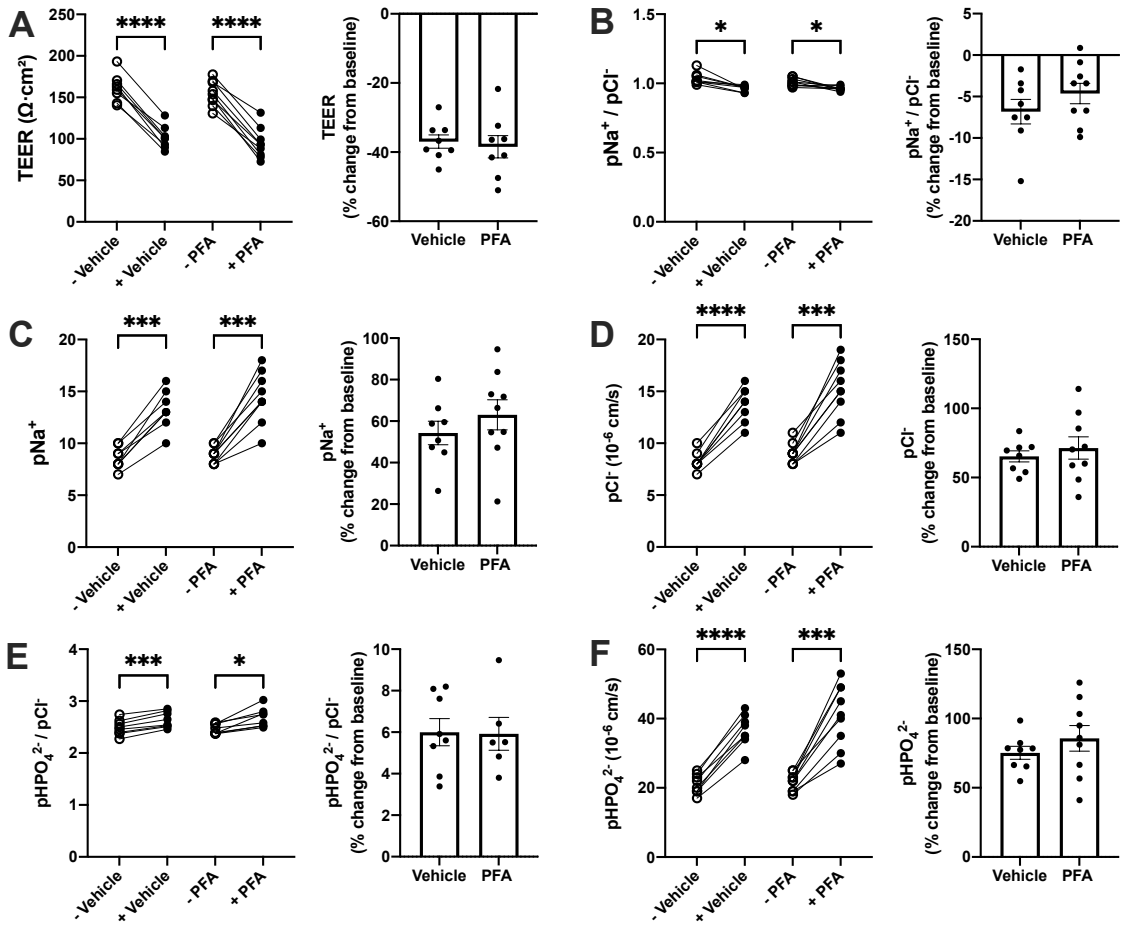

Figure 3.10. Phosphonoformate (PFA) does not alter paracellular HPO_4^{2-} transport in Caco-2 bbe cells. Effect of PFA (5 mM) or vehicle (water) at pH 8.0 on **(A)** TEER, **(B)** sodium to chloride permeability (pNa^+ / pCl^-), **(C)** sodium permeability (pNa^+), **(D)** chloride permeability (pCl^-), **(E)** Pi to chloride permeability ($pHPO_4^{2-}$ / pCl^-) and **(F)** Pi permeability ($pHPO_4^{2-}$) in caco-2 bbe cells mounted in Ussing chambers. Raw values are presented and the % change from baseline for each parameter; asterisks indicate a statistical difference between conditions (student's paired t-test; *P < 0.05, **P < 0.01, ***P < 0.001, ****P < 0.0001).

3.4.3 The transcellular pathway meditates intestinal absorption of Pi from organic sources

Given the likely systemic absorption of PFA and its confounding effects on renal Pi reabsorption, we repeated the PFA balance study instead with the addition of NTX-1942 (NTX), a non-absorbable Npt2b inhibitor. In brief, WT mice were placed into metabolic cages for 3 days on either the organic P (0.7% wt/wt P, 1% Ca^{2+} wt/wt) or inorganic Pi diet (0.7% wt/wt P, 1% Ca^{2+} wt/wt). After two days in their static cages, the mice were placed back into metabolic cages on either the organic or inorganic Pi diet, with the addition of NTX (6 mg / g chow). There were no alterations in body weight, chow or water intake (Table 3.6). Consistent with the reported increased bioavailability of inorganic Pi (Cupisti & Kalantar-Zadeh, 2013; Saurette & Alexander, 2019) and with our previous balance study **(Figure 3.1)** we observed significantly increased urinary Pi excretion on the inorganic Pi diet (0.15 ± 0.02; urine Pi/P ingested) relative to the organic P diet (0.06 ± 0.02) **(Figure 3.11 A)**. Coadministration of NTX in each diet led to a significant reduction in urinary Pi excretion on the organic P diet, but not the inorganic Pi diet **(Figure 3.11)**. As Npt2b is responsible for the majority of transcellular Pi absorption (Sabbagh et al., 2009; Saurette & Alexander, 2019), this is consistent with liberated Pi from organic sources being absorbed predominantly by the transcellular pathway. Consistent with reduced urine Pi excretion on the organic P diet supplemented with NTX, we observed a significant reduction in Pi bioavailability on the organic P diet, but not the inorganic Pi diet **(Figure 3.11)**. Together, inhibiting Npt2b decreases Pi bioavailability on the organic Pi diet and reduces urinary Pi excretion. This provides support for the hypothesis that Pi liberated from organic sources (*i.e.* protein) is absorbed *via* the secondary active transporter, Npt2b. The reduced absorption of Pi with NTX administration on the organic P diet led to significantly increased wet fecal mass (Table 3.6) compared with no NTX. This may be due to luminal water retention as there is a

compensatory reduction in urine volume when mice are treated with NTX on the organic P diet (Table 3.6).

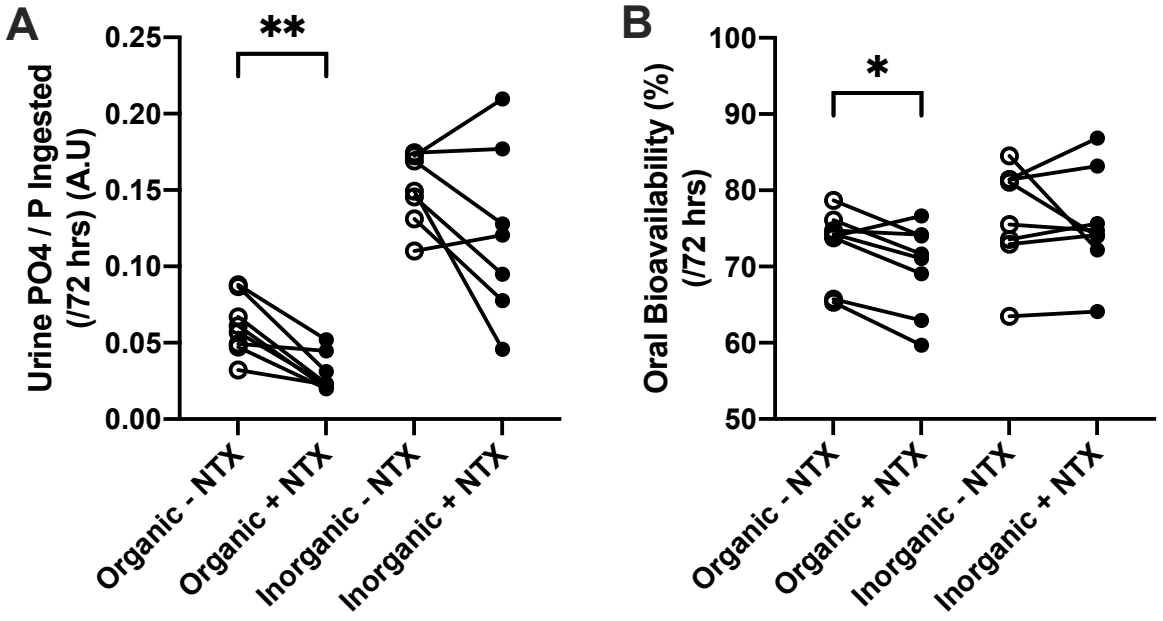

Figure 3.11. NTX1942 reduces urine Pi and oral P bioavailability in wildtype mice on an organic P diet. Mice 10-15 weeks old were placed into metabolic cages for 3 days on an organic P (0.7% P; n = 8 per group) or inorganic Pi (0.7% P; n = 8 per group) diet and subsequently received the same diet supplemented with PFA (6 mg / g chow) for an additional 3 days; the treatment order was reversed for half the mice. **(A)** Urine PO_4^{3-} excretion normalized to amount ingested. **(B)** Bioavailability as a % of P consumed. Raw values are presented; asterisks indicate a statistical difference between conditions (student's paired t-test; *P < 0.05, **P < 0.01).

Table 3.6: *Metabolic cage data for NTX-1942 metabolic cage study.*

	Organic P Diet			**Inorganic Pi Diet**		
	No drug	**NTX-1942**	***P*-value**	**No drug**	**NTX-1942**	***P*-value**
Sample size (n)	8	8		8	8	
Body Weight (g)	27.60 ± 3.79	27.14 ± 3.56	0.66	26.37 ± 2.89	26.74 ± 3.07	0.66
Chow eaten (g/g body weight)	0.15 ± 0.05	0.16 ± 0.03	0.30	0.14 ± 0.03	0.15 ± 0.03	0.25
Water intake (mL/72 hour/g body weight)	0.15 ± 0.04	0.15 ± 0.04	0.58	0.13 ± 0.05	0.12 ± 0.03	0.88
Urine volume (mL/72 hour/g body weight)	0.028 ± 0.010	0.015 ± 0.010	<0.0001	0.036 ± 0.012	0.030 ± 0.018	0.16
Fecal excretion, wet (g/72 hour/g body weight)	0.048 ± 0.018	0.058 ± 0.013	0.04	0.012 ± 0.003	0.014 ± 0.003	0.22

Data presented as mean ± SD compared by unpaired t-test.

Chapter 4 : Claudin-2 Results

Claudin-2 results are modified from published work in Curry JN, *Saurette M* et al., *J Clin Invest.* 2020 Apr 1, 130 (4): 1948-1960

4.1 Delineating the role of claudin-2 in Ca^{2+} homeostasis

4.1.1 Claudin-2 KO mice have hypercalciuria due a defect in proximal tubule Ca^{2+} reabsorption

Claudin-2 is a cation permeable claudin expressed in the gut and renal proximal tubule. Claudin-2 KO mice were first described in 2010, where they were mentioned in passing to have hypercalciuria (Muto et al, 2010). Thus, to understand the role of claudin-2 in maintaining Ca^{2+} homeostasis we first sought to characterize the overall Ca^{2+} balance of claudin-2 KO mice. To do this, we conducted a metabolic balance study by placing WT and claudin-2 KO mice into metabolic cages on a diet containing normal dietary Ca^{2+} (0.95%, PicoLab) for three days. There were no significant differences between WT and claudin-2 KO mice in body weight, water intake, urine volume or fecal excretion (Table 4.1). However, female claudin-2 KO mice ate significantly less than WT mice. Claudin-2 KO mice did not have alterations in their 24 hr urine creatinine, consistent with other reports that whole kidney GFR is unaltered in these mice (Pei et al., 2016) (Table 4.2). As serum Ca^{2+} was also unchanged in the claudin-2 KO mice, this suggests the filtered load of Ca^{2+} is unchanged. However, claudin-2 KO mice have a significantly increased urine Ca^{2+}/ creatinine and fractional excretion of Ca^{2+} ($FECa^{2+}$) (Table 4.2). Therefore, the claudin-2 KO mice display hypercalciuria. Because claudin-2 is predominately expressed in the proximal tubule and is permeable to Ca^{2+} (Yu et al., 2009) this infers the hypercalciuria observed is due to impaired paracellular Ca^{2+} transport in the proximal tubule.

Table 4.1: *Metabolic cage data for wildtype and claudin-2 KO mice on a standard lab chow.*

	Male			**Female**		
	Wildtype	**Cldn-2 KO**	***P*-value**	**Wildtype**	**Cldn-2 KO**	***P*-value**
Sample size (n)	5	7		6	6	
Body Weight (g)	35.93 ± 2.41	36.49 ± 3.72	0.77	24.44 ± 3.21	29.80 ± 2.20	0.007
Chow eaten (g/g body weight)	0.11 ± 0.03	0.12 ± 0.04	0.52	0.16 ± 0.03	0.12 ± 0.03	0.03
Water intake (mL/24 hour/g body weight)	0.12 ± 0.04	0.15 ± 0.05	0.27	0.18 ± 0.03	0.14 ± 0.04	0.12
Urine volume (mL/24 hour/g body weight)	0.03 ± 0.02	0.05 ± 0.02	0.36	0.02 ± 0.01	0.03 ± 0.01	0.24
Fecal excretion, wet (g/24 hour/g body weight)	0.04 ± 0.02	0.05 ± 0.02	0.58	0.07 ± 0.02	0.05 ± 0.01	0.07

Data presented as mean ± SD compared by student's unpaired t-test.

Table 4.2: *Serum, urine and fecal parameters for wildtype and claudin-2 KO mice on a standard lab chow.*

Parameter	Wildtype	Cldn-2 KO	*P*- value
Sample size (n)	11	13	
Serum			
Calcium (mM)	1.92 (1.86-1.98)	1.98 (1.81-2.07)	0.50
Urine			
Creatinine (µmol /24 hr)	8.23 ± 3.99	9.50 ± 2.87	0.37
Ca^{2+}/ Creatinine (/72 hr)	0.32 (0.26-0.38)	0.53 (0.47-0.77)	<0.0001
FE_{Ca}	1.54 ± 0.66	3.69 ± 1.63	0.0008
Mg^{2+}/ Creatinine (/72 hr)	28.72 (11.24-38.90)	43.42 (19.72-80.47)	0.01
Feces			
Total Ca^{2+} (mmol / 72 hr)	0.58 ± 0.24	0.59 ± 0.18	0.83
Ca^{2+} Taken (mmol / 72 hr)	0.83 ± 0.27	0.85 ± 0.23	0.77
Bioavailability (%)	24.70 ± 15.17	38.03 ± 13.59	0.03

Data presented as mean ± SD compared by unpaired t-test, or as median (IQR) compared by Mann-Whitney test. N= 5 male WT, 6 female WT; N= 6 male KO and 7 female KO.

4.1.2 Claudin-2 KO mice do not have altered bone mineral metabolism

As the claudin-2 KO mice had hypercalciuria with no alterations in their serum Ca^{2+} (Table 4.2) it appeared they may be compensating for a negative calcium balance. Therefore, we assessed the tibia of WT and claudin-2 KO mice using micro-computed tomography (μCT) to investigate if enhanced bone resorption in the null mice was responsible for maintaining normocalcemia. Visual inspection did not reveal gross morphological differences between WT and claudin-2 KO tibia **(Figure 4.1)**. Further morphometric analysis by μ-CT of the cortical and trabecular bone did not reveal any significant differences in the microarchitecture (Table 4.3) suggesting there are no alterations in bone mineral metabolism. Additionally, we did not observe altered bone mineral density in either the cortical or trabecular bone suggesting enhanced bone resorption / reduced deposition is not responsible for maintaining serum Ca^{2+} levels. Consistent with this, PTH and vitamin D_3 were unaltered in the claudin-2 KO mice (Curry et al., 2020) suggesting the null mice are not in a negative calcium balance despite the renal Ca^{2+} leak.

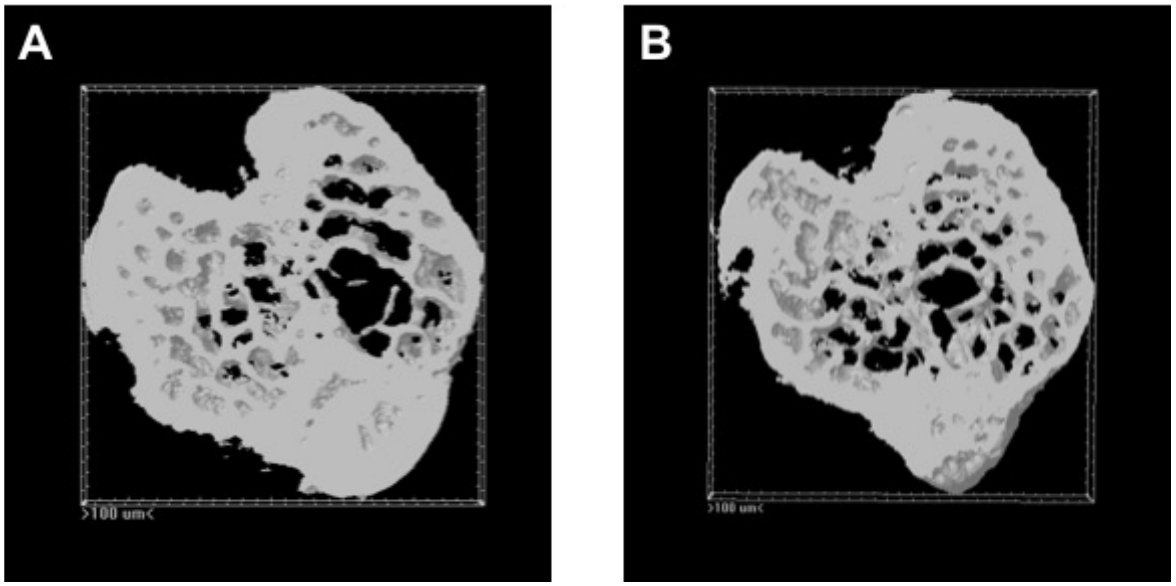

Figure 4.1. Representative images of a 3-dimension reconstruction of the tibia region of interests. A 3-D rendering of the region of interest analyzed was created in CTvol (Bruker, Skyscan) for male A) wild-type and B) Claudin-2 KO mice.

Table 4.3: *Quantitative micro-CT analysis of tibia of 12-week-old wildtype and claudin-2 KO mice*

	Male			Female		
	Wildtype	**Cldn-2 KO**	***P*-value**	**Wildtype**	**Cldn-2 KO**	***P*-value**
Sample size (n)	5	7		6	6	
Trabecular Bone						
BV (mm^3)	0.33 ± 0.06	0.30 ± 0.04	0.94	0.27 ± 0.04	0.31 ± 0.03	0.90
TV (mm^3)	2.52 ± 0.34	2.64 ± 0.78	0.98	2.52 ± 0.09	2.22 ± 0.16	0.82
BV/TV (%)	14.51 ± 4.10	12.33 ± 1.89	0.88	10.78 ± 0.28	13.87 ± 1.15	0.72
TS (mm^2)	16.46 ± 1.39	17.00 ± 1.29	0.98	15.78 ± 0.50	14.15 ± 0.89	0.70
BS (mm^2)	17.28 ± 3.17	15.21 ± 1.69	0.84	13.92 ± 0.42	15.05 ± 1.32	0.96
BS/BV (1/mm)	52.94 ± 1.41	51.26 ± 1.03	0.87	51.62 ± 1.67	49.47 ± 2.07	0.76
BS/TV (1/mm)	7.56 ±2.03	6.25 ± 0.91	0.81	5.54 ± 0.10	6.80 ± 0.52	0.81
SMI	1.77 ± 0.14	1.79 ± 0.12	0.99	1.78 ± 0.12	1.64 ± 0.12	0.84
Tb.Th (mm)	0.069 ± 0.002	0.072 ± 0.002	0.86	0.074 ± 0.003	0.076 ± 0.004	0.97
Tb.N (1/mm)	2.06 ± 0.55	1.71 ± 0.26	0.81	1.45 ± 0.03	1.83 ± 0.16	0.77
Tb.Sp (mm)	0.281 ± 0.027	0.304 ± 0.038	0.67	0.314 ± 0.003	0.288 ± 0.007	0.60
BMD (g/cm^3)	0.47 ± 0.01	0.54 ± 0.01	0.09	0.60 ± 0.02	0.58 ±0.02	0.80
Cortical Bone						
BV (mm^3)	0.57 ± 0.05	0.65 ± 0.05	0.51	0.62 ± 0.02	0.69 ±0.03	0.63
Ct.Th (mm)	0.120 ± 0.006	0.129 ± 0.007	0.60	0.148 ± 0.004	0.157 ± 0.004	0.63

Data presented as mean ± SEM. Groups were compared by one-way ANOVA and Tukey's HSD test for multiple comparison ($p < 0.05$).

4.1.3 Claudin-2 KO mice do not have altered expression of intestinal Ca^{2+} transport mediators

Given the absence of reduced bone mineral density but hypercalciuria we next assessed fecal calcium excretion. The claudin-2 KO mice displayed increased Ca^{2+} bioavailability (38.03 ± 13.59 %) compared with WT mice (24.70 ± 15.17 %) (P = 0.03, Table 4.2), thereby compensating for urine loss. Therefore, in addition to the renal Ca^{2+} leak, net increased intestinal Ca^{2+} absorption either contributed to the hypercalciuria or was in response to help maintain serum Ca^{2+}. To examine these possibility, Curry *et al* placed claudin-2 KO animals on a Ca^{2+} deficient diet (<0.01 % Ca^{2+}) for three days in metabolic cages and found this reduced the $FECa^{2+}$ compared to the regular Ca^{2+} diet but was still increased relative to WT mice (2020). This is consistent with a primary renal leak and compensatory intestinal calcium reabsorption.

To elucidate the mechanism by which the claudin-2 KO mice increased net intestinal Ca^{2+} absorption, we measured the expression of intestinal Ca^{2+} transport mediators throughout the small intestine and proximal colon. In the duodenum, we did not observe alterations in expression of the transcellular Ca^{2+} transport machinery *TRPV6*, *S100g* (Calbindin-D9k), *NCX* or *Atp2b1* (PMCA1b) **(Figure 4.2 A-D)**. Further, expression of claudin-12 and -15 was unaltered. This suggests transcellular Ca^{2+} transport in the duodenum was not increased. Similarly, the expression of claudin-12 and -15 in the jejunum **(Figure 4.3)** and ileum **(Figure 4.4)** was not altered in claudin-12 KO mice suggesting enhanced transcription of the main claudins conferring Ca^{2+} permeability in the intestine did not facilitate the net increased intestinal Ca^{2+} absorption. The proximal colon also contributes to Ca^{2+} absorption (Hylander et al., 1990) and is acutely regulated by the CaSR (J. J. Lee et al., 2019) suggesting a role of this segment in intestinal Ca^{2+} transport. Therefore, we assessed the expression of transcellular Ca^{2+} mediators in this segment and did not observe any alterations in *TRPV6*, *S100g* (Calbindin-D9k), *NCX* or *Atp2b1*

(PMCA1b) **(Figure 4.5 C-E).** Further, there were no alteration claudin-12 expression in this segment **(Figure 4.5 A)**.

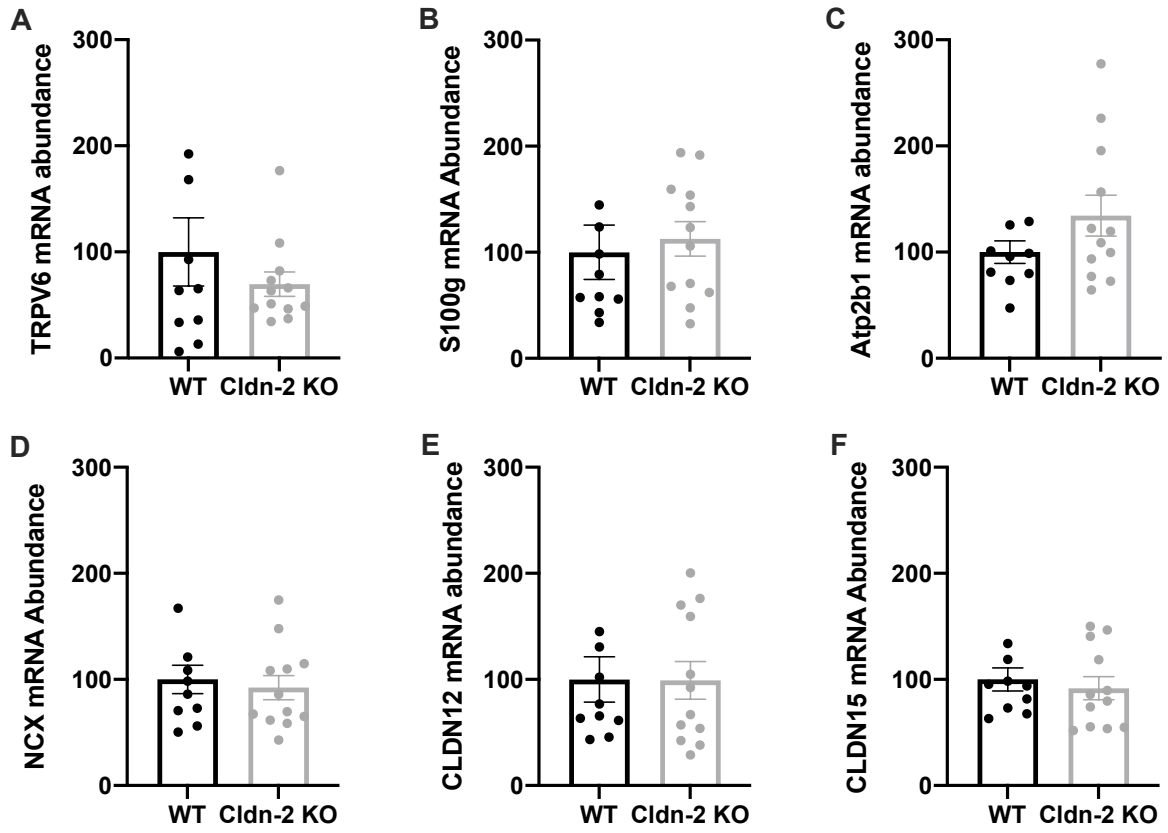

Figure 4.2. Expression of intestinal calcium transporters in the duodenum of Cldn-2 KO mice and wild-type controls. (Figure adapted from Curry and *Saurette* et al 2020). Quantitative RT-PCR was used to measure the expression of calcium transport proteins in the duodenum of wild-type (WT) and Cldn-2 KO mice. Expression of **(A)** TRPV6 ($P > 0.99$, Mann-Whitney), **(B)** S100g encoding CalbD-9k ($P = 0.34$, Mann-Whitney), **(C)** Atp2b1 encoding PMCA1b ($P = 0.15$, student's unpaired t-test), **(D)** NCX encoding sodium-chloride exchanger ($P = 0.66$, student's unpaired t-test), **(E)** Claudin-12 ($P = 0.92$, Mann-Whitney) and **(F)** Claudin-15 ($P = 0.45$, Mann-Whitney). Results are normalized to *Ezrin* and expressed relative to WT. Data presented as mean ± SD; n = 10 WT and 12 Cldn-2 KO.

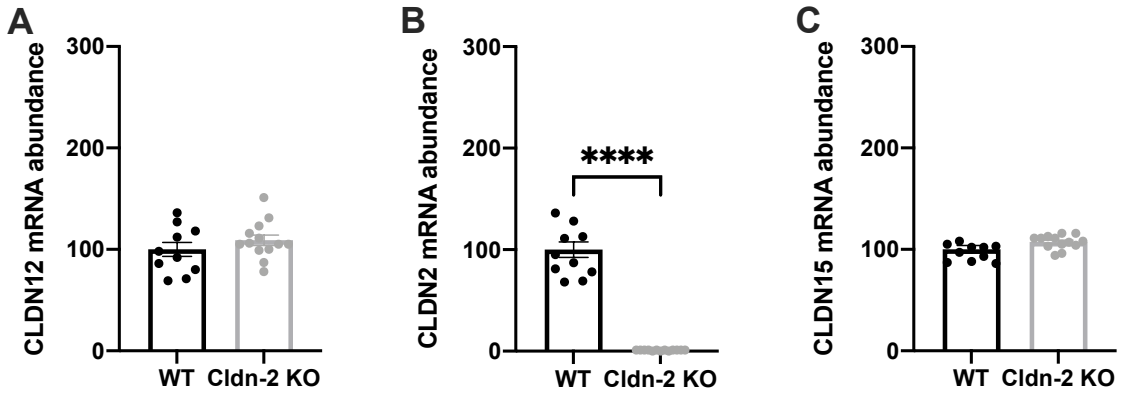

Figure 4.3. Expression of intestinal calcium transporters in the jejunum of Cldn-2 KO mice and wild-type controls. (Figure adapted from Curry, *Saurette* et al 2020). Quantitative RT-PCR was used to measure the expression of paracellular calcium transport proteins in the jejunum of wild-type (WT) and Cldn-2 KO mice. Expression of **(A)** Claudin-12 (P = 0.29, student's unpaired t-test), **(B)** Claudin-2 (P < 0.0001, Mann-Whitney non-parametric test) and **(C)** Claudin-15 (P = 0.08, student's unpaired t-test). Results are normalized to *Ezrin* and expressed relative to WT. Data presented as mean ± SD; n = 11 WT (5 male and 6 female) and 13 Cldn-2 KO (6 male and 7 female); ****P < 0.0001.

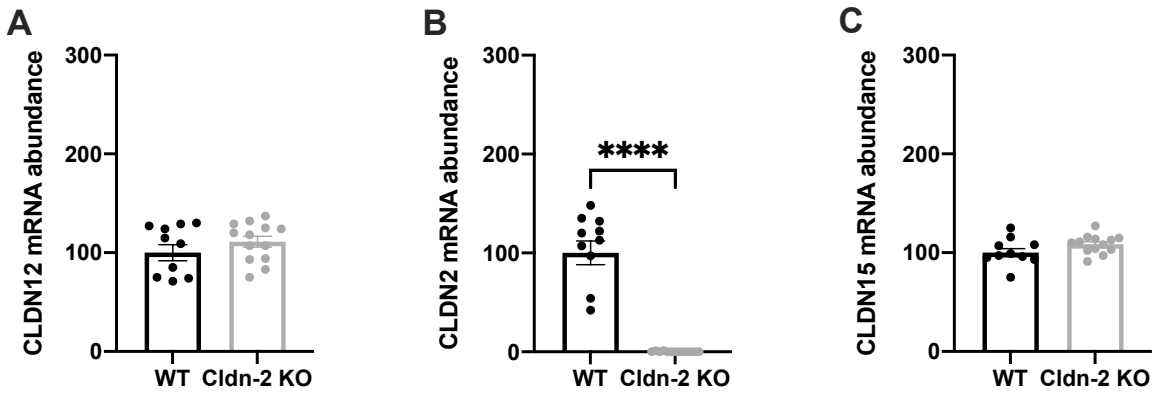

Figure 4.4. Expression of intestinal calcium transporters in the ileum of Cldn-2 KO mice and wild-type controls. (Figure adapted from Curry, *Saurette* et al 2020). Quantitative RT-PCR was used to measure the expression of paracellular calcium transport proteins in the ileum of wild-type (WT) and Cldn-2 KO mice. Expression of **(A)** Claudin-12 (P = 0.25, student's unpaired t-test), **(B)** Claudin-2 (P < 0.0001, Mann-Whitney non-parametric test) and **(C)** Claudin-15 (P = 0.08, student's unpaired t-test). Results are normalized to *Ezrin* and expressed relative to WT. Data presented as mean ± SD; n = 11 WT (5 male and 6 female) and 13 Cldn-2 KO (6 male and 7 female); ****P < 0.0001.

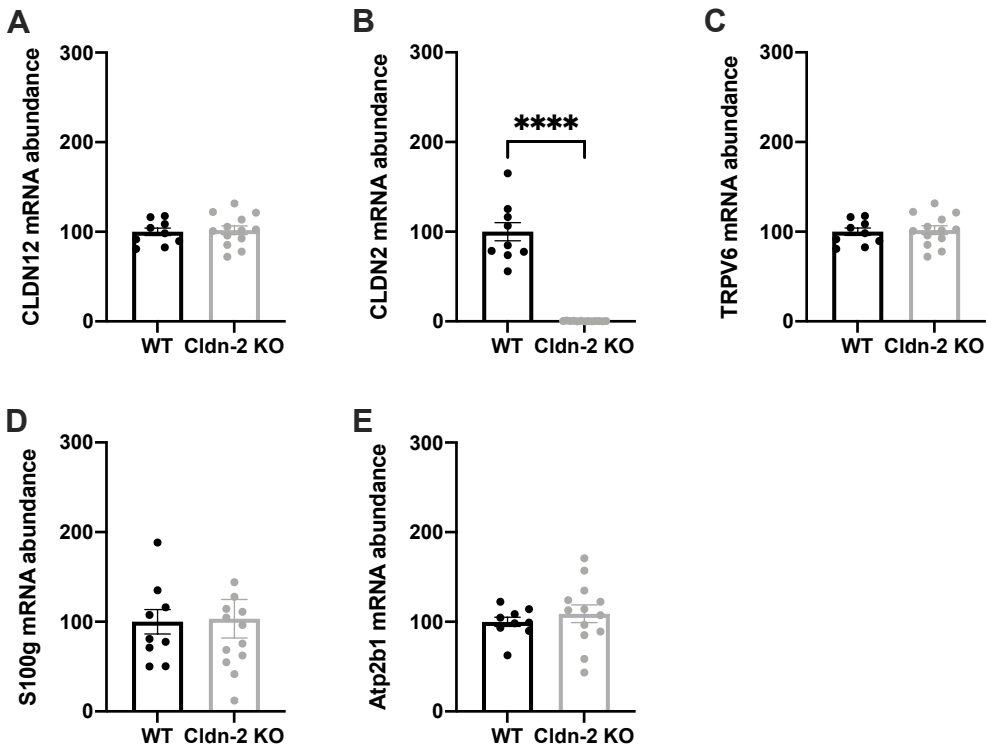

Figure 4.5. Expression of intestinal calcium transporters in the proximal colon of Cldn-2 KO mice and wild-type controls. (Figure adapted from Curry, *Saurette* et al 2020). Quantitative RT-PCR was used to measure the expression of calcium transport proteins in the ileum of wild-type (WT) and Cldn-2 KO mice. Expression of **(A)** Claudin-12 ($P = 0.78$, student's unpaired t-test), **(B)** Claudin-2 ($P < 0.0001$, Mann-Whitney non-parametric test), **(C)** TRPV6 ($P = 0.78$, student's unpaired t-test), **(D)** S100g encoding Calbindin-d9K ($P = 0.90$, student's unpaired t-test) and **(E)** Atp2b1 encoding PMCA1b ($P = 0.47$, student's unpaired t-test). Results are normalized to *GAPDH* and expressed relative to WT. Data presented as mean ± SD; n = 10 WT (5 male and 5 female) and 13 Cldn-2 KO (6 male and 7 female); ****$P < 0.0001$.

4.1.4 Claudin-2 KO mice do not have altered Ca^{2+} permeability in the ileum

While we did not observe any alterations in mRNA expression of claudins involved in Ca^{2+} absorption throughout the small intestine and colon, we investigated if claudin-2 KO mice had altered paracellular Ca^{2+} permeability and thus transport, *ex-vivo*. To assess if enhanced paracellular Ca^{2+} transport was responsible for the increased net intestinal Ca^{2+} absorption, we mounted ileal tissue in Ussing chambers and conducted a bionic dilution potential experiment in WT and claudin-12 KO mice. The majority of Ca^{2+} absorption in the small intestine occurs in this segment *in-vivo* (Duflos et al., 1995) and is entirely paracellular (Beggs & Alexander, 2017). The TEER was not significantly different between WT (46.06 ± 6.07 Ω•cm^2) and the claudin-2 KO mice (39.34 ± 12.38 Ω•cm^2) in this segment (Table 4.4). We first imposed a Na^+ to Cl^- dilution potential and measured the diffusion potential across the ileum. The relative permeability of Na^+ to Cl^- (pNa^+/ pCl^-) was calculated using the GHK equation. We did not observe any differences in pNa^+/ pCl^- (Table 4.4). We then imposed a Ca^{2+} to Na^+ dilution potential and calculated the relative permeability of Ca^{2+} to Na^+ (pCa^{2+} / pNa^+) which was unaltered in the KO mice. Using pNa^+/ pCl^- and pCa^{2+} / pNa^+ and the TEER, we calculated the absolute permeabilities of Na^+, Cl^- and Ca^{2+}. All these parameters were unaltered between genotypes (Table 4.4) suggesting that in the ileum paracellular Ca^{2+} transport is not enhanced in the claudin-2 KO mice, consitent with unaltered Ca^{2+} efflux from ileal gut sacs in claudin-2 KO mice (Curry et al., 2020).

Additional experiments conducted by Curry *et al* determined that pCa^{2+} was unaltered in all small intestinal segments (2020). In contrast, everted sacs of proximal colon demonstrated reduced efflux when claudin-2 was deleted and pCa^{2+} across the proximal colon was also reduced (Curry et al., 2020). This led to the conclusion that claudin-2 is a Ca^{2+} permeable pore in

the intestine and that its removal reduced Ca^{2+} secretion in the proximal colon leading to a net increased intestinal Ca^{2+} absorption.

Table 4.4: *Calcium permeability in the ileum of wildtype and Cldn-2 KO mice.*

	Wildtype	**Cldn-2 KO**	***P*- value**
Sample size (n)	3	3	
TEER (Ω*cm^2)	46.06 ± 6.07	39.34 ± 12.38	0.44
pNa^+/ pCl^-	2.51 ± 0.57	3.14 ± 0.91	0.36
pNa^+ (cm/s x 10^{-4})	0.47 ± 0.07	0.68 ± 0.24	0.22
pCl^- (cm/s x 10^{-4})	0.20 ± 0.05	0.21 ± 0.05	0.78
pCa^{2+} / pNa^+	2.53 (2.31-2.54)	2.39 (2.06-2.40)	0.40
pCa^{2+} (cm/s x 10^{-4})	1.14 ± 0.14	1.49 ± 0.44	0.26

Ion permeabilities were determined from biionic dilution potential measurements in Ussing chambers using Ileal tissue from wildtype and Cldn-2 KO mice. Data is presented as mean ± SD compared by unpaired t-test ($p \leq 0.05$) or as median (IQR) compared by Mann-Whitney test. TEER, transepithelial electrical resistance; Px, transepithelial permeability to X.

Chapter 5 : Discussion

Claudin-2 discussion is modified from published work in Curry JN, *Saurette M* et al., *J Clin Invest.* 2020 Apr 1, 130 (4): 1948-1960

Claudin-12 is a cation permeable tight junction protein expressed in the epithelia of the gastrointestinal tract and the proximal tubule in the kidney, which is regulated by vitamin D_3 (Fujita et al., 2008). Previous studies performed in the Alexander Laboratory revealed that feeding claudin-12 KO mice synthetic diets with inorganic Pi and altered Ca^{2+} content, but not regular organic chow, resulted in increased urinary Pi excretion (Plain et al., 2020). This suggested that claudin-12 may block intestinal Pi absorption. Additionally, inhibition of NHE3 in the gastrointestinal tract by minimally absorbed small molecules (i.e. Tenapanor hydrochloride, SAR218034) enhances fecal Pi excretion and decreased urinary Pi excretion in healthy rodents (King et al., 2018; Linz et al., 2012; Spencer et al., 2014) and models of chronic kidney disease (CKD) (Labonte et al., 2015). Therefore, in this thesis we hypothesized that claudin-12 forms a paracellular Pi barrier. To test this hypothesis, the jejunum of WT and claudin-12 KO mice were dissected and mounted in Ussing chambers and we measured the permeability to Pi *ex-vivo* (N.B Npt2b is minimally expressed in this segment under normal dietary Pi conditions). Claudin-12 KO mice had a significantly increased pPi in this intestinal segment **(Figure 3.3 F)**, consistent with claudin-12 being a paracellular Pi barrier. This is also consistent with claudin-12 forming cation permeable pores (Fujita et al., 2008; Plain et al., 2020) as the charge selectivity in the first ECL, which allows permeation of cations, may be predicted to have the opposite effect on anions. Given claudin-12 behaves as a paracellular Pi blocker, we used the claudin-12 KO mouse model to investigate how the different types of Pi (*i.e.* organic P or inorganic Pi) are absorbed across the gastrointestinal tract.

Dietary phosphorus occurs as a mixture of organic phosphorus found in meat, poultry, fish and legumes (Kalantar-Zadeh et al., 2010), and inorganic phosphate found in sodium and potassium phosphate additives and preservatives. Unfortunately, inorganic Pi salts are frequently

found in a Western diet (Carrigan et al., 2014; Leon et al., 2013) and have a much higher bioavailability (> 80%) relative to P from organic sources. Diets with inorganic Pi therefore have a greater ability to contribute to the development of hyperphosphatemia, a problem commonly encounter by persons with CKD and ESRD (M. Shimada et al., 2019). In this clinical population as well as the general population, higher blood Pi is associated with cardiovascular disease and mortality (Dhingra et al., 2007; Gutierrez et al., 2015; Palmer et al., 2011). Despite the clinical relevance of understanding why the different forms of Pi have such different bioavailability, the mechanisms underpinning this difference are not understood. Therefore, it was a goal of this thesis to determine how organic and inorganic Pi are absorbed across the gastrointestinal tract to better understand the reason for differing bioavailability. Using the claudin-12 KO mouse model as a means to alter paracellular Pi transport and pharmacological inhibitors of Npt2b, the main Pi transporter in the intestine (Sabbagh et al., 2009), to manipulate the transcellular pathway, we provide evidence supporting our hypothesis that inorganic Pi is able to move down its concentration gradient *via* the paracellular pathway, while organic P requires a secondarily active process to be absorbed transcellularly. Evidence for this comes primarily from two observations: 1) Urine Pi excretion and bioavailability are increased in claudin-12 KO mice relative to wild-type mice when fed an inorganic Pi diet but not an organic P diet and 2) NTX-1942, a non-absorbable Npt2b inhibitor, decreased urine Pi excretion and bioavailability when animals consumed an organic P diet, but not inorganic Pi diet.

5.1 Proposed model for the different bioavailability of organic P and inorganic Pi

5.1.1 Inorganic Pi is absorbed predominantly via the paracellular pathway

We first developed two diets with the same total dietary P (0.7%) and matched closely for the other minerals and macronutrients (Table 2.1, 2.2). The "inorganic Pi" diet had a portion of the dietary P (0.3%, Table 2.1) supplemented from Pi salts, while the P in the "organic P" diet was solely from organic sources (0.4% total P from protein, 0.3% from phytate). Having a portion of the P in the inorganic Pi diet from protein avoids protein malnutrition, which would confound the results. Consistent with the reported increased bioavailability of inorganic Pi (Cupisti & Kalantar-Zadeh, 2013), the inorganic Pi diet had increased bioavailability in both male and female WT mice **(Figure 3.2)** and led to enhanced urinary Pi excretion **(Figure 3.1)** reflecting increased intestinal absorption. Importantly, the claudin-12 KO mice had a further increase in Pi bioavailability **(Figure 3.2)** and urinary Pi excretion **(Figure 3.1)** on the inorganic Pi, but not the organic P diet. As claudin-12 was determined to be a paracellular Pi blocker *ex-vivo* in Ussing chamber **(Figure 3.3 F)**, this suggests inorganic Pi is able to move down its electrochemical gradient from the gut lumen to blood along the paracellular pathway as deletion of a Pi barrier enhanced Pi absorption and urinary Pi excretion only on the inorganic Pi diet **(Figure 5.1)**. While claudin-12 is also expressed in the renal proximal tubule (Plain et al., 2020), it likely also behaves as a paracellular Pi barrier here, as proximal tubule Pi reabsorption is felt to occur only by the transcellular pathway (Kaufman & Hamburger, 1987). However, if claudin-12 reduces pPi in the PT, this would imply the KO mice would have enhanced renal Pi reabsorption. Thus, it is unlikely that deletion of claudin-12 in the kidney would enhance renal Pi excretion. However, microperfusion studies assessing Pi permeability in PTs of claudin-12 KO animals would be needed to definitively determine whether this is the case.

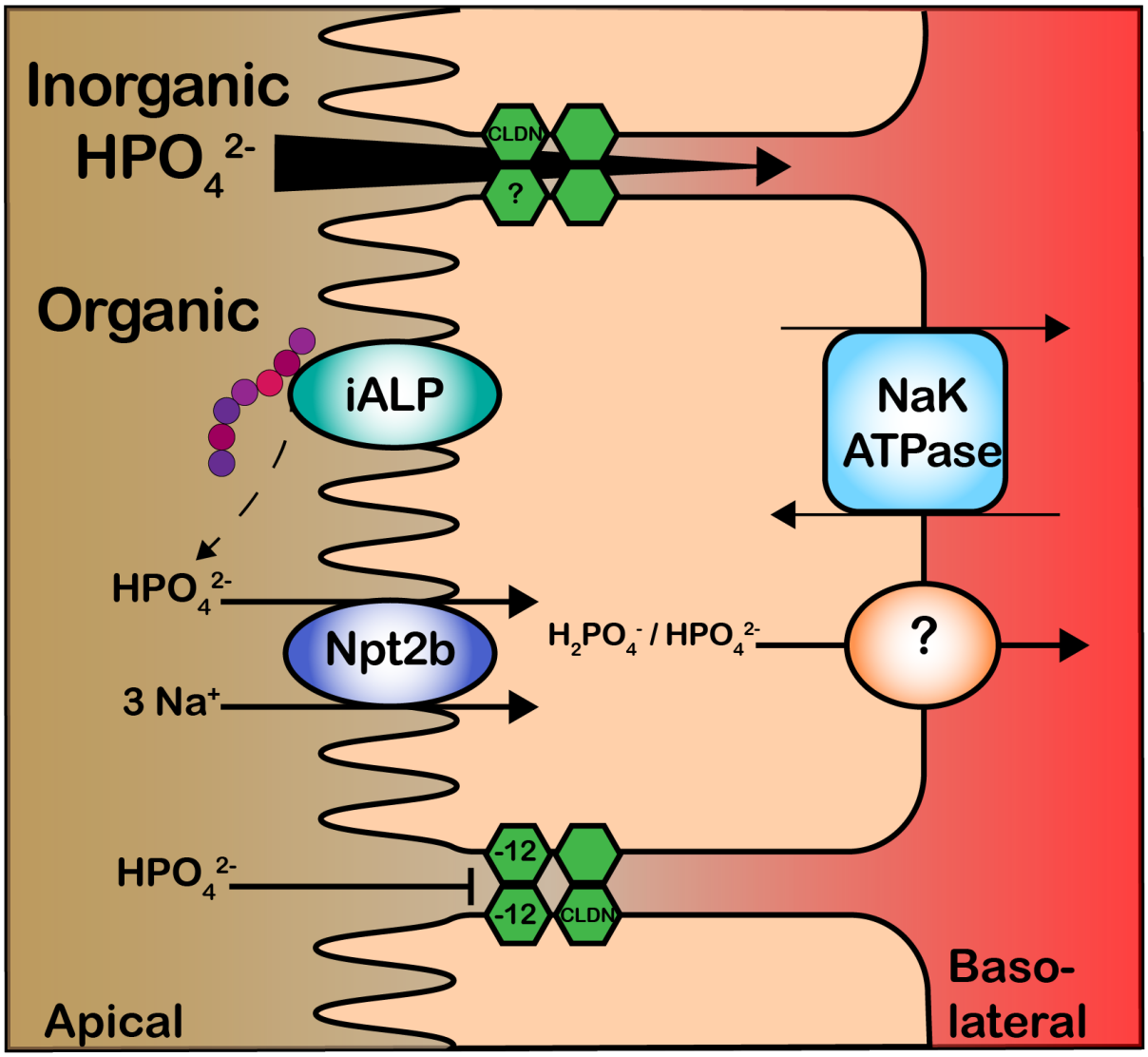

Figure 5.1. Proposed model for the difference in bioavailability between organic P and inorganic Pi. Pi must first be liberated from organic molecules (*i.e.* protein, casein) by intestinal alkaline phosphatase (iALP), leading to lower concentrations in the intestinal lumen which necessitates absorption using a secondarily active transport process (Npt2b). Conversely, inorganic Pi is unbound and free to move down its electrochemical gradient via the paracellular pathway (top-junction), although it is unclear which claudins create the Pi pore. Claudin-12 reduces the permeability of the epithelium to Pi (*i.e.* paracellular Pi blocker) and reduces intestinal absorption of Pi from inorganic, but not organic sources.

The alteration in urinary Pi excretion in the claudin-12 KO mice could also be a non-specific effect causing increased urinary excretion of other ions as well. However, we did not observe altered urinary excretion of other ions in claudin-12 KO mice (Table 3.2 and 3.3) on the inorganic Pi diet. The alterations in urinary excretion of Ca^{2+}, Mg^{2+} and K^{+} between diets is due to the altered mineral contents between diets (Table 2.1). Despite having the same Cl^{-} content in both diets, urine Cl^{-} excretion was significantly lower in WT mice on the inorganic Pi diet (Table 3.2). Cl^{-} may be moving through the same parcellular pore as Pi, therefore, increased free luminal Pi on the inorganic Pi diet may reduce the amount of Cl^{-} absorbed in WT mice when claudin-12 is present and blocking Pi absorption (Table 3.2). When claudin-12 is removed, this may provide an alternate route for Pi absorption normalizing intestinal Cl^{-} absorption and increasing urine Cl^{-} in the claudin-12 KO mice. Additionally, on an organic P diet, there is significantly decreased serum K^{+} in the claudin-12 KO mice (Table 3.4) without alterations to urinary K^{+} excretion (Table 3.2 and 3.3). As K^{+} moves paracellularly in the small intestine (King et al., 2018), this suggests claudin-12 confers permeability to K^{+} in the intestine and suggests reduced paracellular intestinal K^{+} uptake in the null mice.

5.1.2 Novel model for hyperphosphatemia

Hyperphosphatemia often occurs in CKD and ESRD (Hruska et al., 2008) as renal Pi excretion decreases with declining glomerular filtration, and responsiveness of the kidney to FGF-23 declines (Hu et al., 2013). Hyperphosphatemia is rare in the absence of renal dysfunction in mice. However, the claudin-12 KO mice develop hyperphosphatemia on an inorganic Pi diet (Table 3.4) due to enhanced intestinal Pi absorption. This is therefore a novel model to study hyperphosphatemia in the absence of renal dysfunction and should prove helpful

for dissecting out the link that epidemiological studies highlight between hyperphosphatemia and cardiovascular disease, left-ventricular hypertrophy and mortality (Cozzolino et al., 2019; Da et al., 2015; Dhingra et al., 2007; Okuno et al., 2007).

In the claudin-12 KO model of hyperphosphatemia, alterations in dietary Pi source leads to altered Pi status and hormonal alterations in FGF-23, but not PTH **(Figure 3.4)**. FGF-23 secretion is enhanced in response to high blood Pi, which occurs in WT and claudin-12 KO mice on an inorganic Pi diet, which serves to enhance renal Pi excretion. The hypocalcemia and hyperphosphatemia that occur on an inorganic Pi diet would reduce CaSR activity in parathyroid chief cells and contribute to enhanced PTH production and release (Almaden et al., 1996; P. P. Centeno et al., 2019). However, elevated FGF-23 decreases PTH secretion *in-vitro* (Krajisnik et al., 2007) and *in-vivo* (Ben-Dov et al., 2007). Therefore, PTH may be unaltered on the inorganic Pi diet due to increased FGF-23 inhibition of PTH production and secretion. Additionally, FGF-23 negatively regulates vitamin D_3 synthesis in the kidney in a VDR dependent manner (Miyamoto et al., 2005) by decreasing transcription of *CYP27b1* and enhancing transcription of *CYP24a1* encoding 1-α-hydroxylase and 24-hydroxylase respectively. While vitamin D_3 levels were not directly assessed, this would be consistent with the reduced serum Ca^{2+} levels we observed in mice on an inorganic Pi diet (Table 3.4). Alternatively, the reduction in serum Ca^{2+} may be due to reduced Ca^{2+} absorption from the intestine. Increased Pi in the intestinal lumen on an inorganic Pi diet may decrease absorption by binding free Ca^{2+} in the lumen and enhance its fecal excretion. Claudin-2 and -12 are expressed in the intestine, form Ca^{2+} permeable pores and are regulated by vitamin D_3 (Fujita et al., 2008). We observed significantly decreased expression of claudin-2 in the duodenum **(Figure 3.5 F)**, suggesting a reduced paracellular Ca^{2+}

permeability and therefore possibly absorption from this segment. As transcellular Ca^{2+} transport machinery in the intestine, including TRPV6, CABP9K, NCX and PMCA1b, is also regulated by vitamin D_3 (Hoenderop et al., 2005), decreased expression of these transport mediators may also contribute to a reduced serum Ca^{2+}. Additionally, an FGF-23 mediated reduction in vitamin D_3 may also explain the decreased mRNA expression of Npt2b in the ileum **(Figure 3.7).** While Np2tb is also regulated by dietary Pi content, and potentially the form as inorganic Pi is predicted to have greater luminal concentrations, it is unlikely this is responsible as it occurs at the post-transcriptional level (Segawa et al., 2004).

5.1.3 Organic P is absorbed predominantly via the transcellular pathway

To test our hypothesis that Pi liberated from organic dietary sources leads to lower luminal concentrations that necessitate transport via secondarily active transporters, we used pharmacological inhibitors of Npt2b to manipulate the transcellular pathway. If Pi liberated from organic molecules moves transcellularly, we predicted that we would observe decreased Pi bioavailability on the organic P diet, but not the inorganic Pi diet. We attempted to use PFA, a common Npt2b inhibitor, however, it is likely absorbed systemically as we observed enhanced urinary Pi excretion in both WT and claudin-12 KO mice (Table 3.8), consistent with its known inhibition on Npt2a and 2c (Loghman-Adham, 1996). Therefore, NTX-1942, a Npt2b specific inhibitor, was employed as it is not absorbed across the intestine (Navre et al., 2011). Using NTX we demonstrated that inhibition of the major transcellular Pi transport pathway (Marks et al., 2006; Sabbagh et al., 2009) reduces Pi absorption on the organic but not the inorganic Pi diet **(Figure 3.11)**. This implies that Npt2b likely plays a more prominent role in intestinal Pi absorption for diets composed of organic P (*i.e*. protein), while Western diets with increased

inorganic Pi content may rely more on the paracellular pathway. It is unlikely that manipulating Npt2b influences paracellular transport, thereby confounding our interpretation, as intestine-specific Npt2b KO mice do not display altered Pi permeability in any segment (Knopfel et al., 2019).

5.2 Proposed role of claudin-2 in renal and intestinal Ca^{2+} transport

Claudin-2 is a cation permeable pore expressed in epithelial of the intestine, proximal tubule and thin descending limbs of the loop of Henle (Curry et al., 2020; Muto et al., 2010; Plain et al., 2020; Yu et al., 2009). Constitutive deletion of claudin-2 in mice leads to hypercalciuria (Table 4.2) caused by a primary renal Ca^{2+} leak. While renal Ca^{2+} loss may lead to a negative Ca^{2+} balance with consequent increased PTH and vitamin D_3 (Hoenderop et al., 2005), no alterations in serum Ca^{2+} (Table 4.2) or calciotropic hormones were observed (Curry et al., 2020). Consistent with unaltered calciotropic hormones, we demonstrated that altered bone mineral metabolism was not responsible for maintaining serum Ca^{2+} levels as bone architecture and mineral metabolism was unchanged in the KO mice **(Figure 4.1 and Table 4.3)**. However, we observed increased Ca^{2+} bioavailability and net intestinal Ca^{2+} absorption (Table 4.2) suggesting intestinal compensation for renal Ca^{2+} loss. This simultaneous increased renal Ca^{2+} loss and intestinal hyperabsorption is consistent with the phenotype of patients with idiopathic hypercalciuria (O. W. Moe, 2006). It was suggested that enhanced intestinal Ca^{2+} absorption was due to reduced colonic Ca^{2+} secretion as the permeability to Ca^{2+} was significantly reduced in the proximal colon (Curry et al., 2020) and we did not observe alterations in pCa^{2+} in the ileum (Table 4.4) or the gene expression of trancellular Ca^{2+} transporters and claudins which mediate paracellular Ca^{2+} transport **(Figures 4.2-4.5)**. This observation highlights that the absorption of dietary Ca^{2+} is accompanied by a

continuous backleak of Ca^{2+} through the claudin-2 pore in the colon which allows for enhanced fecal Ca^{2+} excretion, in addition to renal Ca^{2+} excretion given hypercalcemia. As hypercalciuria is a major risk factor for developing kidney stones (Worcester & Coe, 2010), it is unsurprising that claudin-2 KO mice develop nephrocalcinosis (Curry et al., 2020). Due to reduced proximal tubule Ca^{2+} absorption, there is increased delivery of Ca^{2+} to the loops of Henle. Claudin-2 KO mice developed intratubular plugs of hydroxyapatite in the descending and ascending thin limbs of the loop of Henle (Curry et al., 2020) and by 6 months of age, the majority of these deposits are located in the intersititium suggesting the tubules degenerated as the depositions grew. As the phenotype of the claudin-2 KO mice resembled patients with idiopathic hypercalciuria that develop kidney stones, a genome-wide association study (GWAS) was conducted to evaluate the association of single-nucleotide polymorphisms (SNPs) within the *CLDN2* locus and risk of kidney stone formation. A number of SNPs associated with nephrolithiasis were genotyped and the risk alleles identified were found to associate with decreased claudin-2 in pancreatic tissue (N.B. there is not enough renal data to say whether these alleles associate with reduced claudin-2 expression in the kidney). Consistent with the observed nephrolithiasis in claudin-2 KO mice, risk alleles that result in decreased expression of claudin-2 produce a similar phenotype in humans. The association of reduced claudin-2 expression / function and the development of kidney stones is further supported by the observation that patients with a rare missense mutation in *CLDN2* (p. Gly161Arg) were found to have a history of kidney stones and were hypercalciuric (Askari et al., 2019). Together, this demonstrates that claudin-2 is crucial in regulating Ca^{2+} absorption in renal and intestinal epithelia and that its loss / reduced expression results in nephrolithiasis in both mice and humans.

5.3 Therapeutic considerations

As hyperphosphatemia is commonly observed in patients with CKD and ESRD (Cannata-Andia & Martin, 2016; Hruska et al., 2008) and is associated with a number of negative sequelae including cardiovascular disease, worsening renal function and death (W. Bai et al., 2016; Palmer et al., 2011; Ritter & Slatopolsky, 2016), reducing serum Pi in this population is a clinical recommendation (Kidney Disease: Improving Global Outcomes, 2017). Given declining renal function in these patients, intestinal Pi absorption is targeted to reduce serum Pi (Fouque et al., 2018). Dietary counselling for these patients includes recommendations to reduce dietary Pi by avoiding foods with a high phosphorus to protein ratio, such as egg yolk, and with Pi additives, such as soft drinks (Cupisti & Kalantar-Zadeh, 2013). Our findings that inorganic Pi diets are more highly bioavailable due to absorption by the paracellular pathway support the recommendation to include education about dietary Pi form as an element in this type of intervention and preferentially avoid foods with inorganic Pi additives.

Additionally, drugs that reduce serum Pi target intestinal Pi absorption. However, a non-absorbable Npt2b-specific inhibitor unfortunately failed to reduce serum Pi in patients with ESRD on maintenance hemodialysis (Larsson et al., 2018). This is consistent with the paracellular pathway playing a more physiologically relevant role under most dietary Pi conditions, especially in humans consuming a Western diet containing large amounts of inorganic Pi (Saurette & Alexander, 2019). Therefore, drugs that target this pathway will likely prove helpful in reducing serum Pi. Tenapanor hydrocholoride is one of these drugs that reduces intestinal Pi absorption by decreasing paracellular Pi permeability (King et al., 2018). As tenapanor inhibits NHE3 it also reduces intestinal Na^+ absorption and decreases extracellular fluid volume (Spencer et al., 2014). Drugs that directly modulate the tight junction to reduce Pi

absorption may be warranted when clinicians want to specifically target intestinal Pi transport without altering sodium or fluid balance. To this end, drugs which increase intestinal expression of claudin-12 may prove useful in reducing Pi absorption. However, a better strategy would be to block the intestinal paracellular Pi pore. Unfortunately, the identity of this pore remains elusive.

Similarly, developing pharmacological strategies to enhance renal claudin-2 expression would prove useful in treating idiopathic hypercalciuria and preventing nephrolithiasis. Thiazide diuretics are commonly prescribed to patients with CKD, to reduce extracellular fluid volume and to enhance renal Ca^{2+} reabsorption and reduce hypercalciuria, a major risk factor for developing kidney stones. These drugs target the DCT and reduce NaCl reabosorption via the sodium chloride cotransporter (NCC). Distal Na^{+} loss leads to proximal tubule hyperabsorption of Na^{+}; as Ca^{2+} reabsorption depends on Na^{+} reabsorption this leads to hypocalciuria (Alexander & Dimke, 2017). However, thiazide diuretics are contraindicated for some patients due to off target effects including hypokalemia. Therefore, pharmacologically enhancing claudin-2 expression would serve to enhance renal Ca^{2+} reabsorption and fecal Ca^{2+} excretion via secretion in the proximal colon reducing hypercalciuria and therefore the risk of developing kidney stones in these patients.

5.4 Conclusion

In conclusion, we demonstrate the altered bioavailability between organic P and inorganic Pi is due to a difference in how these Pi forms are absorbed across the intestine. Claudin-12 KO mice, which display enhanced paracellular Pi permeability *ex-vivo*, were used to interrogate how alterations in paracellular Pi transport affects the absorption of these two forms of Pi. Using these mice, we demonstrate that inorganic Pi is absorbed primarily *via* the paracellular pathway. Conversely, pharmacological inhibition of the major transcellular Pi absorptive pathway selectively reduces absorption of Pi from organic sources. This supports the conclusion that Pi liberated from organic molecules such as protein require secondarily active transport via Npt2b. Further, we highlight that claudin-2 which forms Ca^{2+} permeable pores in intestinal and renal epithelia is necessary for Ca^{2+} homeostasis. Loss of the protein leads to a primary renal Ca^{2+} leak which is compensated for through enhanced intestinal Ca^{2+} absorption. Ultimately, loss or decreased function of claudin-2 leads to nephrolithiasis in mice, thereby increasing the risk of stone formation in humans.

5.5 Future directions

Using claudin-12 KO mice, a transgenic model of enhanced paracellular Pi permeability, we demonstrated that inorganic Pi is absorbed predominantly via the paracellular pathway. To further support this hypothesis, the organic to inorganic Pi metabolic balance study should be repeated in WT mice with the addition of tenapanor to pharmacologically manipulate the paracellular pathway. If inorganic Pi is predominantly absorbed paracellularly, a reduced Pi bioavailability should be observed on the inorganic Pi diet, but not on the organic P. To further implicate the transcellular pathway as the main route of Pi absorption from diets of organic P, the

organic to inorganic Pi metabolic balance study could be conducted using intestinal specific Npt2b KO mice. In this genetic model, reduced Pi bioavailability and urine Pi excretion should be observed when the mice are fed an organic P diet, but not the inorganic Pi diet.

By feeding inorganic Pi to claudin-12 KO mice, we have established a novel model of hyperphosphatemia in the absence of renal dysfunction. Hyperphosphatemia is associated with cardiovascular disease, including left-ventricular hypertrophy and vascular calcification, and all-cause mortality in CKD/ESRD patients as well as the general population (W. Bai et al., 2016; Da et al., 2015). However, the exact mechanism whereby this occurs is unclear and whether it is a direct effect of inorganic Pi or mediated by FGF-23 / other hormones is unknown. Having established a model of hyperphosphatemia, the effects of chronic inorganic Pi diet administration can be assessed in the claudin-12 KO mice and the mechanism linking disturbance in Pi homeostasis and cardiovascular disease can be investigated. Emerging evidence suggests a pro-inflammatory response to hyperphosphatemia may mediate the relationship to the development of vascular calcification and cardiovascular disease (Voelkl et al., 2021). This model will allow this potential link to be assessed.

A central question in the field of Pi transport concerns the identity of the Pi pore. As the composition of claudins in a tight junction determines the permeability of the epithelium to an ion, the question is more specifically: which claudin(s) confers paracellular Pi permeability. Therefore, a crucial future direction is to identify which claudin(s) compose the Pi pore. As the background expression of claudins influences the permeability properties of the epithelium, caco2bbe cells could be stably transfected with the claudins endogenously expressed in the intestinal epithelium. Using a Tet-off system, the expression of each claudin could be selectively inactivated and Pi–Cl^- diffusion potential experiments conducted in Ussing chambers *ex-vivo* to

determine which claudin confers Pi permeability to the epithelium. Determining the identity of the Pi pore would establish it as a drug target to pharmacologically block paracellular intestinal Pi transport directly. As this route mediates the bulk of intestinal Pi transport under most conditions, this would greatly improve the ability of clinicians to treat hyperphosphatemia that develops in CKD and ESRD.

References

Agus, Z. S., Gardner, L. B., Beck, L. H., & Goldberg, M. (1973). Effects of parathyroid hormone on renal tubular reabsorption of calcium, sodium, and phosphate. *Am J Physiol, 224*(5), 1143-1148. doi:10.1152/ajplegacy.1973.224.5.1143

Alexander, R. T. (2020). Increased intestinal phosphate absorption, an often-overlooked effect of vitamin D. *J Physiol*. doi:10.1113/JP281095

Alexander, R. T., Beggs, M. R., Zamani, R., Marcussen, N., Frische, S., & Dimke, H. (2015). Ultrastructural and immunohistochemical localization of plasma membrane Ca2+-ATPase 4 in Ca2+-transporting epithelia. *Am J Physiol Renal Physiol, 309*(7), F604-616. doi:10.1152/ajprenal.00651.2014

Alexander, R. T., & Dimke, H. (2017). Effect of diuretics on renal tubular transport of calcium and magnesium. *Am J Physiol Renal Physiol, 312*(6), F998-F1015. doi:10.1152/ajprenal.00032.2017

Alexander, R. T., Rievaj, J., & Dimke, H. (2014). Paracellular calcium transport across renal and intestinal epithelia. *Biochem Cell Biol, 92*(6), 467-480. doi:10.1139/bcb-2014-0061

Almaden, Y., Canalejo, A., Hernandez, A., Ballesteros, E., Garcia-Navarro, S., Torres, A., . . . Rodriguez, M. (1996). Direct effect of phosphorus on PTH secretion from whole rat parathyroid glands in vitro. *Journal of Bone and Mineral Research, 11*(7), 970-976. doi:https://doi.org/10.1002/jbmr.5650110714

Almeida, A. L., Kudo, L. H., & Rocha, A. S. (1981). Calcium transport in isolated perfused pars recta of proximal tubule. *Braz J Med Biol Res, 14*(1), 43-49. Retrieved from https://www.ncbi.nlm.nih.gov/pubmed/7306722

Amasheh, S., Meiri, N., Gitter, A. H., Schoneberg, T., Mankertz, J., Schulzke, J. D., & Fromm, M. (2002). Claudin-2 expression induces cation-selective channels in tight junctions of epithelial cells. *J Cell Sci, 115*(Pt 24), 4969-4976. doi:10.1242/jcs.00165

Anderson, J. M., & Van Itallie, C. M. (2009). Physiology and function of the tight junction. *Cold Spring Harb Perspect Biol, 1*(2), a002584. doi:10.1101/cshperspect.a002584

Andrukhova, O., Zeitz, U., Goetz, R., Mohammadi, M., Lanske, B., & Erben, R. G. (2012). FGF23 acts directly on renal proximal tubules to induce phosphaturia through activation of the ERK1/2-SGK1 signaling pathway. *Bone, 51*(3), 621-628. doi:10.1016/j.bone.2012.05.015

Ansermet, C., Moor, M. B., Centeno, G., Auberson, M., Hu, D. Z., Baron, R., . . . Firsov, D. (2017). Renal Fanconi Syndrome and Hypophosphatemic Rickets in the Absence of Xenotropic and Polytropic Retroviral Receptor in the Nephron. *J Am Soc Nephrol, 28*(4), 1073-1078. doi:10.1681/ASN.2016070726

Askari, M., Karamzadeh, R., Ansari-Pour, N., Karimi-Jafari, M. H., Almadani, N., Sadighi Gilani, M. A., . . . Totonchi, M. (2019). Identification of a missense variant in CLDN2 in obstructive azoospermia. *Journal of Human Genetics, 64*(10), 1023-1032. doi:10.1038/s10038-019-0642-0

Bai, L., Collins, J. F., & Ghishan, F. K. (2000). Cloning and characterization of a type III Na-dependent phosphate cotransporter from mouse intestine. *Am J Physiol Cell Physiol, 279*(4), C1135-1143. doi:10.1152/ajpcell.2000.279.4.C1135

Bai, W., Li, J., & Liu, J. (2016). Serum phosphorus, cardiovascular and all-cause mortality in the general population: A meta-analysis. *Clin Chim Acta, 461*, 76-82. doi:10.1016/j.cca.2016.07.020

Balla, T. (2013). Phosphoinositides: tiny lipids with giant impact on cell regulation. *Physiol Rev, 93*(3), 1019-1137. doi:10.1152/physrev.00028.2012

Barratt, L. J., Rector, F. C., Jr., Kokko, J. P., & Seldin, D. W. (1974). Factors governing the transepithelial potential difference across the proximal tubule of the rat kidney. *J Clin Invest, 53*(2), 454-464. doi:10.1172/JCI107579

Barry, P. H., & Lynch, J. W. (1991). Liquid junction potentials and small cell effects in patch-clamp analysis. *J Membr Biol, 121*(2), 101-117. doi:10.1007/BF01870526

Beck, L. H., & Goldberg, M. (1973). Effects of acetazolamide and parathyroidectomy on renal transport of sodium, calcium, and phosphate. *Am J Physiol, 224*(5), 1136-1142. doi:10.1152/ajplegacy.1973.224.5.1136

Beggs, M. R., & Alexander, R. T. (2017). Intestinal absorption and renal reabsorption of calcium throughout postnatal development. *Exp Biol Med (Maywood), 242*(8), 840-849. doi:10.1177/1535370217699536

Ben-Dov, I. Z., Galitzer, H., Lavi-Moshayoff, V., Goetz, R., Kuro-o, M., Mohammadi, M., . . . Silver, J. (2007). The parathyroid is a target organ for FGF23 in rats. *J Clin Invest, 117*(12), 4003-4008. doi:10.1172/JCI32409

Benn, B. S., Ajibade, D., Porta, A., Dhawan, P., Hediger, M., Peng, J. B., . . . Christakos, S. (2008). Active intestinal calcium transport in the absence of transient receptor potential vanilloid type 6 and calbindin-D9k. *Endocrinology, 149*(6), 3196-3205. doi:10.1210/en.2007-1655

Bergwitz, C., & Juppner, H. (2010). Regulation of phosphate homeostasis by PTH, vitamin D, and FGF23. *Annu Rev Med, 61*, 91-104. doi:10.1146/annurev.med.051308.111339

Bergwitz, C., Roslin, N. M., Tieder, M., Loredo-Osti, J. C., Bastepe, M., Abu-Zahra, H., . . . Juppner, H. (2006). SLC34A3 mutations in patients with hereditary hypophosphatemic rickets with hypercalciuria predict a key role for the sodium-phosphate cotransporter NaPi-IIc in maintaining phosphate homeostasis. *Am J Hum Genet, 78*(2), 179-192. doi:10.1086/499409

Berndt, T., Craig, T. A., Bowe, A. E., Vassiliadis, J., Reczek, D., Finnegan, R., . . . Kumar, R. (2003). Secreted frizzled-related protein 4 is a potent tumor-derived phosphaturic agent. *J Clin Invest, 112*(5), 785-794. doi:10.1172/JCI18563

Bhadada, S. K., & Rao, S. D. (2021). Role of Phosphate in Biomineralization. *Calcified Tissue International, 108*(1), 32-40. doi:10.1007/s00223-020-00729-9

Bianco, S. D., Peng, J. B., Takanaga, H., Suzuki, Y., Crescenzi, A., Kos, C. H., . . . Hediger, M. A. (2007). Marked disturbance of calcium homeostasis in mice with targeted disruption of the Trpv6 calcium channel gene. *J Bone Miner Res, 22*(2), 274-285. doi:10.1359/jbmr.061110

Biber, J., Hernando, N., & Forster, I. (2013). Phosphate transporters and their function. *Annu Rev Physiol, 75*, 535-550. doi:10.1146/annurev-physiol-030212-183748

Biemesderfer, D., Rutherford, P. A., Nagy, T., Pizzonia, J. H., Abu-Alfa, A. K., & Aronson, P. S. (1997). Monoclonal antibodies for high-resolution localization of NHE3 in adult and neonatal rat kidney. *Am J Physiol, 273*(2 Pt 2), F289-299. doi:10.1152/ajprenal.1997.273.2.F289

Birge, S. J., Peck, W. A., Berman, M., & Whedon, G. D. (1969). Study of calcium absorption in man: a kinetic analysis and physiologic model. *J Clin Invest, 48*(9), 1705-1713. doi:10.1172/JCI106136

Blaine, J., Chonchol, M., & Levi, M. (2015). Renal control of calcium, phosphate, and magnesium homeostasis. *Clin J Am Soc Nephrol, 10*(7), 1257-1272. doi:10.2215/CJN.09750913

Blau, J. E., & Collins, M. T. (2015). The PTH-Vitamin D-FGF23 axis. *Reviews in Endocrine and Metabolic Disorders, 16*(2), 165-174. doi:10.1007/s11154-015-9318-z

Bon, N., Frangi, G., Sourice, S., Guicheux, J., Beck-Cormier, S., & Beck, L. (2018). Phosphate-dependent FGF23 secretion is modulated by PiT2/Slc20a2. *Molecular Metabolism, 11*, 197-204. doi:https://doi.org/10.1016/j.molmet.2018.02.007

Bookstein, C., DePaoli, A. M., Xie, Y., Niu, P., Musch, M. W., Rao, M. C., & Chang, E. B. (1994). Na+/H+ exchangers, NHE-1 and NHE-3, of rat intestine. Expression and localization. *J Clin Invest, 93*(1), 106-113. doi:10.1172/JCI116933

Borowitz, S. M., & Ghishan, F. K. (1989). Phosphate transport in human jejunal brush-border membrane vesicles. *Gastroenterology, 96*(1), 4-10. Retrieved from https://www.ncbi.nlm.nih.gov/pubmed/2909436

Bottger, P., Hede, S. E., Grunnet, M., Hoyer, B., Klaerke, D. A., & Pedersen, L. (2006). Characterization of transport mechanisms and determinants critical for Na+-dependent Pi symport of the PiT family paralogs human PiT1 and PiT2. *Am J Physiol Cell Physiol, 291*(6), C1377-1387. doi:10.1152/ajpcell.00015.2006

Boyce, A. M., Lee, A. E., Roszko, K. L., & Gafni, R. I. (2020). Hyperphosphatemic Tumoral Calcinosis: Pathogenesis, Clinical Presentation, and Challenges in Management. *Front Endocrinol (Lausanne), 11*, 293. doi:10.3389/fendo.2020.00293

Breiderhoff, T., Himmerkus, N., Stuiver, M., Mutig, K., Will, C., Meij, I. C., . . . Muller, D. (2012). Deletion of claudin-10 (Cldn10) in the thick ascending limb impairs paracellular sodium permeability and leads to hypermagnesemia and nephrocalcinosis. *Proc Natl Acad Sci U S A, 109*(35), 14241-14246. doi:10.1073/pnas.1203834109

Bronner, F. (2003). Mechanisms of intestinal calcium absorption. *J Cell Biochem, 88*(2), 387-393. doi:10.1002/jcb.10330

Bronner, F., & Pansu, D. (1999). Nutritional aspects of calcium absorption. *J Nutr, 129*(1), 9-12. doi:10.1093/jn/129.1.9

Bronner, F., Pansu, D., & Stein, W. D. (1986). An analysis of intestinal calcium transport across the rat intestine. *Am J Physiol, 250*(5 Pt 1), G561-569. doi:10.1152/ajpgi.1986.250.5.G561

Campean, V., Kricke, J., Ellison, D., Luft, F. C., & Bachmann, S. (2001). Localization of thiazide-sensitive Na(+)-Cl(-) cotransport and associated gene products in mouse DCT. *Am J Physiol Renal Physiol, 281*(6), F1028-1035. doi:10.1152/ajprenal.0148.2001

Canaff, L., & Hendy, G. N. (2002). Human calcium-sensing receptor gene. Vitamin D response elements in promoters P1 and P2 confer transcriptional responsiveness to 1,25-dihydroxyvitamin D. *J Biol Chem, 277*(33), 30337-30350. doi:10.1074/jbc.M201804200

Candeal, E., Caldas, Y. A., Guillen, N., Levi, M., & Sorribas, V. (2017). Intestinal phosphate absorption is mediated by multiple transport systems in rats. *Am J Physiol Gastrointest Liver Physiol, 312*(4), G355-G366. doi:10.1152/ajpgi.00244.2016

Cannata-Andia, J. B., & Martin, K. J. (2016). The challenge of controlling phosphorus in chronic kidney disease. *Nephrol Dial Transplant, 31*(4), 541-547. doi:10.1093/ndt/gfv055

Carrigan, A., Klinger, A., Choquette, S. S., Luzuriaga-McPherson, A., Bell, E. K., Darnell, B., & Gutierrez, O. M. (2014). Contribution of food additives to sodium and phosphorus content of diets rich in processed foods. *J Ren Nutr, 24*(1), 13-19, 19e11. doi:10.1053/j.jrn.2013.09.003

Centeno, P. P., Herberger, A., Mun, H. C., Tu, C., Nemeth, E. F., Chang, W., . . . Ward, D. T. (2019). Phosphate acts directly on the calcium-sensing receptor to stimulate parathyroid hormone secretion. *Nat Commun, 10*(1), 4693. doi:10.1038/s41467-019-12399-9

Centeno, V. A., Diaz de Barboza, G. E., Marchionatti, A. M., Alisio, A. E., Dallorso, M. E., Nasif, R., & Tolosa de Talamoni, N. G. (2004). Dietary calcium deficiency increases Ca2+ uptake and Ca2+ extrusion mechanisms in chick enterocytes. *Comp Biochem Physiol A Mol Integr Physiol, 139*(2), 133-141. doi:10.1016/j.cbpb.2004.08.002

Cha, S. K., Wu, T., & Huang, C. L. (2008). Protein kinase C inhibits caveolae-mediated endocytosis of TRPV5. *Am J Physiol Renal Physiol, 294*(5), F1212-1221. doi:10.1152/ajprenal.00007.2008

Chakraborty, A., Kim, S., & Snyder, S. H. (2011). Inositol pyrophosphates as mammalian cell signals. *Sci Signal, 4*(188), re1. doi:10.1126/scisignal.2001958

Chanchlani, R., Nemer, P., Sinha, R., Nemer, L., Krishnappa, V., Sochett, E., . . . Raina, R. (2020). An Overview of Rickets in Children. *Kidney Int Rep, 5*(7), 980-990. doi:10.1016/j.ekir.2020.03.025

Chiu, Y. W., Teitelbaum, I., Misra, M., de Leon, E. M., Adzize, T., & Mehrotra, R. (2009). Pill burden, adherence, hyperphosphatemia, and quality of life in maintenance dialysis patients. *Clin J Am Soc Nephrol, 4*(6), 1089-1096. doi:10.2215/CJN.00290109

Cho, C. H., Lee, S. Y., Shin, H. S., Philipson, K. D., & Lee, C. O. (2003). Partial rescue of the Na+-Ca2+ exchanger (NCX1) knock-out mouse by transgenic expression of NCX1. *Exp Mol Med, 35*(2), 125-135. doi:10.1038/emm.2003.18

Cho, H. Y., Choi, H. J., Sun, H. J., Yang, J. Y., An, J. H., Cho, S. W., . . . Shin, C. S. (2010). Transgenic mice overexpressing secreted frizzled-related proteins (sFRP)4 under the control of serum amyloid P promoter exhibit low bone mass but did not result in disturbed phosphate homeostasis. *Bone, 47*(2), 263-271. doi:10.1016/j.bone.2010.05.010

Christakos, S. (2012). Mechanism of action of 1,25-dihydroxyvitamin D3 on intestinal calcium absorption. *Rev Endocr Metab Disord, 13*(1), 39-44. doi:10.1007/s11154-011-9197-x

Christov, M., Koren, S., Yuan, Q., Baron, R., & Lanske, B. (2011). Genetic ablation of sfrp4 in mice does not affect serum phosphate homeostasis. *Endocrinology, 152*(5), 2031-2036. doi:10.1210/en.2010-1351

Colegio, O. R., Van Itallie, C., Rahner, C., & Anderson, J. M. (2003). Claudin extracellular domains determine paracellular charge selectivity and resistance but not tight junction fibril architecture. *Am J Physiol Cell Physiol, 284*(6), C1346-1354. doi:10.1152/ajpcell.00547.2002

Collins, J. F., Bai, L., & Ghishan, F. K. (2004). The SLC20 family of proteins: dual functions as sodium-phosphate cotransporters and viral receptors. *Pflugers Arch, 447*(5), 647-652. doi:10.1007/s00424-003-1088-x

Consortium, A. (2000). Autosomal dominant hypophosphataemic rickets is associated with mutations in FGF23. *Nat Genet, 26*(3), 345-348. doi:10.1038/81664

Cozzolino, M., Ciceri, P., Galassi, A., Mangano, M., Carugo, S., Capelli, I., & Cianciolo, G. (2019). The Key Role of Phosphate on Vascular Calcification. *Toxins (Basel), 11*(4). doi:10.3390/toxins11040213

Cupisti, A., & Kalantar-Zadeh, K. (2013). Management of natural and added dietary phosphorus burden in kidney disease. *Semin Nephrol, 33*(2), 180-190. doi:10.1016/j.semnephrol.2012.12.018

Curry, J. N., Saurette, M., Askari, M., Pei, L., Filla, M. B., Beggs, M. R., . . . Yu, A. S. (2020). Claudin-2 deficiency associates with hypercalciuria in mice and human kidney stone disease. *J Clin Invest, 130*(4), 1948-1960. doi:10.1172/JCI127750

Curthoys, N. P., & Moe, O. W. (2014). Proximal tubule function and response to acidosis. *Clin J Am Soc Nephrol, 9*(9), 1627-1638. doi:10.2215/CJN.10391012

Da, J., Xie, X., Wolf, M., Disthabanchong, S., Wang, J., Zha, Y., . . . Wang, H. (2015). Serum Phosphorus and Progression of CKD and Mortality: A Meta-analysis of Cohort Studies. *Am J Kidney Dis, 66*(2), 258-265. doi:10.1053/j.ajkd.2015.01.009

David, V., Martin, A., Hedge, A. M., & Rowe, P. S. (2009). Matrix extracellular phosphoglycoprotein (MEPE) is a new bone renal hormone and vascularization modulator. *Endocrinology, 150*(9), 4012-4023. doi:10.1210/en.2009-0216

Davis, G. R., Zerwekh, J. E., Parker, T. F., Krejs, G. J., Pak, C. Y., & Fordtran, J. S. (1983). Absorption of phosphate in the jejunum of patients with chronic renal failure before and after correction of vitamin D deficiency. *Gastroenterology, 85*(4), 908-916. Retrieved from https://www.ncbi.nlm.nih.gov/pubmed/6688402

De Beur, S. M., Finnegan, R. B., Vassiliadis, J., Cook, B., Barberio, D., Estes, S., . . . Schiavi, S. C. (2002). Tumors associated with oncogenic osteomalacia express genes important in bone and mineral metabolism. *J Bone Miner Res, 17*(6), 1102-1110. doi:10.1359/jbmr.2002.17.6.1102

de Groot, T., Lee, K., Langeslag, M., Xi, Q., Jalink, K., Bindels, R. J., & Hoenderop, J. G. (2009). Parathyroid hormone activates TRPV5 via PKA-dependent phosphorylation. *J Am Soc Nephrol, 20*(8), 1693-1704. doi:10.1681/ASN.2008080873

Dhingra, R., Sullivan, L. M., Fox, C. S., Wang, T. J., D'Agostino, R. B., Sr., Gaziano, J. M., & Vasan, R. S. (2007). Relations of serum phosphorus and calcium levels to the incidence of cardiovascular disease in the community. *Arch Intern Med, 167*(9), 879-885. doi:10.1001/archinte.167.9.879

Di Stefano, A., Wittner, M., Nitschke, R., Braitsch, R., Greger, R., Bailly, C., . . . de Rouffignac, C. (1990). Effects of parathyroid hormone and calcitonin on Na+, Cl-, K+, Mg2+ and Ca2+ transport in cortical and medullary thick ascending limbs of mouse kidney. *Pflugers Arch, 417*(2), 161-167. doi:10.1007/BF00370694

Dimke, H., Desai, P., Borovac, J., Lau, A., Pan, W., & Alexander, R. T. (2013). Activation of the Ca(2+)-sensing receptor increases renal claudin-14 expression and urinary Ca(2+) excretion. *Am J Physiol Renal Physiol, 304*(6), F761-769. doi:10.1152/ajprenal.00263.2012

Dobbie, H., Unwin, R. J., Faria, N. J., & Shirley, D. G. (2008). Matrix extracellular phosphoglycoprotein causes phosphaturia in rats by inhibiting tubular phosphate reabsorption. *Nephrol Dial Transplant, 23*(2), 730-733. doi:10.1093/ndt/gfm535

DuBose, T. D., Jr., Pucacco, L. R., Seldin, D. W., Carter, N. W., & Kokko, J. P. (1979). Microelectrode determination of pH and PCO2 in rat proximal tubule after benzolamide: evidence for hydrogen ion secretion. *Kidney Int, 15*(6), 624-629. doi:10.1038/ki.1979.82

Duflos, C., Bellaton, C., Pansu, D., & Bronner, F. (1995). Calcium solubility, intestinal sojourn time and paracellular permeability codetermine passive calcium absorption in rats. *J Nutr, 125*(9), 2348-2355. doi:10.1093/jn/125.9.2348

Edwards, B. R., Baer, P. G., Sutton, R. A., & Dirks, J. H. (1973). Micropuncture study of diuretic effects on sodium and calcium reabsorption in the dog nephron. *J Clin Invest, 52*(10), 2418-2427. doi:10.1172/JCI107432

Enck, A. H., Berger, U. V., & Yu, A. S. (2001). Claudin-2 is selectively expressed in proximal nephron in mouse kidney. *Am J Physiol Renal Physiol, 281*(5), F966-974. doi:10.1152/ajprenal.2001.281.5.F966

Fallingborg, J. (1999). Intraluminal pH of the human gastrointestinal tract. *Dan Med Bull, 46*(3), 183-196. Retrieved from https://www.ncbi.nlm.nih.gov/pubmed/10421978

Feng, J. Q., Ward, L. M., Liu, S., Lu, Y., Xie, Y., Yuan, B., . . . White, K. E. (2006). Loss of DMP1 causes rickets and osteomalacia and identifies a role for osteocytes in mineral metabolism. *Nat Genet, 38*(11), 1310-1315. doi:10.1038/ng1905

Fissell, R. B., Karaboyas, A., Bieber, B. A., Sen, A., Li, Y., Lopes, A. A., . . . Tentori, F. (2016). Phosphate binder pill burden, patient-reported non-adherence, and mineral bone disorder markers: Findings from the DOPPS. *Hemodial Int, 20*(1), 38-49. doi:10.1111/hdi.12315

Forster, I. C., Loo, D. D., & Eskandari, S. (1999). Stoichiometry and Na+ binding cooperativity of rat and flounder renal type II Na+-Pi cotransporters. *Am J Physiol, 276*(4), F644-649. doi:10.1152/ajprenal.1999.276.4.F644

Fouque, D., Vervloet, M., & Ketteler, M. (2018). Targeting Gastrointestinal Transport Proteins to Control Hyperphosphatemia in Chronic Kidney Disease. *Drugs, 78*(12), 1171-1186. doi:10.1007/s40265-018-0950-2

Frische, S., Alexander, R. T., Ferreira, P., Tan, R. S. G., Wang, W., Svenningsen, P., . . . Dimke, H. (2021). Localization and regulation of claudin-14 in experimental models of hypercalcemia. *Am J Physiol Renal Physiol, 320*(1), F74-F86. doi:10.1152/ajprenal.00397.2020

Fujita, H., Sugimoto, K., Inatomi, S., Maeda, T., Osanai, M., Uchiyama, Y., . . . Chiba, H. (2008). Tight junction proteins claudin-2 and -12 are critical for vitamin D-dependent Ca2+ absorption between enterocytes. *Mol Biol Cell, 19*(5), 1912-1921. doi:10.1091/mbc.E07-09-0973

Gawenis, L. R., Stien, X., Shull, G. E., Schultheis, P. J., Woo, A. L., Walker, N. M., & Clarke, L. L. (2002). Intestinal NaCl transport in NHE2 and NHE3 knockout mice. *Am J Physiol Gastrointest Liver Physiol, 282*(5), G776-784. doi:10.1152/ajpgi.00297.2001

Geall, M. G., & Summerskill, W. H. (1969). Electric-potential difference--a neglected parameter of gut integrity and function? *Gut, 10*(6), 418-421. Retrieved from https://www.ncbi.nlm.nih.gov/pubmed/4891737
https://gut.bmj.com/content/gutjnl/10/6/418.full.pdf

Gensure, R. C., Gardella, T. J., & Jüppner, H. (2005). Parathyroid hormone and parathyroid hormone-related peptide, and their receptors. *Biochem Biophys Res Commun, 328*(3), 666-678. doi:10.1016/j.bbrc.2004.11.069

Giral, H., Caldas, Y., Sutherland, E., Wilson, P., Breusegem, S., Barry, N., . . . Levi, M. (2009). Regulation of rat intestinal Na-dependent phosphate transporters by dietary phosphate. *Am J Physiol Renal Physiol, 297*(5), F1466-1475. doi:10.1152/ajprenal.00279.2009

Gisler, S. M., Stagljar, I., Traebert, M., Bacic, D., Biber, J., & Murer, H. (2001). Interaction of the Type IIa Na/Pi Cotransporter with PDZ Proteins*. *Journal of Biological Chemistry, 276*(12), 9206-9213. doi:https://doi.org/10.1074/jbc.M008745200

Goel, M., Sinkins, W. G., Zuo, C. D., Estacion, M., & Schilling, W. P. (2006). Identification and localization of TRPC channels in the rat kidney. *Am J Physiol Renal Physiol, 290*(5), F1241-1252. doi:10.1152/ajprenal.00376.2005

Gong, Y., Renigunta, V., Himmerkus, N., Zhang, J., Renigunta, A., Bleich, M., & Hou, J. (2012). Claudin-14 regulates renal Ca(+)(+) transport in response to CaSR signalling via a novel microRNA pathway. *EMBO J, 31*(8), 1999-2012. doi:10.1038/emboj.2012.49

Gonzalez-Parra, E., Gracia-Iguacel, C., Egido, J., & Ortiz, A. (2012). Phosphorus and nutrition in chronic kidney disease. *Int J Nephrol, 2012*, 597605. doi:10.1155/2012/597605

Goretti Penido, M., & Alon, U. S. (2012). Phosphate homeostasis and its role in bone health. *Pediatr Nephrol, 27*(11), 2039-2048. doi:10.1007/s00467-012-2175-z

Greger, R., & Schlatter, E. (1983). Properties of the lumen membrane of the cortical thick ascending limb of Henle's loop of rabbit kidney. *Pflugers Arch, 396*(4), 315-324. doi:10.1007/BF01063937

Gunzel, D., Stuiver, M., Kausalya, P. J., Haisch, L., Krug, S. M., Rosenthal, R., . . . Muller, D. (2009). Claudin-10 exists in six alternatively spliced isoforms that exhibit distinct localization and function. *J Cell Sci, 122*(Pt 10), 1507-1517. doi:10.1242/jcs.040113

Gunzel, D., & Yu, A. S. (2013). Claudins and the modulation of tight junction permeability. *Physiol Rev, 93*(2), 525-569. doi:10.1152/physrev.00019.2012

Gustke, R. F., McCormick, P., Ruppin, H., Soergel, K. H., Whalen, G. E., & Wood, C. M. (1981). Human intestinal potential difference: recording method and biophysical implications. *J Physiol, 321*, 571-582. doi:10.1113/jphysiol.1981.sp014003

Gutierrez, O. M., Luzuriaga-McPherson, A., Lin, Y., Gilbert, L. C., Ha, S. W., & Beck, G. R., Jr. (2015). Impact of Phosphorus-Based Food Additives on Bone and Mineral Metabolism. *J Clin Endocrinol Metab, 100*(11), 4264-4271. doi:10.1210/jc.2015-2279

Habener, J. F., Kemper, B., & Potts, J. T., Jr. (1975). Calcium-dependent intracellular degradation of parathyroid hormone: a possible mechanism for the regulation of hormone stores. *Endocrinology, 97*(2), 431-441. doi:10.1210/endo-97-2-431

Han, X., Yang, J., Li, L., Huang, J., King, G., & Quarles, L. D. (2016). Conditional Deletion of Fgfr1 in the Proximal and Distal Tubule Identifies Distinct Roles in Phosphate and Calcium Transport. *PLoS One, 11*(2), e0147845. doi:10.1371/journal.pone.0147845

Hashimoto, N., Matsui, I., Ishizuka, S., Inoue, K., Matsumoto, A., Shimada, K., . . . Isaka, Y. (2020). Lithocholic acid increases intestinal phosphate and calcium absorption in a vitamin D receptor dependent but transcellular pathway independent manner. *Kidney Int, 97*(6), 1164-1180. doi:10.1016/j.kint.2020.01.032

Hattenhauer, O., Traebert, M., Murer, H., & Biber, J. (1999). Regulation of small intestinal Na-P(i) type IIb cotransporter by dietary phosphate intake. *Am J Physiol, 277*(4), G756-762. doi:10.1152/ajpgi.1999.277.4.G756

Haussler, M. R., Whitfield, G. K., Kaneko, I., Forster, R., Saini, R., Hsieh, J. C., . . . Jurutka, P. W. (2012). The role of vitamin D in the FGF23, klotho, and phosphate bone-kidney endocrine axis. *Rev Endocr Metab Disord, 13*(1), 57-69. doi:10.1007/s11154-011-9199-8

Hernando, N., Myakala, K., Simona, F., Knopfel, T., Thomas, L., Murer, H., . . . Biber, J. (2015). Intestinal Depletion of NaPi-IIb/Slc34a2 in Mice: Renal and Hormonal Adaptation. *J Bone Miner Res, 30*(10), 1925-1937. doi:10.1002/jbmr.2523

Hernando, N., Pastor-Arroyo, E. M., Marks, J., Schnitzbauer, U., Knopfel, T., Burki, M., . . . Wagner, C. A. (2020). 1,25(OH)2 vitamin D3 stimulates active phosphate transport but

not paracellular phosphate absorption in mouse intestine. *J Physiol*. doi:10.1113/JP280345

Hilfiker, H., Hattenhauer, O., Traebert, M., Forster, I., Murer, H., & Biber, J. (1998). Characterization of a murine type II sodium-phosphate cotransporter expressed in mammalian small intestine. *Proceedings of the National Academy of Sciences, 95*(24), 14564-14569. doi:10.1073/pnas.95.24.14564

Hoenderop, J. G., Nilius, B., & Bindels, R. J. (2005). Calcium absorption across epithelia. *Physiol Rev, 85*(1), 373-422. doi:10.1152/physrev.00003.2004

Hoenderop, J. G., van Leeuwen, J. P., van der Eerden, B. C., Kersten, F. F., van der Kemp, A. W., Merillat, A. M., . . . Bindels, R. J. (2003). Renal Ca2+ wasting, hyperabsorption, and reduced bone thickness in mice lacking TRPV5. *J Clin Invest, 112*(12), 1906-1914. doi:10.1172/JCI19826

Hofmeister, M. V., Fenton, R. A., & Praetorius, J. (2009). Fluorescence isolation of mouse late distal convoluted tubules and connecting tubules: effects of vasopressin and vitamin D3 on Ca2+ signaling. *American Journal of Physiology-Renal Physiology, 296*(1), F194-F203. doi:10.1152/ajprenal.90495.2008

Holick, M. F., Frommer, J. E., McNeill, S. C., Richtand, N. M., Henley, J. W., & Potts, J. T., Jr. (1977). Photometabolism of 7-dehydrocholesterol to previtamin D3 in skin. *Biochem Biophys Res Commun, 76*(1), 107-114. doi:10.1016/0006-291x(77)91674-6

Hoogerwerf, W. A., Tsao, S. C., Devuyst, O., Levine, S. A., Yun, C. H., Yip, J. W., . . . Donowitz, M. (1996). NHE2 and NHE3 are human and rabbit intestinal brush-border proteins. *Am J Physiol, 270*(1 Pt 1), G29-41. doi:10.1152/ajpgi.1996.270.1.G29

Hou, J., Renigunta, A., Konrad, M., Gomes, A. S., Schneeberger, E. E., Paul, D. L., . . . Goodenough, D. A. (2008). Claudin-16 and claudin-19 interact and form a cation-selective tight junction complex. *J Clin Invest, 118*(2), 619-628. doi:10.1172/JCI33970

Hou, J., Renigunta, A., Yang, J., & Waldegger, S. (2010). Claudin-4 forms paracellular chloride channel in the kidney and requires claudin-8 for tight junction localization. *Proc Natl Acad Sci U S A, 107*(42), 18010-18015. doi:10.1073/pnas.1009399107

Hou, J., Shan, Q., Wang, T., Gomes, A. S., Yan, Q., Paul, D. L., . . . Goodenough, D. A. (2007). Transgenic RNAi depletion of claudin-16 and the renal handling of magnesium. *J Biol Chem, 282*(23), 17114-17122. doi:10.1074/jbc.M700632200

Hruska, K. A., Mathew, S., Lund, R., Qiu, P., & Pratt, R. (2008). Hyperphosphatemia of chronic kidney disease. *Kidney Int, 74*(2), 148-157. doi:10.1038/ki.2008.130

Hu, M. C., Shiizaki, K., Kuro-o, M., & Moe, O. W. (2013). Fibroblast growth factor 23 and Klotho: physiology and pathophysiology of an endocrine network of mineral metabolism. *Annu Rev Physiol, 75*, 503-533. doi:10.1146/annurev-physiol-030212-183727

Huqun, Izumi, S., Miyazawa, H., Ishii, K., Uchiyama, B., Ishida, T., . . . Hagiwara, K. (2007). Mutations in the SLC34A2 gene are associated with pulmonary alveolar microlithiasis. *Am J Respir Crit Care Med, 175*(3), 263-268. doi:10.1164/rccm.200609-1274OC

Hylander, E., Ladefoged, K., & Jarnum, S. (1980). The importance of the colon in calcium absorption following small-intestinal resection. *Scand J Gastroenterol, 15*(1), 55-60. doi:10.3109/00365528009181432

Hylander, E., Ladefoged, K., & Jarnum, S. (1990). Calcium absorption after intestinal resection. The importance of a preserved colon. *Scand J Gastroenterol, 25*(7), 705-710. doi:10.3109/00365529008997596

Ikuta, K., Segawa, H., Sasaki, S., Hanazaki, A., Fujii, T., Kushi, A., . . . Miyamoto, K. I. (2018). Effect of Npt2b deletion on intestinal and renal inorganic phosphate (Pi) handling. *Clin Exp Nephrol, 22*(3), 517-528. doi:10.1007/s10157-017-1497-3

Jaeger, P., Karlmark, B., Stanton, B., Kirk, R. G., Duplinsky, T., & Giebisch, G. (1980). Micropuncture study of distal tubular activation of phosphate reabsorption in the rat. *Adv Exp Med Biol, 128*, 77-82. doi:10.1007/978-1-4615-9167-2_9

Jain, A., Fedarko, N. S., Collins, M. T., Gelman, R., Ankrom, M. A., Tayback, M., & Fisher, L. W. (2004). Serum levels of matrix extracellular phosphoglycoprotein (MEPE) in normal humans correlate with serum phosphorus, parathyroid hormone and bone mineral density. *J Clin Endocrinol Metab, 89*(8), 4158-4161. doi:10.1210/jc.2003-032031

Jono, S., McKee, M. D., Murry, C. E., Shioi, A., Nishizawa, Y., Mori, K., . . . Giachelli, C. M. (2000). Phosphate regulation of vascular smooth muscle cell calcification. *Circ Res, 87*(7), E10-17. doi:10.1161/01.res.87.7.e10

Kalantar-Zadeh, K., Gutekunst, L., Mehrotra, R., Kovesdy, C. P., Bross, R., Shinaberger, C. S., . . . Kopple, J. D. (2010). Understanding sources of dietary phosphorus in the treatment of patients with chronic kidney disease. *Clin J Am Soc Nephrol, 5*(3), 519-530. doi:10.2215/CJN.06080809

Karbach, U. (1989). Mechanism of intestinal calcium transport and clinical aspects of disturbed calcium absorption. *Dig Dis, 7*(1), 1-18. doi:10.1159/000171202

Karbach, U. (1992). Paracellular calcium transport across the small intestine. *J Nutr, 122*(3 Suppl), 672-677. doi:10.1093/jn/122.suppl_3.672

Katai, K., Miyamoto, K., Kishida, S., Segawa, H., Nii, T., Tanaka, H., . . . Takeda, E. (1999). Regulation of intestinal Na+-dependent phosphate co-transporters by a low-phosphate diet and 1,25-dihydroxyvitamin D3. *Biochem J, 343 Pt 3*, 705-712. Retrieved from https://www.ncbi.nlm.nih.gov/pubmed/10527952

Kato, K., Jeanneau, C., Tarp, M. A., Benet-Pages, A., Lorenz-Depiereux, B., Bennett, E. P., . . . Clausen, H. (2006). Polypeptide GalNAc-transferase T3 and familial tumoral calcinosis. Secretion of fibroblast growth factor 23 requires O-glycosylation. *J Biol Chem, 281*(27), 18370-18377. doi:10.1074/jbc.M602469200

Kaufman, J. S., & Hamburger, R. J. (1987). Lack of influence of volume flux on phosphate reabsorption in the proximal tubule. *Miner Electrolyte Metab, 13*(3), 158-164. Retrieved from https://www.ncbi.nlm.nih.gov/pubmed/3627047

Kellett, G. L. (2011). Alternative perspective on intestinal calcium absorption: proposed complementary actions of Ca(v)1.3 and TRPV6. *Nutr Rev, 69*(7), 347-370. doi:10.1111/j.1753-4887.2011.00395.x

Khundmiri, S. J., Murray, R. D., & Lederer, E. (2016). PTH and Vitamin D. *Compr Physiol, 6*(2), 561-601. doi:10.1002/cphy.c140071

Kidney Disease: Improving Global Outcomes, C. K. D. M. B. D. U. W. G. (2017). KDIGO 2017 Clinical Practice Guideline Update for the Diagnosis, Evaluation, Prevention, and Treatment of Chronic Kidney Disease-Mineral and Bone Disorder (CKD-MBD). *Kidney Int Suppl (2011), 7*(1), 1-59. doi:10.1016/j.kisu.2017.04.001

Kido, S., Miyamoto, K., Mizobuchi, H., Taketani, Y., Ohkido, I., Ogawa, N., . . . Takeda, E. (1999). Identification of regulatory sequences and binding proteins in the type II sodium/phosphate cotransporter NPT2 gene responsive to dietary phosphate. *J Biol Chem, 274*(40), 28256-28263. doi:10.1074/jbc.274.40.28256

Kimizuka, H., & Koketsu, K. (1964). Ion transport through cell membrane. *J Theor Biol, 6*(2), 290-305. doi:10.1016/0022-5193(64)90035-9

King, A. J., Siegel, M., He, Y., Nie, B., Wang, J., Koo-McCoy, S., . . . Caldwell, J. S. (2018). Inhibition of sodium/hydrogen exchanger 3 in the gastrointestinal tract by tenapanor reduces paracellular phosphate permeability. *Sci Transl Med, 10*(456). doi:10.1126/scitranslmed.aam6474

Kitanaka, S., Takeyama, K., Murayama, A., Sato, T., Okumura, K., Nogami, M., . . . Kato, S. (1998). Inactivating mutations in the 25-hydroxyvitamin D3 1alpha-hydroxylase gene in patients with pseudovitamin D-deficiency rickets. *N Engl J Med, 338*(10), 653-661. doi:10.1056/NEJM199803053381004

Kliewer, S. A., Umesono, K., Mangelsdorf, D. J., & Evans, R. M. (1992). Retinoid X receptor interacts with nuclear receptors in retinoic acid, thyroid hormone and vitamin D3 signalling. *Nature, 355*(6359), 446-449. doi:10.1038/355446a0

Knöpfel, T. (2017). *Mechanisms of intestinal phosphate absorption.* (PhD). University of Zurich, Germany. Retrieved from https://doi.org/10.5167/uzh-129184 Available from Zurich open repository and archive

Knopfel, T., Himmerkus, N., Gunzel, D., Bleich, M., Hernando, N., & Wagner, C. A. (2019). Paracellular transport of phosphate along the intestine. *Am J Physiol Gastrointest Liver Physiol*. doi:10.1152/ajpgi.00032.2019

Knopfel, T., Pastor-Arroyo, E. M., Schnitzbauer, U., Kratschmar, D. V., Odermatt, A., Pellegrini, G., . . . Wagner, C. A. (2017). The intestinal phosphate transporter NaPi-IIb (Slc34a2) is required to protect bone during dietary phosphate restriction. *Sci Rep, 7*(1), 11018. doi:10.1038/s41598-017-10390-2

Ko, S. H., Lee, G. S., Vo, T. T., Jung, E. M., Choi, K. C., Cheung, K. W., . . . Jeung, E. B. (2009). Dietary calcium and 1,25-dihydroxyvitamin D3 regulate transcription of calcium transporter genes in calbindin-D9k knockout mice. *J Reprod Dev, 55*(2), 137-142. doi:10.1262/jrd.20139

Kornberg, A. (1979). The enzymatic replication of DNA. *CRC Crit Rev Biochem, 7*(1), 23-43. doi:10.3109/10409237909102568

Koster, H. P. G., Hartog, A., Van os, C. H., & Bindels, R. J. M. (1995). Calbindin-D28K facilitates cytosolic calcium diffusion without interfering with calcium signaling. *Cell Calcium, 18*(3), 187-196. doi:https://doi.org/10.1016/0143-4160(95)90063-2

Krajisnik, T., Bjorklund, P., Marsell, R., Ljunggren, O., Akerstrom, G., Jonsson, K. B., . . . Larsson, T. E. (2007). Fibroblast growth factor-23 regulates parathyroid hormone and 1alpha-hydroxylase expression in cultured bovine parathyroid cells. *J Endocrinol, 195*(1), 125-131. doi:10.1677/JOE-07-0267

Krug, S. M., Gunzel, D., Conrad, M. P., Rosenthal, R., Fromm, A., Amasheh, S., . . . Fromm, M. (2012). Claudin-17 forms tight junction channels with distinct anion selectivity. *Cell Mol Life Sci, 69*(16), 2765-2778. doi:10.1007/s00018-012-0949-x

Kullenberg, D., Taylor, L. A., Schneider, M., & Massing, U. (2012). Health effects of dietary phospholipids. *Lipids Health Dis, 11*, 3. doi:10.1186/1476-511X-11-3

Kurosu, H., Ogawa, Y., Miyoshi, M., Yamamoto, M., Nandi, A., Rosenblatt, K. P., . . . Kuro-o, M. (2006). Regulation of fibroblast growth factor-23 signaling by klotho. *J Biol Chem, 281*(10), 6120-6123. doi:10.1074/jbc.C500457200

Labonte, E. D., Carreras, C. W., Leadbetter, M. R., Kozuka, K., Kohler, J., Koo-McCoy, S., . . . Charmot, D. (2015). Gastrointestinal Inhibition of Sodium-Hydrogen Exchanger 3

Reduces Phosphorus Absorption and Protects against Vascular Calcification in CKD. *J Am Soc Nephrol, 26*(5), 1138-1149. doi:10.1681/ASN.2014030317

Lameris, A. L., Nevalainen, P. I., Reijnen, D., Simons, E., Eygensteyn, J., Monnens, L., . . . Hoenderop, J. G. (2015). Segmental transport of Ca(2)(+) and Mg(2)(+) along the gastrointestinal tract. *Am J Physiol Gastrointest Liver Physiol, 308*(3), G206-216. doi:10.1152/ajpgi.00093.2014

Lardy, H. A., & Ferguson, S. M. (1969). Oxidative phosphorylation in mitochondria. *Annu Rev Biochem, 38*, 991-1034. doi:10.1146/annurev.bi.38.070169.005015

Larsson, T. E., Kameoka, C., Nakajo, I., Taniuchi, Y., Yoshida, S., Akizawa, T., & Smulders, R. A. (2018). NPT-IIb Inhibition Does Not Improve Hyperphosphatemia in CKD. *Kidney Int Rep, 3*(1), 73-80. doi:10.1016/j.ekir.2017.08.003

Lee, G. S., Lee, K. Y., Choi, K. C., Ryu, Y. H., Paik, S. G., Oh, G. T., & Jeung, E. B. (2007). Phenotype of a calbindin-D9k gene knockout is compensated for by the induction of other calcium transporter genes in a mouse model. *J Bone Miner Res, 22*(12), 1968-1978. doi:10.1359/jbmr.070801

Lee, J. J., Liu, X., O'Neill, D., Beggs, M. R., Weissgerber, P., Flockerzi, V., . . . Alexander, R. T. (2019). Activation of the calcium sensing receptor attenuates TRPV6-dependent intestinal calcium absorption. *JCI Insight, 5*. doi:10.1172/jci.insight.128013

Lee, J. J., Plain, A., Beggs, M. R., Dimke, H., & Alexander, R. T. (2017). Effects of phospho- and calciotropic hormones on electrolyte transport in the proximal tubule. *F1000Res, 6*, 1797. doi:10.12688/f1000research.12097.1

Legati, A., Giovannini, D., Nicolas, G., Lopez-Sanchez, U., Quintans, B., Oliveira, J. R., . . . Coppola, G. (2015). Mutations in XPR1 cause primary familial brain calcification associated with altered phosphate export. *Nat Genet, 47*(6), 579-581. doi:10.1038/ng.3289

Leon, J. B., Sullivan, C. M., & Sehgal, A. R. (2013). The prevalence of phosphorus-containing food additives in top-selling foods in grocery stores. *J Ren Nutr, 23*(4), 265-270 e262. doi:10.1053/j.jrn.2012.12.003

Lieben, L., Masuyama, R., Torrekens, S., Van Looveren, R., Schrooten, J., Baatsen, P., . . . Carmeliet, G. (2012). Normocalcemia is maintained in mice under conditions of calcium malabsorption by vitamin D-induced inhibition of bone mineralization. *J Clin Invest, 122*(5), 1803-1815. doi:10.1172/JCI45890

Linz, D., Wirth, K., Linz, W., Heuer, H. O., Frick, W., Hofmeister, A., . . . Ruetten, H. (2012). Antihypertensive and laxative effects by pharmacological inhibition of sodium-proton-exchanger subtype 3-mediated sodium absorption in the gut. *Hypertension, 60*(6), 1560-1567. doi:10.1161/HYPERTENSIONAHA.112.201590

Liu, S., Tang, W., Zhou, J., Stubbs, J. R., Luo, Q., Pi, M., & Quarles, L. D. (2006). Fibroblast growth factor 23 is a counter-regulatory phosphaturic hormone for vitamin D. *J Am Soc Nephrol, 17*(5), 1305-1315. doi:10.1681/ASN.2005111185

Loffing, J., & Kaissling, B. (2003). Sodium and calcium transport pathways along the mammalian distal nephron: from rabbit to human. *Am J Physiol Renal Physiol, 284*(4), F628-643. doi:10.1152/ajprenal.00217.2002

Loffing, J., Loffing-Cueni, D., Valderrabano, V., Klausli, L., Hebert, S. C., Rossier, B. C., . . . Kaissling, B. (2001). Distribution of transcellular calcium and sodium transport pathways along mouse distal nephron. *Am J Physiol Renal Physiol, 281*(6), F1021-1027. doi:10.1152/ajprenal.0085.2001

Loghman-Adham, M. (1996). Use of phosphonocarboxylic acids as inhibitors of sodium-phosphate cotransport. *Gen Pharmacol, 27*(2), 305-312. doi:10.1016/0306-3623(95)02017-9

Lopez, I., Rodriguez-Ortiz, M. E., Almaden, Y., Guerrero, F., de Oca, A. M., Pineda, C., . . . Aguilera-Tejero, E. (2011). Direct and indirect effects of parathyroid hormone on circulating levels of fibroblast growth factor 23 in vivo. *Kidney Int, 80*(5), 475-482. doi:10.1038/ki.2011.107

Lorenz-Depiereux, B., Benet-Pages, A., Eckstein, G., Tenenbaum-Rakover, Y., Wagenstaller, J., Tiosano, D., . . . Strom, T. M. (2006). Hereditary hypophosphatemic rickets with hypercalciuria is caused by mutations in the sodium-phosphate cotransporter gene SLC34A3. *Am J Hum Genet, 78*(2), 193-201. doi:10.1086/499410

Lu, Y., Yuan, B., Qin, C., Cao, Z., Xie, Y., Dallas, S. L., . . . Feng, J. Q. (2011). The biological function of DMP-1 in osteocyte maturation is mediated by its 57-kDa C-terminal fragment. *J Bone Miner Res, 26*(2), 331-340. doi:10.1002/jbmr.226

Ma, Y. L., Cain, R. L., Halladay, D. L., Yang, X., Zeng, Q., Miles, R. R., . . . Onyia, J. E. (2001). Catabolic effects of continuous human PTH (1--38) in vivo is associated with sustained stimulation of RANKL and inhibition of osteoprotegerin and gene-associated bone formation. *Endocrinology, 142*(9), 4047-4054. doi:10.1210/endo.142.9.8356

MacDonald, T., Saurette, M., Beggs, M. R., & Todd Alexander, R. (2021). Developmental Changes in Phosphate Homeostasis. *Rev Physiol Biochem Pharmacol*. doi:10.1007/112_2020_52

Mandon, B., Siga, E., Roinel, N., & de Rouffignac, C. (1993). Ca2+, Mg2+ and K+ transport in the cortical and medullary thick ascending limb of the rat nephron: influence of transepithelial voltage. *Pflugers Arch, 424*(5-6), 558-560. doi:10.1007/BF00374924

Marks, J., Churchill, L. J., Debnam, E. S., & Unwin, R. J. (2008). Matrix extracellular phosphoglycoprotein inhibits phosphate transport. *J Am Soc Nephrol, 19*(12), 2313-2320. doi:10.1681/ASN.2008030315

Marks, J., Debnam, E. S., & Unwin, R. J. (2010). Phosphate homeostasis and the renal-gastrointestinal axis. *Am J Physiol Renal Physiol, 299*(2), F285-296. doi:10.1152/ajprenal.00508.2009

Marks, J., Lee, G. J., Nadaraja, S. P., Debnam, E. S., & Unwin, R. J. (2015). Experimental and regional variations in Na+-dependent and Na+-independent phosphate transport along the rat small intestine and colon. *Physiol Rep, 3*(1). doi:10.14814/phy2.12281

Marks, J., Srai, S. K., Biber, J., Murer, H., Unwin, R. J., & Debnam, E. S. (2006). Intestinal phosphate absorption and the effect of vitamin D: a comparison of rats with mice. *Exp Physiol, 91*(3), 531-537. doi:10.1113/expphysiol.2005.032516

Marneros, A. G. (2021). Magnesium and Calcium Homeostasis Depend on KCTD1 Function in the Distal Nephron. *Cell Rep, 34*(2), 108616. doi:10.1016/j.celrep.2020.108616

Martin, A., David, V., & Quarles, L. D. (2012). Regulation and function of the FGF23/klotho endocrine pathways. *Physiol Rev, 92*(1), 131-155. doi:10.1152/physrev.00002.2011

Martin, A., Liu, S., David, V., Li, H., Karydis, A., Feng, J. Q., & Quarles, L. D. (2011). Bone proteins PHEX and DMP1 regulate fibroblastic growth factor Fgf23 expression in osteocytes through a common pathway involving FGF receptor (FGFR) signaling. *FASEB J, 25*(8), 2551-2562. doi:10.1096/fj.10-177816

Matsumoto, N., Hemmi, A., Yamato, H., Ohnishi, R., Segawa, H., Ohno, S., & Miyamoto, K. (2010). Immunohistochemical analyses of parathyroid hormone-dependent

downregulation of renal type II Na-Pi cotransporters by cryobiopsy. *J Med Invest, 57*(1-2), 138-145. Retrieved from https://www.ncbi.nlm.nih.gov/pubmed/20299753 https://www.jstage.jst.go.jp/article/jmi/57/1%2C2/57_1%2C2_138/_pdf

McHardy, G. J. R., & Parsons, D. S. (1956). THE ABSORPTION OF INORGANIC PHOSPHATE FROM THE SMALL INTESTINE OF THE RAT. *Quarterly Journal of Experimental Physiology and Cognate Medical Sciences, 41*(4), 398-409. doi:doi:10.1113/expphysiol.1956.sp001211

Milatz, S., Krug, S. M., Rosenthal, R., Gunzel, D., Muller, D., Schulzke, J. D., . . . Fromm, M. (2010). Claudin-3 acts as a sealing component of the tight junction for ions of either charge and uncharged solutes. *Biochim Biophys Acta, 1798*(11), 2048-2057. doi:10.1016/j.bbamem.2010.07.014

Miyagawa, A., Tatsumi, S., Takahama, W., Fujii, O., Nagamoto, K., Kinoshita, E., . . . Miyamoto, K. I. (2018). The sodium phosphate cotransporter family and nicotinamide phosphoribosyltransferase contribute to the daily oscillation of plasma inorganic phosphate concentration. *Kidney Int, 93*(5), 1073-1085. doi:10.1016/j.kint.2017.11.022

Miyamoto, K., Ito, M., Kuwahata, M., Kato, S., & Segawa, H. (2005). Inhibition of intestinal sodium-dependent inorganic phosphate transport by fibroblast growth factor 23. *Ther Apher Dial, 9*(4), 331-335. doi:10.1111/j.1744-9987.2005.00292.x

Moe, O. W. (2006). Kidney stones: pathophysiology and medical management. *The Lancet, 367*(9507), 333-344. doi:https://doi.org/10.1016/S0140-6736(06)68071-9

Moe, S. M., Zidehsarai, M. P., Chambers, M. A., Jackman, L. A., Radcliffe, J. S., Trevino, L. L., . . . Asplin, J. R. (2011). Vegetarian Compared with Meat Dietary Protein Source and Phosphorus Homeostasis in Chronic Kidney Disease. *Clinical Journal of the American Society of Nephrology, 6*(2), 257-264. doi:10.2215/cjn.05040610

Moog, F., & Glazier, H. S. (1972). Phosphate absorption and alkaline phosphatase activity in the small intestine of the adult mouse and of the chick embryo and hatched chick. *Comp Biochem Physiol A Comp Physiol, 42*(2), 321-336. Retrieved from https://www.ncbi.nlm.nih.gov/pubmed/4404366

Morgan, E. L., Mace, O. J., Helliwell, P. A., Affleck, J., & Kellett, G. L. (2003). A role for Ca(v)1.3 in rat intestinal calcium absorption. *Biochem Biophys Res Commun, 312*(2), 487-493. doi:10.1016/j.bbrc.2003.10.138

Moz, Y., Silver, J., & Naveh-Many, T. (1999). Protein-RNA interactions determine the stability of the renal NaPi-2 cotransporter mRNA and its translation in hypophosphatemic rats. *J Biol Chem, 274*(36), 25266-25272. doi:10.1074/jbc.274.36.25266

Moz, Y., Silver, J., & Naveh-Many, T. (2003). Characterization of cis-acting element in renal NaPi-2 cotransporter mRNA that determines mRNA stability. *Am J Physiol Renal Physiol, 284*(4), F663-670. doi:10.1152/ajprenal.00332.2002

Muto, S., Hata, M., Taniguchi, J., Tsuruoka, S., Moriwaki, K., Saitou, M., . . . Furuse, M. (2010). Claudin-2-deficient mice are defective in the leaky and cation-selective paracellular permeability properties of renal proximal tubules. *Proc Natl Acad Sci U S A, 107*(17), 8011-8016. doi:10.1073/pnas.0912901107

Nakamura, S., Irie, K., Tanaka, H., Nishikawa, K., Suzuki, H., Saitoh, Y., . . . Fujiyoshi, Y. (2019). Morphologic determinant of tight junctions revealed by claudin-3 structures. *Nat Commun, 10*(1), 816. doi:10.1038/s41467-019-08760-7

Navre, M., Labonte, E., & Carreras, C. (2011). *Novel Non-Systemic NaP2b Inhibitors Block Intestinal Phosphate Uptake.* Paper presented at the Proceedings of ASN meeting.

Ng, R. C., Rouse, D., & Suki, W. N. (1984). Calcium transport in the rabbit superficial proximal convoluted tubule. *J Clin Invest, 74*(3), 834-842. doi:10.1172/JCI111500

Nijenhuis, T., Hoenderop, J. G., van der Kemp, A. W., & Bindels, R. J. (2003). Localization and regulation of the epithelial Ca2+ channel TRPV6 in the kidney. *J Am Soc Nephrol, 14*(11), 2731-2740. doi:10.1097/01.asn.0000094081.78893.e8

Nordin, B. E. C. (1976). *Calcium, phosphate, and magnesium metabolism : clinical physiology and diagnostic procedures / edited by B. E. C. Nordin*. Edinburgh ; New York : New York: Churchill Livingstone ; distributed in the United States of America by Longman.

Office of the Surgeon, G. (2004). Reports of the Surgeon General. In *Bone Health and Osteoporosis: A Report of the Surgeon General*. Rockville (MD): Office of the Surgeon General (US).

Okuno, S., Ishimura, E., Kitatani, K., Fujino, Y., Kohno, K., Maeno, Y., . . . Nishizawa, Y. (2007). Presence of abdominal aortic calcification is significantly associated with all-cause and cardiovascular mortality in maintenance hemodialysis patients. *Am J Kidney Dis, 49*(3), 417-425. doi:10.1053/j.ajkd.2006.12.017

Olauson, H., Lindberg, K., Amin, R., Jia, T., Wernerson, A., Andersson, G., & Larsson, T. E. (2012). Targeted deletion of Klotho in kidney distal tubule disrupts mineral metabolism. *J Am Soc Nephrol, 23*(10), 1641-1651. doi:10.1681/ASN.2012010048

Palmer, S. C., Hayen, A., Macaskill, P., Pellegrini, F., Craig, J. C., Elder, G. J., & Strippoli, G. F. (2011). Serum levels of phosphorus, parathyroid hormone, and calcium and risks of death and cardiovascular disease in individuals with chronic kidney disease: a systematic review and meta-analysis. *JAMA, 305*(11), 1119-1127. doi:10.1001/jama.2011.308

Pan, W., Borovac, J., Spicer, Z., Hoenderop, J. G., Bindels, R. J., Shull, G. E., . . . Alexander, R. T. (2012). The epithelial sodium/proton exchanger, NHE3, is necessary for renal and intestinal calcium (re)absorption. *Am J Physiol Renal Physiol, 302*(8), F943-956. doi:10.1152/ajprenal.00504.2010

Peacock, M. (2021). Phosphate Metabolism in Health and Disease. *Calcified Tissue International, 108*(1), 3-15. doi:10.1007/s00223-020-00686-3

Pei, L., Solis, G., Nguyen, M. T., Kamat, N., Magenheimer, L., Zhuo, M., . . . Yu, A. S. (2016). Paracellular epithelial sodium transport maximizes energy efficiency in the kidney. *J Clin Invest, 126*(7), 2509-2518. doi:10.1172/JCI83942

Perazella, M., Rosner, M., & Lerma, E. V. (2018). *CURRENT Diagnosis & Treatment Nephrology & Hypertension* (A. Fielding & K. J. Davis. Eds. 2 ed.). London, United States: McGraw Hill Professional.

Perwad, F., Zhang, M. Y., Tenenhouse, H. S., & Portale, A. A. (2007). Fibroblast growth factor 23 impairs phosphorus and vitamin D metabolism in vivo and suppresses 25-hydroxyvitamin D-1alpha-hydroxylase expression in vitro. *Am J Physiol Renal Physiol, 293*(5), F1577-1583. doi:10.1152/ajprenal.00463.2006

Picard, N., Capuano, P., Stange, G., Mihailova, M., Kaissling, B., Murer, H., . . . Wagner, C. A. (2010). Acute parathyroid hormone differentially regulates renal brush border membrane phosphate cotransporters. *Pflugers Arch, 460*(3), 677-687. doi:10.1007/s00424-010-0841-1

Plain, A., Pan, W., O'Neill, D., Ure, M., Beggs, M. R., Farhan, M., . . . Alexander, R. T. (2020). Claudin-12 Knockout Mice Demonstrate Reduced Proximal Tubule Calcium Permeability. *Int J Mol Sci, 21*(6). doi:10.3390/ijms21062074

Prasad, V., Okunade, G. W., Miller, M. L., & Shull, G. E. (2004). Phenotypes of SERCA and PMCA knockout mice. *Biochem Biophys Res Commun, 322*(4), 1192-1203. doi:10.1016/j.bbrc.2004.07.156

Radanovic, T., Wagner, C. A., Murer, H., & Biber, J. (2005). Regulation of intestinal phosphate transport. I. Segmental expression and adaptation to low-P(i) diet of the type IIb Na(+)-P(i) cotransporter in mouse small intestine. *Am J Physiol Gastrointest Liver Physiol, 288*(3), G496-500. doi:10.1152/ajpgi.00167.2004

Rajagopal, A., Braslavsky, D., Lu, J. T., Kleppe, S., Clement, F., Cassinelli, H., . . . Lee, B. H. (2014). Exome sequencing identifies a novel homozygous mutation in the phosphate transporter SLC34A1 in hypophosphatemia and nephrocalcinosis. *J Clin Endocrinol Metab, 99*(11), E2451-2456. doi:10.1210/jc.2014-1517

Reilly, R. F., Shugrue, C. A., Lattanzi, D., & Biemesderfer, D. (1993). Immunolocalization of the Na+/Ca2+ exchanger in rabbit kidney. *Am J Physiol, 265*(2 Pt 2), F327-332. doi:10.1152/ajprenal.1993.265.2.F327

Rievaj, J., Pan, W., Cordat, E., & Alexander, R. T. (2013a). The Na(+)/H(+) exchanger isoform 3 is required for active paracellular and transcellular Ca(2)(+) transport across murine cecum. *Am J Physiol Gastrointest Liver Physiol, 305*(4), G303-313. doi:10.1152/ajpgi.00490.2012

Rievaj, J., Pan, W., Cordat, E., & Alexander, R. T. (2013b). The Na^+/H^+ exchanger isoform 3 is required for active paracellular and transcellular Ca^{2+} transport across murine cecum. *Am J Physiol Gastrointest Liver Physiol, 305*(4), G303-313. doi:10.1152/ajpgi.00490.2012

Ritter, C. S., & Slatopolsky, E. (2016). Phosphate Toxicity in CKD: The Killer among Us. *Clin J Am Soc Nephrol, 11*(6), 1088-1100. doi:10.2215/CJN.11901115

Rizzuto, R., Pinton, P., Ferrari, D., Chami, M., Szabadkai, G., Magalhães, P. J., . . . Pozzan, T. (2003). Calcium and apoptosis: facts and hypotheses. *Oncogene, 22*(53), 8619-8627. doi:10.1038/sj.onc.1207105

Robert, P. H. (2012). *Phosphorus. In Present Knowledge in Nutrition.* (E. JW, M. IA, & Z. SH Eds. 10 ed.). Washington, DC: Wiley-Blackwell.

Rowe, P. S., Kumagai, Y., Gutierrez, G., Garrett, I. R., Blacher, R., Rosen, D., . . . Mundy, G. R. (2004). MEPE has the properties of an osteoblastic phosphatonin and minhibin. *Bone, 34*(2), 303-319. doi:10.1016/j.bone.2003.10.005

Sabbagh, Y., Carpenter, T. O., & Demay, M. B. (2005). Hypophosphatemia leads to rickets by impairing caspase-mediated apoptosis of hypertrophic chondrocytes. *Proc Natl Acad Sci U S A, 102*(27), 9637-9642. doi:10.1073/pnas.0502249102

Sabbagh, Y., Giral, H., Caldas, Y., Levi, M., & Schiavi, S. C. (2011). Intestinal phosphate transport. *Adv Chronic Kidney Dis, 18*(2), 85-90. doi:10.1053/j.ackd.2010.11.004

Sabbagh, Y., O'Brien, S. P., Song, W., Boulanger, J. H., Stockmann, A., Arbeeny, C., & Schiavi, S. C. (2009). Intestinal npt2b plays a major role in phosphate absorption and homeostasis. *J Am Soc Nephrol, 20*(11), 2348-2358. doi:10.1681/ASN.2009050559

Sandin, K., Hegbrant, J., & Kloo, L. (2006). A theoretical investigation of the supersaturation of basic calcium phosphate in serum of dialysis patients. *J Appl Biomater Biomech, 4*(2), 80-86. Retrieved from https://www.ncbi.nlm.nih.gov/pubmed/20799206

Saurette, M., & Alexander, R. T. (2019). Intestinal phosphate absorption: The paracellular pathway predominates? *Exp Biol Med (Maywood)*, 1535370219831220. doi:10.1177/1535370219831220

Schiavi, S. C., Tang, W., Bracken, C., O'Brien, S. P., Song, W., Boulanger, J., . . . Sabbagh, Y. (2012). Npt2b deletion attenuates hyperphosphatemia associated with CKD. *J Am Soc Nephrol, 23*(10), 1691-1700. doi:10.1681/ASN.2011121213

Schlingmann, K. P., Ruminska, J., Kaufmann, M., Dursun, I., Patti, M., Kranz, B., . . . Konrad, M. (2016). Autosomal-Recessive Mutations in SLC34A1 Encoding Sodium-Phosphate Cotransporter 2A Cause Idiopathic Infantile Hypercalcemia. *J Am Soc Nephrol, 27*(2), 604-614. doi:10.1681/ASN.2014101025

Schnermann, J., Huang, Y., & Mizel, D. (2013). Fluid reabsorption in proximal convoluted tubules of mice with gene deletions of claudin-2 and/or aquaporin1. *Am J Physiol Renal Physiol, 305*(9), F1352-1364. doi:10.1152/ajprenal.00342.2013

Schultheis, P. J., Clarke, L. L., Meneton, P., Miller, M. L., Soleimani, M., Gawenis, L. R., . . . Shull, G. E. (1998). Renal and intestinal absorptive defects in mice lacking the NHE3 Na+/H+ exchanger. *Nat Genet, 19*(3), 282-285. doi:10.1038/969

Segawa, H., Kaneko, I., Yamanaka, S., Ito, M., Kuwahata, M., Inoue, Y., . . . Miyamoto, K. (2004). Intestinal Na-P(i) cotransporter adaptation to dietary P(i) content in vitamin D receptor null mice. *Am J Physiol Renal Physiol, 287*(1), F39-47. doi:10.1152/ajprenal.00375.2003

Segawa, H., Onitsuka, A., Furutani, J., Kaneko, I., Aranami, F., Matsumoto, N., . . . Miyamoto, K. (2009). Npt2a and Npt2c in mice play distinct and synergistic roles in inorganic phosphate metabolism and skeletal development. *Am J Physiol Renal Physiol, 297*(3), F671-678. doi:10.1152/ajprenal.00156.2009

Segawa, H., Yamanaka, S., Ito, M., Kuwahata, M., Shono, M., Yamamoto, T., & Miyamoto, K. (2005). Internalization of renal type IIc Na-Pi cotransporter in response to a high-phosphate diet. *Am J Physiol Renal Physiol, 288*(3), F587-596. doi:10.1152/ajprenal.00097.2004

Seldin, D. W. (1999). Renal handling of calcium. *Nephron, 81 Suppl 1*, 2-7. doi:10.1159/000046292

Shaikh, A., Berndt, T., & Kumar, R. (2008). Regulation of phosphate homeostasis by the phosphatonins and other novel mediators. *Pediatr Nephrol, 23*(8), 1203-1210. doi:10.1007/s00467-008-0751-z

Shibasaki, Y., Etoh, N., Hayasaka, M., Takahashi, M. O., Kakitani, M., Yamashita, T., . . . Hanaoka, K. (2009). Targeted deletion of the tybe IIb Na(+)-dependent Pi-co-transporter, NaPi-IIb, results in early embryonic lethality. *Biochem Biophys Res Commun, 381*(4), 482-486. doi:10.1016/j.bbrc.2009.02.067

Shimada, M., Shutto-Uchita, Y., & Yamabe, H. (2019). Lack of Awareness of Dietary Sources of Phosphorus Is a Clinical Concern. *In Vivo, 33*(1), 11-16. doi:10.21873/invivo.11432

Shimada, T., Hasegawa, H., Yamazaki, Y., Muto, T., Hino, R., Takeuchi, Y., . . . Yamashita, T. (2004). FGF-23 is a potent regulator of vitamin D metabolism and phosphate homeostasis. *J Bone Miner Res, 19*(3), 429-435. doi:10.1359/JBMR.0301264

Shinkyo, R., Sakaki, T., Kamakura, M., Ohta, M., & Inouye, K. (2004). Metabolism of vitamin D by human microsomal CYP2R1. *Biochem Biophys Res Commun, 324*(1), 451-457. doi:10.1016/j.bbrc.2004.09.073

Silver, J., & Naveh-Many, T. (2010). FGF23 and the parathyroid glands. *Pediatr Nephrol, 25*(11), 2241-2245. doi:10.1007/s00467-010-1565-3

Silver, J., Russell, J., & Sherwood, L. M. (1985). Regulation by vitamin D metabolites of messenger ribonucleic acid for preproparathyroid hormone in isolated bovine parathyroid cells. *Proc Natl Acad Sci U S A, 82*(12), 4270-4273. doi:10.1073/pnas.82.12.4270

Sommer, S., Berndt, T., Craig, T., & Kumar, R. (2007). The phosphatonins and the regulation of phosphate transport and vitamin D metabolism. *J Steroid Biochem Mol Biol, 103*(3-5), 497-503. doi:10.1016/j.jsbmb.2006.11.010

Spencer, A. G., Labonte, E. D., Rosenbaum, D. P., Plato, C. F., Carreras, C. W., Leadbetter, M. R., . . . Charmot, D. (2014). Intestinal inhibition of the Na+/H+ exchanger 3 prevents cardiorenal damage in rats and inhibits Na+ uptake in humans. *Sci Transl Med, 6*(227), 227ra236. doi:10.1126/scitranslmed.3007790

Stoll, R., Kinne, R., & Murer, H. (1979). Effect of dietary phosphate intake on phosphate transport by isolated rat renal brush-border vesicles. *Biochem J, 180*(3), 465-470. doi:10.1042/bj1800465

Suki, W. N. (1979). Calcium transport in the nephron. *Am J Physiol, 237*(1), F1-6. doi:10.1152/ajprenal.1979.237.1.F1

Suki, W. N., Rouse, D., Ng, R. C., & Kokko, J. P. (1980). Calcium transport in the thick ascending limb of Henle. Heterogeneity of function in the medullary and cortical segments. *J Clin Invest, 66*(5), 1004-1009. doi:10.1172/JCI109928

Sutton, R. A., & Dirks, J. H. (1975). The renal excretion of calcium: a review of micropuncture data. *Can J Physiol Pharmacol, 53*(6), 979-988. doi:10.1139/y75-136

Swaan, P. W., & Tukker, J. J. (1995). Carrier-mediated transport mechanism of foscarnet (trisodium phosphonoformate hexahydrate) in rat intestinal tissue. *J Pharmacol Exp Ther, 272*(1), 242-247. Retrieved from https://www.ncbi.nlm.nih.gov/pubmed/7815338

Tachibana, T., Hagiwara, K., & Johkoh, T. (2009). Pulmonary alveolar microlithiasis: review and management. *Curr Opin Pulm Med, 15*(5), 486-490. doi:10.1097/MCP.0b013e32832d03bb

Tamura, A., Hayashi, H., Imasato, M., Yamazaki, Y., Hagiwara, A., Wada, M., . . . Tsukita, S. (2011). Loss of claudin-15, but not claudin-2, causes Na+ deficiency and glucose malabsorption in mouse small intestine. *Gastroenterology, 140*(3), 913-923. doi:10.1053/j.gastro.2010.08.006

Tamura, A., Kitano, Y., Hata, M., Katsuno, T., Moriwaki, K., Sasaki, H., . . . Tsukita, S. (2008). Megaintestine in claudin-15-deficient mice. *Gastroenterology, 134*(2), 523-534. doi:10.1053/j.gastro.2007.11.040

Taniguchi, K., Terai, K., & Terada, Y. (2015). Novel NaPi-IIb inhibitor ASP3325 inhibits phosphate absorption in intestine and reduces plasma phosphorus level in rats with renal failure. *Journal of American Society of Nephrology*(583A), FR-PO936.

Tatsumi, S., Segawa, H., Morita, K., Haga, H., Kouda, T., Yamamoto, H., . . . Takeda, E. (1998). Molecular cloning and hormonal regulation of PiT-1, a sodium-dependent phosphate cotransporter from rat parathyroid glands. *Endocrinology, 139*(4), 1692-1699. doi:10.1210/endo.139.4.5925

Tenenhouse, H. S., Martel, J., Gauthier, C., Segawa, H., & Miyamoto, K. (2003). Differential effects of Npt2a gene ablation and X-linked Hyp mutation on renal expression of Npt2c. *Am J Physiol Renal Physiol, 285*(6), F1271-1278. doi:10.1152/ajprenal.00252.2003

Traebert, M., Hattenhauer, O., Murer, H., Kaissling, B., & Biber, J. (1999). Expression of type II Na-P(i) cotransporter in alveolar type II cells. *Am J Physiol, 277*(5), L868-873. doi:10.1152/ajplung.1999.277.5.L868

Ullrich, K. J., Rumrich, G., & Kloss, S. (1976). Active Ca2+ reabsorption in the proximal tubule of the rat kidney. Dependence on sodium- and buffer transport. *Pflugers Arch, 364*(3), 223-228. doi:10.1007/BF00581759

Villa-Bellosta, R., & Sorribas, V. (2010). Compensatory regulation of the sodium/phosphate cotransporters NaPi-IIc (SCL34A3) and Pit-2 (SLC20A2) during Pi deprivation and acidosis. *Pflugers Arch, 459*(3), 499-508. doi:10.1007/s00424-009-0746-z

Virkki, L. V., Murer, H., & Forster, I. C. (2006). Voltage clamp fluorometric measurements on a type II Na+-coupled Pi cotransporter: shedding light on substrate binding order. *J Gen Physiol, 127*(5), 539-555. doi:10.1085/jgp.200609496

Voelkl, J., Egli-Spichtig, D., Alesutan, I., & Wagner, C. A. (2021). Inflammation: a putative link between phosphate metabolism and cardiovascular disease. *Clin Sci (Lond), 135*(1), 201-227. doi:10.1042/CS20190895

Wallimann, T., Tokarska-Schlattner, M., & Schlattner, U. (2011). The creatine kinase system and pleiotropic effects of creatine. *Amino Acids, 40*(5), 1271-1296. doi:10.1007/s00726-011-0877-3

Walton, J., & Gray, T. K. (1979). Absorption of inorganic phosphate in the human small intestine. *Clin Sci (Lond), 56*(5), 407-412. Retrieved from https://www.ncbi.nlm.nih.gov/pubmed/477225
http://www.clinsci.org/content/56/5/407.long

Wang, Y., Wilson, C., Cartwright, E. J., & Lei, M. (2017). Plasma membrane Ca(2+) -ATPase 1 is required for maintaining atrial Ca(2+) homeostasis and electrophysiological stability in the mouse. *J Physiol, 595*(24), 7383-7398. doi:10.1113/JP274110

Wasserman, R. H., Corradino, R. A., & Taylor, A. N. (1969). Binding proteins from animals with possible transport function. *J Gen Physiol, 54*(1), 114-137. doi:10.1085/jgp.54.1.114

Wasserman, R. H., & Taylor, A. N. (1966). Vitamin d3-induced calcium-binding protein in chick intestinal mucosa. *Science, 152*(3723), 791-793. doi:10.1126/science.152.3723.791

Weber, C. R., Liang, G. H., Wang, Y., Das, S., Shen, L., Yu, A. S., . . . Turner, J. R. (2015). Claudin-2-dependent paracellular channels are dynamically gated. *Elife, 4*, e09906. doi:10.7554/eLife.09906

Weber, C. R., & Turner, J. R. (2017). Dynamic modeling of the tight junction pore pathway. *Ann N Y Acad Sci, 1397*(1), 209-218. doi:10.1111/nyas.13374

Weinman, E. J., Steplock, D., Cha, B., Kovbasnjuk, O., Frost, N. A., Cunningham, R., . . . Donowitz, M. (2009). PTH transiently increases the percent mobile fraction of Npt2a in OK cells as determined by FRAP. *Am J Physiol Renal Physiol, 297*(6), F1560-1565. doi:10.1152/ajprenal.90657.2008

Weinman, E. J., Steplock, D., Shenolikar, S., & Biswas, R. (2011). Fibroblast growth factor-23-mediated inhibition of renal phosphate transport in mice requires sodium-hydrogen exchanger regulatory factor-1 (NHERF-1) and synergizes with parathyroid hormone. *J Biol Chem, 286*(43), 37216-37221. doi:10.1074/jbc.M111.288357

Wettschureck, N., Lee, E., Libutti, S. K., Offermanns, S., Robey, P. G., & Spiegel, A. M. (2007). Parathyroid-specific double knockout of Gq and G11 alpha-subunits leads to a phenotype resembling germline knockout of the extracellular Ca2+ -sensing receptor. *Mol Endocrinol, 21*(1), 274-280. doi:10.1210/me.2006-0110

Wilkins, G. E., Granleese, S., Hegele, R. G., Holden, J., Anderson, D. W., & Bondy, G. P. (1995). Oncogenic osteomalacia: evidence for a humoral phosphaturic factor. *J Clin Endocrinol Metab, 80*(5), 1628-1634. doi:10.1210/jcem.80.5.7745010

Worcester, E. M., & Coe, F. L. (2010). Clinical practice. Calcium kidney stones. *N Engl J Med, 363*(10), 954-963. doi:10.1056/NEJMcp1001011

Woudenberg-Vrenken, T. E., Lameris, A. L., Weissgerber, P., Olausson, J., Flockerzi, V., Bindels, R. J., . . . Hoenderop, J. G. (2012). Functional TRPV6 channels are crucial for transepithelial Ca2+ absorption. *Am J Physiol Gastrointest Liver Physiol, 303*(7), G879-885. doi:10.1152/ajpgi.00089.2012

Yamada, S., Tokumoto, M., Tatsumoto, N., Taniguchi, M., Noguchi, H., Nakano, T., . . . Kitazono, T. (2014). Phosphate overload directly induces systemic inflammation and malnutrition as well as vascular calcification in uremia. *Am J Physiol Renal Physiol, 306*(12), F1418-1428. doi:10.1152/ajprenal.00633.2013

Yu, A. S. (2015). Claudins and the kidney. *J Am Soc Nephrol, 26*(1), 11-19. doi:10.1681/ASN.2014030284

Yu, A. S., Cheng, M. H., Angelow, S., Gunzel, D., Kanzawa, S. A., Schneeberger, E. E., . . . Coalson, R. D. (2009). Molecular basis for cation selectivity in claudin-2-based paracellular pores: identification of an electrostatic interaction site. *J Gen Physiol, 133*(1), 111-127. doi:10.1085/jgp.200810154

Yuan, B., Feng, J. Q., Bowman, S., Liu, Y., Blank, R. D., Lindberg, I., & Drezner, M. K. (2013). Hexa-D-arginine treatment increases 7B2*PC2 activity in hyp-mouse osteoblasts and rescues the HYP phenotype. *J Bone Miner Res, 28*(1), 56-72. doi:10.1002/jbmr.1738

Yuan, B., Takaiwa, M., Clemens, T. L., Feng, J. Q., Kumar, R., Rowe, P. S., . . . Drezner, M. K. (2008). Aberrant Phex function in osteoblasts and osteocytes alone underlies murine X-linked hypophosphatemia. *J Clin Invest, 118*(2), 722-734. doi:10.1172/JCI32702

Zachos, N. C., Tse, M., & Donowitz, M. (2005). Molecular physiology of intestinal Na+/H+ exchange. *Annu Rev Physiol, 67*, 411-443. doi:10.1146/annurev.physiol.67.031103.153004

Zhang, M. I., & O'Neil, R. G. (1996). Regulated calcium channel in apical membranes renal proximal tubule cells. *Am J Physiol, 271*(5 Pt 1), C1757-1764. doi:10.1152/ajpcell.1996.271.5.C1757